2020

Study Of Scalar Extensions For Physics Beyond The Standard Model

Marco Antonio Merchand Medina
William & Mary - Arts & Sciences, mmerchandd_5@hotmail.com

Study of Scalar Extensions for Physics Beyond the Standard Model

Marco Antonio Merchand Medina

Villa de Alvarez, Colima, Mexico

Masters of Science, College of William & Mary, 2016
Bachelor of Science, University of Colima, 2014

A Dissertation presented to the Graduate Faculty
of The College of William & Mary in Candidacy for the Degree of
Doctor of Philosophy

Department of Physics

College of William & Mary
August, 2020

APPROVAL PAGE

This Dissertation is submitted in partial fulfillment of
the requirements for the degree of

Doctor of Philosophy

Marco Antonio Merchand Medina

Reviewed by the Committee May 2020

Committee Chair
Marc Sher, Professor, Physics
College of William & Mary

Christopher Carone, Professor, Physics
College of William & Mary

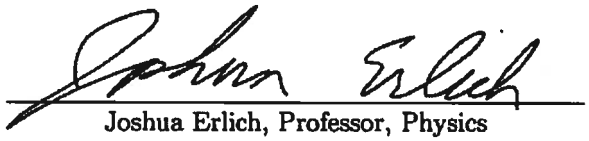

Joshua Erlich, Professor, Physics
College of William & Mary

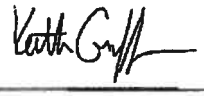

Keith Griffioen, Professor, Physics
College of William & Mary

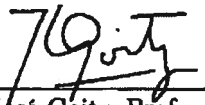

José Goity, Professor, Physics
Hampton University and Jefferson Laboratory

ABSTRACT

In this thesis we investigate the phenomenology of beyond the Standard Model scenarios with extra scalar fields. A review and motivation of extended electroweak symmetry breaking is presented. Then we address observational evidence of new physics such as possible lepton flavor violating processes and the relic abundance of dark matter by implementing models with three Higgs doublets. The complementarity between theoretical restrictions and experimental bounds on some of the predicted signals is leveraged to sharpen the allowed parameter space. After that we study embeddings of two-Higgs doublets into the Randall-Sundrum model with emphasis on the scalar fluctuations of the metric tensor and the stabilization mechanism: i) the viability of Higgs-radion unification is reappraised as well as some amendments to it, ii) additionally, kinetic mixing between radion and two Higgs doublets is explored. Theoretical predictions are tested against the most current experimental data and new avenues of discovery are highlighted. We devote the last part of this thesis to study how the axion solution to the strong CP problem can be unified with the dynamical flavor symmetry explanation for the huge hierarchies observed on the fermions.

TABLE OF CONTENTS

Acknowledgments iv

Dedications v

List of Tables vi

List of Figures viii

Chapter 1. Introduction 1

1.1 The Electroweak Sector 3

1.1.1 Fermion Masses 5

Chapter 2. Extended Higgs Models 7

2.1 Introduction 7

2.2 The Two-Higgs doublet model 8

2.3 Minimal Flavor Violation 9

2.3.1 Natural Flavor Conservation 10

2.3.2 Yukawa Alignment 10

2.4 Three Higgs doublet Model 11

2.4.1 Three doublet lepton-specific model 11

2.4.2 The I(1+2)HDM 15

2.4.2.1 The Model 16

2.4.2.2 Paremeter Scan 17

2.4.2.3 Collider Constraints 21

2.5 Conclusions 22

Chapter 3. The Randall-Sundrum Model 25
3.1 Introduction 25
3.1.1 The radion 27
3.2 Bulk Higgs Models 30
3.2.1 Higgs-radion Unification 32
3.2.2 Bulk Fermions 38
3.2.3 2HDM in the bulk 42
3.2.3.1 Superpotential 46
3.2.3.2 Scalar Perturbations 49
3.3 2HDM-radion mixing 53
3.3.1 Custodialy Symmetric 2HDM 54
3.3.2 Radion interactions 55
3.3.3 Mass Eigenstates 59
3.3.4 Model Predictions 62
3.3.4.1 Constraints From Current LHC Higgs Data 62
3.3.4.2 Collider Signals 65
3.3.4.3 Constraints From Heavy Higgs searches 67
3.4 Conclusion 74

Chapter 4. The Strong CP Problem and Flavor Symmetry 76
4.1 Introduction 76
4.2 Flavorful Axion from the double Tetrahedral Group 79
4.2.1 The Model 81
4.2.2 The Flavon Potential 83
4.2.3 Fit to quarks and charged leptons 86
4.2.4 The Flavorful Axion 88
4.2.5 Constraints from meson decays 91

4.2.6 Neutrino Sector 93
4.3 High Quality Flaxion 97
4.3.1 Quark Sector Model 98
4.3.2 Extension with Leptons 107
4.3.3 The Model 109
4.3.4 Model Constraints 111
4.4 Conclusion 112

Chapter 5. Conclusions 115

Appendices 118

Appendix A. Bulk Gauge bosons 119

Appendix B. Bulk Fermions 121

Appendix C. Background Solution 125

Appendix D. LHC Data 128

Bibliography 130

ACKNOWLEDGMENTS

I want to express my gratitude to my advisor Marc Sher for his guidance, support and valuable insights that have helped in the development of my scientific career. My appreciation to Chris Carone, Josh Erlich and Keith Thrasher from whom I have learned and been fortunate to collaborate with.
Finally I am thankful to all my physics professors, family and friends who have helped me in many different ways throughout my physics career.

I would like to dedicate this dissertation to my parents

LIST OF TABLES

1.1 Quantum charges for any generation of SM fermions. 5

2.1 2HDMs with discrete Z_2 symmetry. 10

3.1 Couplings of h_r to gauge bosons and fermions 37

3.2 A set of bulk mass parameters that reproduces the quark spectrum. Since each generation has three parameters and two masses, many other choices can be made. The predictions made in this section are only weakly sensitive to the specific choices; we have scanned the entire set of parameters and our conclusion in this section are unaffected. 40

3.3 Branching fractions to different decay channels of the SM Higgs boson and the Higgs-radion. The values of the c parameters corresponds to those in table 3.2. 41

4.1 Charge assignments. The index $a = 1, 2$ is a generation label. The first four columns correspond to complex scalar fields, while the remainder are either right-handed standard model fermion fields or Dirac adjoints of left-handed ones. 81

4.2 Fit to the charged fermion masses and mixing angles. All masses are given in GeV. (Note that m_t is the $\overline{MS}$ mass, not the pole mass.) The value of the quantity $\widetilde{\chi}^2$ defined in the text is 12.3. Running from the flavor scale M_F down to the Z mass is taken into account, with $M_F = 4 \times 10^{16}$ GeV, (see Sec. 4.2.6) chosen for the purpose of illustration. 88

4.3 Experimental constraints on the branching fractions of heavy mesons decays (second column), derived bounds on the axion decay constant times flavor rotation matrix elements from Ref. [197] (third column) and lower bound on the axion decay constant using the numerical value of the matrix element from the fit presented in Sec. 4.2.3 (fourth column). 92

4.4 Example of a viable parameter choice for the neutrino sector. 96

4.5 Charge assignments under the gauged flavor symmetry, $\mathrm{U}(1)_F$, the standard model gauge group, $\mathrm{SU}(3)_C \times \mathrm{SU}(2)_W \times \mathrm{U}(1)_Y$, and the accidental global $\mathrm{U}(1) \times \mathrm{U}(1)'$ symmetries discussed in the text. Indices range from $i = 1 \ldots N$, $j = 1 \ldots 2N$ and $k = 1 \ldots 2$. Aside from d_R^3, all other standard model fields are $\mathrm{U}(1)_F$ singlets. The parameters N and x are determined later by phenomenological constraints. 100

4.6 Values of f_b that saturate the bound on axion quality given in Eq. (4.78) as a function of N, with the associated Landau pole scale for standard model hypercharge. 105

4.7 Charge assignments under the gauged flavor symmetry, $\mathrm{U}(1)_F$, the standard model gauge group, $\mathrm{SU}(3)_C \times \mathrm{SU}(2)_W \times \mathrm{U}(1)_Y$, and the accidental global $\mathrm{U}(1) \times \mathrm{U}(1)'$ symmetries discussed in the text. Indices range from $i = 1 \ldots N$, $j = 1 \ldots 5$ and $k = 1 \ldots 5N$. Aside from d_R^3 and L^3, all other standard model fields are $\mathrm{U}(1)_F$ singlets. The parameters N and x are determined later by phenomenological constraints. 109

4.8 Values of f_b that saturate the bound on axion quality given in Eq. (4.89) as a function of N, with the associated value of the axion decay constant and the Landau pole scale for standard model hypercharge. 112

D.0.1 Measured Higgs Signal Strengths 129

LIST OF FIGURES

2.1 Branching ratios of H_1. ξ is the charged Higgs coupling to quarks. The image was taken from Ref. [71]. 14

2.2 Results of the parameter scan in the $m_\chi - m_\eta$ plane with a color bar representing the value of the relic density. In the vertical axis we took the square root of the absolute value of inert sector mass parameter m_η so that negative allowed values correspond to $-m_\eta^2$ in the scalar potential. Image from [72]. 19

2.3 Parameter space points in the $\cos(\beta - \alpha)$-$\tan\beta$. All points survived the parameter scan while the pink dots are also compliant with Planck lower limit. Image from [72]. 20

2.4 LDM+HDM (left) and LDM (right) regions where points colored brown would be excluded by LZ projected upper limits while points colored green would still be allowed. Image from [72]. 21

3.1 The top plots show the allowed regions for the type-I model and the bottom plots show the allowed regions in the type-II model. The blue (red, black) points shown are used for the $\Lambda = 3(5, 100)$ TeV cases. Values of the curvature scalar couplings, ξ_1, ξ_2 were allowed to range between $[-4, 4]$. We have varied the radion and heavy Higgs masses over the range 200 to 1000 GeV. Image from [170]. 64

3.2 Theoretically allowed ξ_1-ξ_2 parameter space for different values of $\tan\beta$. The blue (red) region is for $\Lambda = 3(5)$TeV. Image from [170]. 65

3.3 The parameter space of ξ_1 and ξ_2 allowed by the chi-square goodness of fit. The blue and red points correspond to $\Lambda = 3$ TeV and $\Lambda = 5$ TeV respectively. Image from [170]. 65

3.4 Scatter plots of the amount of mixing between the Higgs and the radion, K_h defined in equation (3.112), as function of the radion mass for the type-I 2HDM. The black region is theoretically allowed and the points colored yellow, green and red are forbidden by heavy scalar searches in the WW, ZZ and hh channels respectively. The benchmark point $\Lambda = 3(5)$TeV was used on the left (right). Due to the custodial symmetry, the charged scalar mass is identical to the pseudoscalar mass, whose value is given above each figure. The heavy neutral Higgs mass, m_H, is varied from 200 to 1000 GeV. Image from [170]. 69

3.5 Scatter plots of the amount of mixing between the heavy Higgs and the radion, K_H defined in equation (3.113), as function of the heavy Higgs mass for the type-I 2HDM. The black region is theoretically allowed and the points colored yellow, green and red are forbidden by heavy scalar searches in the WW, ZZ and hh channels respectively. The benchmark point $\Lambda = 3(5)$TeV was used on the left (right). Due to the custodial symmetry, the charged scalar mass is identical to the pseudoscalar mass, whose value is given above each figure. The radion mass, m_r, is varied from 200 to 1000 GeV. Image from [170]. 71

3.6 The observable $\sigma(gg \to A \to ZX)BR(Z \to l^+l^-)BR(X \to b\bar{b})$ as a function of the resonance mass with $X = H$(red), r(blue) for type-I (top) and type-II (bottom) models. We fixed $\Lambda = 3$ TeV, $m_A = 700$ GeV and $\lambda_4 = 0.1$. Due to the custodial symmetry, the charged scalar mass is identical to the pseudoscalar mass, whose value is given above each figure. The heavy neutral Higgs (radion) mass is varied from 200 to 1000 GeV in the right (left) figures and the values of α and β are chosen to be consistent with the constraints of Figure 3.1. The solid lines represent current and future upper bounds at the LHC. Image from [170]. 72

3.7 The observable $\sigma(gg \to X \to ZA)BR(Z \to l^+l^-)BR(A \to b\bar{b})$ as a function of the resonance mass with $X = H$(red), r(blue) in the type-I (top) and type-II (bottom) models. We fixed $\Lambda = 3$TeV, $m_A = 200$GeV($m_A = 500$GeV) on top (bottom) and $\lambda_4 = 0.1$. Due to the custodial symmetry, the charged scalar mass is identical to the pseudoscalar mass, whose value is given above each figure. The heavy neutral Higgs (radion) mass is varied from 200 to 1000 GeV in the right (left) figures and the values of α and β are chosen to be consistent with the constraints of Figure 3.1. The solid lines represent future upper bounds at the LHC. Image from [170]. 73

Chapter 1

Introduction

The field of High Energy Physics has witnessed substantial verification of the predictions of the Standard Model (SM). The discovery at the LHC of a SM like Higgs boson [1,2] has been the most remarkable particle physics accomplishment of the last decade. In spite of its experimental successes, the Standard Model is incomplete: there are observable phenomena for which the SM cannot offer explanation. In this regard there is overwhelming evidence of the existence of dark matter and the observable universe is asymmetrically populated with more matter than anti-matter.

Besides the aforementioned incontrovertible facts, there are experimental observations which are explained by the SM but are nonetheless peculiar from a theoretical viewpoint. These peculiarities are related to our aesthetic expectations for the values of the free parameters in a theory. Our assumption about the values of the parameters in a theory is related to the notion of Dirac naturalness [3,4] which states that in a fundamental theory with a cut off at a scale Λ, an operator $\mathcal{O}_d$ of mass dimension d is accompanied by a coefficient that scales as

$$c_d \propto c_0 \, \Lambda^{4-d} \tag{1.1}$$

where the coefficient c_0 is a dimensionless $\sim \mathcal{O}(1)$ number. This simple premise has guided our community in developing the underlying mechanisms that cause the apparent violation of naturalness and in the search for new physics.

The notion of naturalness was improved by t'Hooft [5] into what is now known as technical naturalness: in a theory with some operator $\mathcal{O}$ that has coefficient c, if in the limit when $c \to 0$ the theory has an enhanced symmetry then any radiative correction to the size of the parameter c will be proportional to the parameter itself. Therefore it is natural for the parameter to be small.

Within the SM there are several parameters that violate this naturalness principle. Perhaps the most important example being the sensitivity of the Higgs mass, a fundamental scalar in the theory, to physics in the ultraviolet scales. This comes with the name of the electroweak hierarchy problem. In addition to the Higgs mass, there is a strong CP problem related to the size of the θ angle parameter of QCD which is constrained by measurements of the neutron electric dipole moment to be $\theta \leq 10^{-10}$.

The lack of answers to the aforementioned issues justifies the pursuit for theories beyond the SM. In this respect, there has been a vast industry of people in our community that has developed elegant ideas that provide resolutions to these puzzles. Some of these sophisticated models comprise for example, supersymmetry [6], extra dimensions [7, 8], cosmological relaxation [9] or N-naturalness [10].

In many of these incarnations, extra scalar degrees of freedom are either necessary or appear as a consequence of the fundamental theory. In supersymmetric scenarios, two Higgs supermultiplets are used to enforce anomaly cancellations while in compactified extra dimensions the stabilization of the branes separation gives rise to a massive scalar that can mix with the SM Higgs. Other examples include, composite Higgs models [11], Left-Right symmetric models [12] and twin Higgs models [13].

In this dissertation we study the phenomenology of models with extra scalar degrees of freedom. In the remainder of this introductory section we review the basics aspects of electroweak symmetry breaking and the fermion sector in the SM. These are the only ingredients that are relevant for the subequent chapters.

1.1 The Electroweak Sector

The electroweak interactions of the SM have a fundamental gauge symmetry $SU(2)_L \times U(1)_Y$ and the Lagrangian density is given by

$$\mathcal{L}_{\rm EW} = -\frac{1}{4}W^{a\mu\nu}W^a_{\mu\nu} - \frac{1}{4}B^{\mu\nu}B_{\mu\nu} + |D_\mu H|^2 - V(H) + \mathcal{L}_{\rm Yukawa}, \tag{1.2}$$

where the kinetic term for the Abelian part is a simple Maxwell field strength tensor $B_{\mu\nu} = \partial_\mu B_\nu - \partial_\nu B_\mu$ and for the non-Abelian gauge fields, in general, we write their field strength tensor as

$$W^a_{\mu\nu} = \partial_\mu W^a_\nu - \partial_\nu W^a_\mu + g f^{abc} W^b_\mu W^c_\nu, \tag{1.3}$$

where for the $SU(2)$ group, the fine structure constants are simply given by the Levi-Civita symbol, i.e. $f^{abc} = \epsilon^{abc}$ and g denotes the gauge coupling constant. The covariant derivative of the Higgs doublet is

$$D_\mu H = \partial_\mu H - ig\frac{\sigma^a}{2}W^a_\mu H - i\frac{1}{2}g' B_\mu H, \tag{1.4}$$

with g' the gauge coupling of $U(1)_Y$ and we explicitly wrote the canonically normalized generators of $SU(2)$.

The Higgs potential is given by

$$V(H^\dagger H) = -m^2 H^\dagger H + \lambda (H^\dagger H)^2 \tag{1.5}$$

where the constraints $-m^2 < 0$ and $\lambda > 0$ are imposed in order for the vacuum to achieve spontaneous electroweak symmetry breaking down to the Abelian $U(1)_{\rm em}$ of electromagnetism. The minimization condition on the potential yield the relation $\lambda v^2 = m^2$. Where $v = 246$ GeV is determined experimentally from measurements of the muon decay.

With the usual hypercharge quantum numbers in the SM, the Higgs doublet can be

non-linearly parametrized as

$$H = \frac{1}{\sqrt{2}} e^{i\xi^a \sigma^a / v} \begin{pmatrix} 0 \\ v + h \end{pmatrix}, \tag{1.6}$$

where the gauge freedom to remove three rotational degrees of freedom is explicitly manifest. This gauge fixing in which we can ignore the rotational degrees of freedom and only the massive radial mode remains is known as the unitary gauge.

After symmetry breaking the gauge bosons get mass terms from the kinetic term of the Higgs doublet

$$\mathcal{L}_{\text{EW}} \supseteq \frac{g^2 v^2}{4} W_\mu^+ W^{-\mu} + \frac{g^2 v^2}{4 c_{\theta_W}} Z_\mu Z^\mu, \tag{1.7}$$

where the we following linear combinations define the physical charged and neutral gauge massive bosons

$$W_\mu^\pm \equiv \frac{W_\mu^1 \mp i W_\mu^2}{\sqrt{2}}, \tag{1.8}$$

$$Z_\mu \equiv c_{\theta_W} W_\mu^3 - s_{\theta_W} B_\mu, \tag{1.9}$$

where masses are given by

$$m_W = \frac{gv}{2}, \quad m_Z = \frac{m_W}{\cos\theta_W}, \tag{1.10}$$

and the mixing defined by the ratio of gauge couplings

$$\tan\theta_W = \frac{g'}{g}, \tag{1.11}$$

known as the Weinberg angle.

It is common lore to say that in the unitary gauge, the Goldstone bosons get "eaten" by the gauge bosons to get their mass. There is a linear combination, orthogonal to the neutral massive gauge boson,which doesn't receive a mass and is identified as the photon

$$A_\mu \equiv s_{\theta_W} W_\mu^3 + c_{\theta_W} B_\mu. \tag{1.12}$$

The interactions of the radial mode, the Higgs boson can be found by plugging eq. (1.6) into its kinetic and potential energy terms.

1.1.1 Fermion Masses

We display the SM fermion content and their respective representations under the gauge group in table 1.1 below.

Table 1.1: Quantum charges for any generation of SM fermions.

	Q	u_R	d_R	L	e_R	H
$SU(3)$	**3**	**3**	**3**	**1**	**1**	**1**
$SU(2)_L$	**2**	**1**	**1**	**2**	**1**	**2**
$U(1)_Y$	1/6	2/3	$-1/3$	$-1/2$	-1	1/2

From this table it is evident that the SM is chiral with respect to $SU(2)_L$ treating left- and right-handed fermions differently. Gauge invariance dictates what possible terms one can write down as the Yukawa mass terms. Given the Higgs conjugate $\tilde{H} \equiv i\sigma_2 H^*$ which transforms as a fundamental, the SM fermions obtain their masses from the following terms

$$-\mathcal{L}_{\text{Yukawa}} = Y^d \bar{Q} H d_R + Y^u \bar{Q} \tilde{H} u_R + Y^e \bar{L} H e_R + h.c. \tag{1.13}$$

where generation indices are omitted and Y^d, Y^u and Y^e are complex 3×3 matrices which in general, can be written as $Y^f = U_f M_f K_f^\dagger$ with U_f and K_f two independent unitary matrices and M_f a diagonal mass matrix. After spontaneous symmetry breaking one can perform chiral rotations

$$f_L \to U_f f_L, \quad f_R \to K_f f_R, \tag{1.14}$$

which would bring the mass terms into its diagonal form. The kinetic terms for the right-handed fermions will come out unscathed after such rotations. However for the left-handed ones, the coupling of the charged gauge bosons which appear non-diagonally in their matrix

representation will induce flavor mixing

$$\mathcal{L} \supseteq \frac{g}{2} W_\mu^+ \bar{u_L} \gamma^\mu V d_L + h.c. \tag{1.15}$$

where $V \equiv U_u^\dagger U_d$ is the Cabibbo-Kobayashi-Maskawa (CKM) matrix.

Chapter 2

Extended Higgs Models

2.1 Introduction

Many properties of the Higgs boson, like decay branching fractions and couplings to heavy fermions and gauge bosons have been tested experimentally and they are currently found in excellent agreement with the predictions from the SM [14,15]. Nonetheless BSM models with non-minimal scalar sectors and which are consistent with all experiments have been constructed [6]. Very often these theoretical ideas are designed to explain either observational evidence of new physics or as ultraviolet completions that can allow us to understand the apparent violations of Dirac naturalness.

Perhaps the most simple extension of the electroweak sector is to add to the SM Lagrangian a second Higgs doublet. There are examples galore in the literature where an extra Higgs doublet is a necessary ingredient of the theory. A well known example is the fact that two Higgs doublets are needed in the Minimal Supersymmetric Standard Model (MSSM) [16]. Additionally, in the original axion model of Peccei and Quinn [17] a global and anomalous $U(1)_{\rm PQ}$ symmetry in the Yukawa sector is only conceivable if a second doublet is added. This model is by now completely ruled out experimentally but several variants with more matter content exist and their effective field theory at low energies have two Higgs doublets [18].

The two Higgs doublet model has also been implemented for baryogenesis, see e.g. Refs. [19–25] and Dark Matter [26–49].

2.2 The Two-Higgs doublet model

The most general parametrization for the scalar potential for two Higgs doublets with the same quantum numbers [50, 51] is given by

$$\begin{aligned} V(\Phi_1,\Phi_2) = &-\frac{1}{2}\left(m_{11}^2\Phi_1^\dagger\Phi_1 + m_{22}^2\Phi_2^\dagger\Phi_2 + \left(m_{12}^2\Phi_1^\dagger\Phi_2 + H.c.\right)\right) \\ &+ \frac{\lambda_1}{2}(\Phi_1^\dagger\Phi_1)^2 + \frac{\lambda_2}{2}(\Phi_2^\dagger\Phi_2)^2 + \lambda_3(\Phi_1^\dagger\Phi_1)(\Phi_2^\dagger\Phi_2) + \lambda_4(\Phi_1^\dagger\Phi_2)(\Phi_2^\dagger\Phi_1) \\ &+ \left[\frac{\lambda_5}{2}(\Phi_1^\dagger\Phi_2)^2 + \lambda_6(\Phi_1^\dagger\Phi_1)(\Phi_1^\dagger\Phi_2) + \lambda_7(\Phi_2^\dagger\Phi_2)(\Phi_1^\dagger\Phi_2) + H.c.\right], \end{aligned} \tag{2.1}$$

where m_{11}^2, m_{22}^2, and $\lambda_{1,2,3,4}$ are real by hermiticity and m_{12}^2 and $\lambda_{5,6,7}$ are in general complex. In this expression there are fourteen parameters, however the freedom in the choice of basis can be used to reduce this number down to eleven degrees of freedom that are physical. Throughout this work we will assume that CP is conserved by the potential and that is not spontaneously broken by the vacuum. We will also impose softly broken discrete symmetries that eliminate terms with odd numbers of the same doublets in the quartic terms.

The $SU(2)_L$ Higgs doublets can be parametrized as

$$\Phi_a = \begin{pmatrix} \phi_a^+ \\ \left(v_a + \rho_a + i\eta_a\right)/\sqrt{2} \end{pmatrix}, \quad a = 1, 2. \tag{2.2}$$

where the ratio of vevs defines the mixing angle of the CP odd and charged scalars

$$\tan\beta \equiv \frac{v_2}{v_1}. \tag{2.3}$$

The fields appearing in the expression of the Higgs doublets (2.2) are not the physical scalars. To obtain the physical eigenstates one has to diagonalize the mass matrices that

are constructed using equation (3.73). It is customary to write the rotation matrices as

$$\begin{pmatrix}\eta_1\\ \eta_2\end{pmatrix}=\begin{pmatrix}c_\beta & -s_\beta\\ s_\beta & c_\beta\end{pmatrix}\begin{pmatrix}G^0\\ A\end{pmatrix},\quad \begin{pmatrix}\phi_1^\pm\\ \eta_2^\pm\end{pmatrix}=\begin{pmatrix}c_\beta & -s_\beta\\ s_\beta & c_\beta\end{pmatrix}\begin{pmatrix}G^\pm\\ H^\pm\end{pmatrix},\quad \begin{pmatrix}\rho_1\\ \rho_2\end{pmatrix}=\begin{pmatrix}c_\alpha & -s_\alpha\\ s_\alpha & c_\alpha\end{pmatrix}\begin{pmatrix}H\\ h\end{pmatrix}, \tag{2.4}$$

where $c_\beta = \cos\beta$, $s_\beta = \sin\beta$ etc and α is determined by the parameters of the potential. G^0 and $G^\pm$ are the neutral and charged Goldstone bosons, respectively and A is the physical pseudoscalar. The h and H are CP-even Higgs states. Notice that there are 8 degrees of freedom from the two doublets, three of them would get eaten by the gauge bosons and 5 massive physical states remain as consistent with Goldstone theorem.

2.3 Minimal Flavor Violation

In the SM there is an accidental global symmetry $U(3)^5$ when the Yukawa matrices are taken to zero. The number 5 in the exponent coming from the five types of fermions that were presented in table 1.1 while the number 3 inside the group argument coming from the three generations of matter fields. This accidental symmetry is a direct manifestation of technical naturalness.

In the most general 2HDM, the Yukawa couplings would consist of two copies of the SM Yukawas, i.e.,

$$\begin{aligned}-\mathcal{L}_{\text{Yukawa}} =& Y_1^d\bar{Q}\Phi_1 d_R + Y_1^u\bar{Q}\tilde{\Phi}_1 u_R + Y_1^e\bar{L}\Phi_1 e_R \\ & Y_2^d\bar{Q}\Phi_2 d_R + Y_2^u\bar{Q}\tilde{\Phi}_2 u_R + Y_2^e\bar{L}\Phi_2 e_R + \text{h.c.}\end{aligned} \tag{2.5}$$

An expression such as this would induce flavor changing neutral currents and would be in gross violation with experiments if one does not assume that the Yukawa matrices have certain structure. FCNC's are absent in the SM because it satisfies the requirement of Minimal Flavor Violation (MFV) [52]. The MFV framework has been rigorously defined [52], however for our purposes it suffices to define it as the requirement that all interactions that violate flavor symmetry should originate from the known structure of the three Yukawa

matrices and CP violation arises from the complex phase of the CKM matrix, only.

2.3.1 Natural Flavor Conservation

In models with extended Higgs sectors several mechanisms have been devised that achieve MFV in the Yukawa sector. The Paschos-Glashow-Weinberg theorem [53, 54] states that a sufficient condition to avoid FCNC's at tree-level is if all fermions with the same quantum numbers receive their masses from the same Higgs doublet. This is also known as natural flavor conservation.

In 2HDM natural flavor conservation can be enforced by imposing discrete or continuous symmetries in the Yukawas. For example, a discrete Z_2 symmetry can be imposed under which Φ_1 is odd and thus all fermions couple to Φ_2 (it is convention to always take Φ_2). This is known at the type-I model. Following this logic, there are four different types of models that can be written down. These are displayed in table 2.1

Table 2.1: 2HDMs with discrete Z_2 symmetry.

Model	u_R^i	d_R^i	e_R^i
Type I	Φ_2	Φ_2	Φ_2
Type II	Φ_2	Φ_1	Φ_1
Lepton-specific	Φ_2	Φ_2	Φ_1
Flipped	Φ_2	Φ_1	Φ_2

Each of these scenarios have their own phenomenological signals and have been extensively studied in the literature.

2.3.2 Yukawa Alignment

Another way to avoid tree-level FCNCs was introduced by Pich and Tuzon [55, 56] by adopting the structure of equation 2.5 but assuming that the Yukawas of a particular fermion type are proportional, i.e.

$$Y_1^u = z_u Y_2^u, \quad Y_1^d = z_d Y_2^d, \quad Y_1^e = z_e Y_2^e, \tag{2.6}$$

where the z_i can be complex parameters. In this way the Yukawa interactions are automatically diagonalized in the mass basis. In this scenario, MFV arises as a consequence of the underlying flavor structure which can be independent of the Higgs sector and gives rise to the proportionality relations expressed above.

2.4 Three Higgs doublet Model

Having motivated the study of extended scalar sectors in the first chapter and introduced the basics of the 2HDM in the preceding section we now turn our attention into the possibly next to simplest extension of the Higgs sector, the three-Higgs doublet model (3HDM).

Studies of 3HDMs regarding its symmetry structure and breaking patterns have been presented for discrete symmetries in Refs. [57, 58] and for Abelian symmetries in Refs. [59, 60]. Similarly, models with S_3 [61, 62] and A_4 symmetry [63] have appeared. Perturbative unitarity in inert versions of this model were investigated in Ref. [64]. The phenomenology of a 3HDM with Z_5 was explored in [65, 66]. Other phenomenological investigations can be found in Refs. [67–70].

In the following two subsections we will be mainly concerned with two variants of the 3HDM based on our studies in Refs [71, 72]. In the first case we considered a model that has MFV in the quark sector but permits lepton flavor violation in order to accommodate a signal excess that was reported by experiments at the LHC. In the latter case one of the doublets discrete symmetries in the scalar potential render one Higgs doublet to be inert, meaning it doesn't acquire a vev and its neutral component is a viable DM candidate.

2.4.1 Three doublet lepton-specific model

In 2015 the CMS collaboration conducted the first direct search for lepton-flavor violating decays of the discovered Higgs boson into the $\mu\tau$ final state [73] with an excess of events with a significance of 2.4σ being reported. Although subsequent experimental analyses [74, 75] at higher center of mass energies didn't report significant signal excesses we investigated

in Ref. [71] a 3HDM with naturally large lepton flavor violating Higgs decays but with vanishing tree-level FCNCs in the quark sector. To accomplish this they extended the lepton-specific 2HDM by adding an extra Higgs doublet Φ_3, odd under the Z_2. In this way the two doublets Φ_1 and Φ_3 couple to leptons and by Paschos-Glashow-Weinberg theorem there are tree-level FCNCs in the lepton sector.

A slightly simplified form of the scalar potential was assumed where quartic terms odd in either Φ_1 and Φ_3 were omitted and the parameters were chosen such that all doublets acquire non-vanishing vevs $\langle \Phi_i \rangle = (0, v_i)^T$. By the Goldstone theorem, the spectrum consists of two charged scalars, two pseudoscalars and three neutral scalars. Additionally, there are seven rotation angles that diagonalize the mass matrices: four angles for the charged and pseudoscalars and three angles for the CP-even scalars.

The lepton sector is thus given by

$$\mathcal{L}_{Yukawa} \supseteq -\bar{L}\left(\Phi_1 \eta^1 + \Phi_3 \eta^2\right) e_R + h.c. \tag{2.7}$$

where η^1 and η^2 are general complex Yukawa matrices.

A Higgs basis is defined by a rotation $(\Phi_1, \Phi_3) \to (H_1, H_3)$ such that H_1 has zero vev and $\langle H_3 \rangle = v_{13}/\sqrt{2}$ (with $v_{ij}^2 \equiv v_i^2 + v_j^2$) and can be accomplished by performing the field redefinition

$$\begin{pmatrix} \Phi_1 \\ \Phi_3 \end{pmatrix} = \frac{1}{v_{13}} \begin{pmatrix} v_3 & v_1 \\ -v_1 & v_3 \end{pmatrix} \begin{pmatrix} H_1 \\ H_3 \end{pmatrix}. \tag{2.8}$$

Then in the Higgs basis

$$\mathcal{L}_{lepton} = -\frac{\sqrt{2}}{v_{13}} \bar{L}\left(H_1 N + H_3 M\right) e_R. + h.c. \tag{2.9}$$

where

$$N \equiv \frac{1}{\sqrt{2}}\left(v_3 \eta^1 - v_1 \eta^2\right), \tag{2.10}$$

$$M \equiv \frac{1}{\sqrt{2}}\left(v_1 \eta^1 + v_3 \eta^2\right), \tag{2.11}$$

the lepton masses are generated by the M matrix only. When performing the chiral rotation of the leptons to their mass basis, namely $e_R \to U_R e_R$, $L \to U_L L$ the matrix M will be diagonalized but $U_L^\dagger N U_R = N_d$ is not necessarily diagonal.

Notice since U_R is unknown and N is arbitrary, the N_d coefficients are arbitrary as well. The authors assumed that the coefficients were given by the Cheng-Sher ansatz [76]

$$(N_d)_{ij} = k_{ij}\sqrt{m_i m_j}, \tag{2.12}$$

where $k_{ij} \sim \mathcal{O}(1)$. Due to strong constraints on FCNCs involving the first two generations, we simply assume that k_{12}, k_{13}, k_{21}, k_{31} were absent. Then one has

$$N_d = \begin{pmatrix} k_{11}m_e & 0 & 0 \\ 0 & k_{22}m_\mu & k_{23}\sqrt{m_\mu m_\tau} \\ 0 & k_{32}\sqrt{m_\mu m_\tau} & k_{33}m_\tau \end{pmatrix}. \tag{2.13}$$

Besides the ability to explain the $h \to \mu\tau$ excess, this model leads to interesting phenomenological consequences for the charged Higgs bosons that are completely determined by three mixing angles and two mass parameters.

Requiring that the couplings of the light Higgs boson to be within acceptable ranges from those predicted for the SM Higgs and assuming all additional neutral scalars to be very heavy so that they could be decoupled from the low energy theory, the authors studied constraints on the parameters space from B physics and the decay branching fractions of the charged Higgs bosons above the top quark threshold.

The charged Higgs coupling to quarks is a function of the mixing angles given by

$$\xi^u_{H_1^+} = \frac{\cos\beta_1 \cot\psi - \cos\theta \sin\beta_1}{\sin\theta}, \tag{2.14}$$

where two of the mixing angles are given by ratios of vevs, namely

$$\tan\theta = \frac{v_{12}}{v_3}, \qquad \tan\psi = \frac{v_2}{v_1}, \tag{2.15}$$

and β_1 is a free parameter. It is possible to find points in parameter space which can be quarkphobic without any ratio of vevs being too large. Contrary to the 2HDM case where the charged scalar becomes quarkphobic in the large $\tan\beta$ limit putting at risk perturbativity and unitarity.

The authors were interested in one of the charged Higgs $H_1^\pm$ having suppressed couplings to quarks and derived bounds on the mass of $H_2^\pm$ from B decays and found that the bounds were relatively weak unless the Yukawa coupling was relatively large $\xi^u_{H_2^+} > 1$. They also studied the interesting effect of flavor violating decay $B \to \mu\nu_\tau$ which would appear as a contribution to $B \to \mu\nu_\mu$ since detectors are blind to neutrino flavors. However they found that regions of parameter space in which this process has a significant rate is not consistent with other B physics constraints.

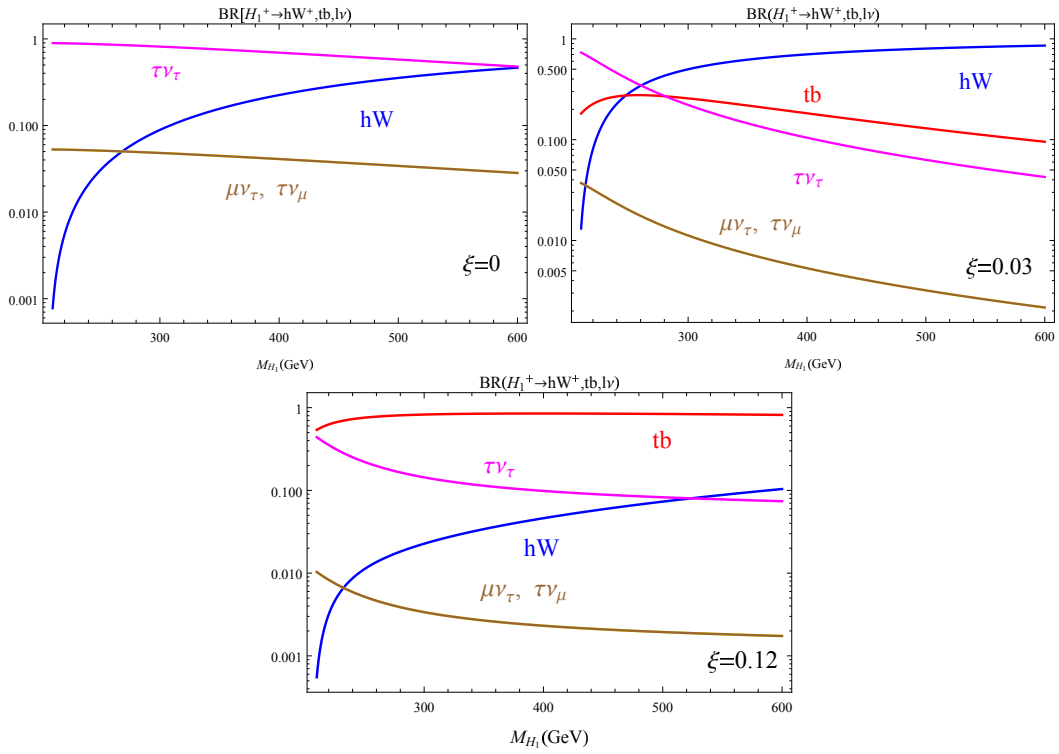

Figure 2.1: Branching ratios of H_1. ξ is the charged Higgs coupling to quarks. The image was taken from Ref. [71].

The most relevant branching fractions are shown in Fig. 2.1 for different values of the

charged Higgs coupling to quarks. One can notice that as the quark Yukawa coupling gets smaller, the decay mode into $\tau\nu_\tau$ becomes dominant for small masses.

The branching fraction into the flavor changing $\mu\nu_\tau$ final state becomes significant and would be the easiest to detect at colliders. The production cross section, via vector boson fusion, for a pair of charged Higgs bosons is model independent and is on the order of a few fb [77]. By the time of writing of this thesis the LHC has completed it last run of 130 fb^{-1} which means about ten events and to the best of our knowledge no upper bounds on flavor violating charged Higgs decays have been imposed, most likely due to overwhelming backgrounds.

2.4.2 The I(1+2)HDM

The data [78] suggests that the energy density of our universe is dominated by dark matter and dark energy and despite the vast amount of experimental evidence for the existence of Dark Matter, its particle physics nature remains, so far, unknown.

The fact that particles with weak scale ($\approx 100\text{GeV}$) cross sections give the right amount of DM abundance, has been called the WIMP miracle and models with WIMP candidates exist in abundance in the literature.

The inert two Higgs doublet model (IDM) [26–29] is one of the simplest extensions of the SM that provides a viable DM candidate while remaining consistent with theoretical and experimental constraints [49]. Its phenomenology has been thoroughly studied [79–81] and it is expected that improved precision measurements in the electroweak sector as well as more sensitive direct detection experiments will further constrain the IDM parameter space.

Inspired by this we investigated [72] a 3HDM where one doublet is inert, thus providing a DM candidate. Another variant of this model is one with two inert doublets. In Ref. [64] these models have been called the I(1+2)HDM and I(2+1)HDM respectively and unitarity and EWPO formulas were derived in both cases.

Furthermore, in [82–84] CP violation in the I(1+2)HDM was studied while in Ref. [85], 1-loop induced charged Higgs decays to electroweak gauge bosons was calculated. For literature on the I(2+1)HDM see Refs. [86–92]

In Ref. [72] we studied the CP conserving I(1+2)HDM with Yukawa structure of type-I and type-II and implemented an updated revision of the parameter space taking into account theoretical and most recent experimental constraints. The predictions for mono object final states were tested against current LHC searches. In the following subsections we will present the model in more detail as well as its constraints, parameter space and mono object predictions.

2.4.2.1 The Model

The model has three Higgs doublets, two active doubles denoted by Φ_1, Φ_2 and one inert doublet η. A dark Z_2 symmetry which stabilizes η is imposed and a softly broken Z_2' is imposed on the active doublets and SM fermions to accomplish MFV. The scalar potential can be written as follows

$$V(\Phi_1, \Phi_2, \eta) = V_{12}(\Phi_1, \Phi_2) + V_3(\eta) + V_{123}(\Phi_1, \Phi_2, \eta), \tag{2.16}$$

where the first term corresponds to the 2HDM potential of eq. (3.73) with $\lambda_6 = \lambda_7 = 0$. The inert doublet potential has the form

$$V_3(\eta) = m_\eta^2 \eta^\dagger \eta + \frac{\lambda_\eta}{2}(\eta^\dagger \eta)^2, \tag{2.17}$$

while the mixing between active and inert doublets is parametrized as

$$\begin{aligned} V_{123}(\Phi_1, \Phi_2, \eta) = {} & \lambda_{1133}(\Phi_1^\dagger \Phi_1)(\eta^\dagger \eta) + \lambda_{2233}(\Phi_2^\dagger \Phi_2)(\eta^\dagger \eta) \\ & + \lambda_{1331}(\Phi_1^\dagger \eta)(\eta^\dagger \Phi_1) + \lambda_{2332}(\Phi_2^\dagger \eta)(\eta^\dagger \Phi_2) \\ & + \frac{1}{2}\left[\lambda_{1313}(\Phi_1^\dagger \eta)^2 + \text{h.c.}\right] + \frac{1}{2}\left[\lambda_{2323}(\Phi_2^\dagger \eta)^2 + \text{h.c.}\right], \end{aligned} \tag{2.18}$$

where all parameters are assumed to be real, consistent with CP conservation.

A simplifying assumption of the quartic couplings, known as the "dark democracy", was adopted

$$\begin{aligned} \lambda_a &\equiv \lambda_{1133} = \lambda_{2233}, \\ \lambda_b &\equiv \lambda_{1331} = \lambda_{2332}, \\ \lambda_c &\equiv \lambda_{1313} = \lambda_{2323}, \end{aligned} \tag{2.19}$$

this simplification reduces the number of parameters significantly. Relaxing this assumption, which is common in IDM studies, can have a substantial effect in this particular model.

Due to the dark Z_2 symmetry, η doesn't couple to fermions at tree-level and the softly broken Z_2' symmetry on the active doublets produces the four types of 2HDM presented in table 2.1. Here we are only interested in type-I and type-II. The mass eigenstates in the active sector are thus obtained by the rotations of eq. 2.4.

Since the interactions between inert and active doublets only arise in the quartic terms, the components of the inert doublet are trivially written in their mass eigenbasis. Fixing $m_h = 125$ GeV, the model is determined by eleven free parameters

$$\text{Free Parameters} = \left\{ m_H, m_A, m_{H^\pm}, m_\chi, m_{\chi_a}, m_{\chi^\pm}, m_\eta^2, m_{12}^2, \alpha, \beta, \lambda_\eta \right\}. \tag{2.20}$$

2.4.2.2 Paremeter Scan

A random scan of the parameters was performed according to the following well motivated ranges

$$2 \leq \tan\beta \leq 10, \tag{2.21}$$

$$0 \leq \beta - \alpha \leq \pi, \tag{2.22}$$

$$10 \text{ GeV} \leq m \leq 1000 \text{ GeV}, \quad \text{with } m = m_H, m_A, m_\chi, m_{\chi_a}, \tag{2.23}$$

$$m_Z/2 \text{ GeV} \leq m \leq 1000 \text{ GeV}, \quad \text{with } m = m_{H^\pm}, m_{\chi^\pm}, \tag{2.24}$$

$$-1 \text{ TeV}^2 \leq m_{12}^2 \leq 1 \text{ TeV}^2, \tag{2.25}$$

$$-1 \text{ TeV}^2 \leq m_\eta^2 \leq 1 \text{ TeV}^2, \tag{2.26}$$

$$0 \leq \lambda_\eta \leq 8\pi. \tag{2.27}$$

During the scan, several theoretical and experimental constraints where imposed:

1 Positivity of the potential at large field values [82].

2 Partial Wave Unitarity bounds on the quartic couplings [64].

3 B-physics constraints on the charged Higgs mass $m_{H^\pm}$ as function of $\tan\beta$ [93].

4 *chi*-square test on the measured S and T parameters [94].

5 Constraints from LEP on the widths of gauge bosons, MSSM limits applied to the IDM and bounds from charged Higgs searches [93, 95–100], .

6 Higgs boson signal strengths and most recent limit on its branching ratio to invisible states as well as exclusion limits from heavy Higgs searches [101–103].

7 Upper limit on DM relic density [104].

8 Upper limit on DM scattering cross section off nucleons [105, 106].

Without loss of generality it is assumed that χ is the DM particle and thus the inequalities $m_\chi < m_{\chi_a}$ and $m_\chi < m_{\chi^\pm}$ are imposed. The model was implemented in FeynRules [107] and micrOMEGAs [108–111] was used to calculate DM observables.

Due to the dark Z_2 symmetry the inert sector fields do not couple to fermions at tree-level and their decay to fermions arises only via Higgs boson annihilation. The Higgs portal coupling is given by

$$\lambda_{abc} \equiv \lambda_a + \lambda_b + \lambda_c = 2\frac{m_\chi^2 - m_\eta^2}{v^2}, \tag{2.28}$$

which is multiplied by $\sin(\beta-\alpha)$ ($\cos(\beta-\alpha)$) for h (H) in the s-channel. We thus see that the mass squared parameter in the inert sector m_η^2 becomes phenomenologically relevant as it moderates DM observables given a DM mass m_χ.

The allowed points from the scan are shown in figure 2.2 in the $m_\chi - m_\eta$ plane where the value of the relic density is shown with a color map. From the plot it is evident that m_χ and m_η are forced to become more degenerate the closer the relic density values are from the Planck upper limit. Many other points away from the line $m_\chi = m_\eta$ are allowed but yield negligible contribution to the DM density and one would need extra dark sectors to satisfy the observed relic abundance.

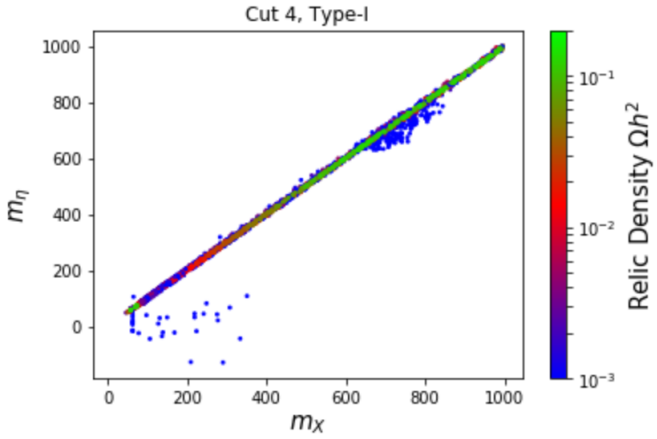

Figure 2.2: Results of the parameter scan in the $m_\chi - m_\eta$ plane with a color bar representing the value of the relic density. In the vertical axis we took the square root of the absolute value of inert sector mass parameter m_η so that negative allowed values correspond to $-m_\eta^2$ in the scalar potential. Image from [72].

Looking at the figure one can pinpoint two regions, colored green, where relic density constraints would be satisfied without needing extra model building. There is a low mass region with $m_\chi \in [57, 73]$ GeV and a high mass region with $m_\chi \in [500, 1000]$ GeV which were referred to as LDM and HDM respectively. This is one of the most salient results from the parameter scan and is independent of the Yukawa type model. This agrees with previous literature [83].

The differences between the type-I and type-II models becomes visible in the $\cos(\beta-\alpha)-$

$\tan\beta$ plane, shown in figure 2.3. The points colored pink satisfy the Planck constraints and thus DM constraints do not affect the mixing angles. The allowed values of the mixing angles are primarily constrained by the Higgs boson signal strengths with stronger constraints in the type-II model, see also [112].

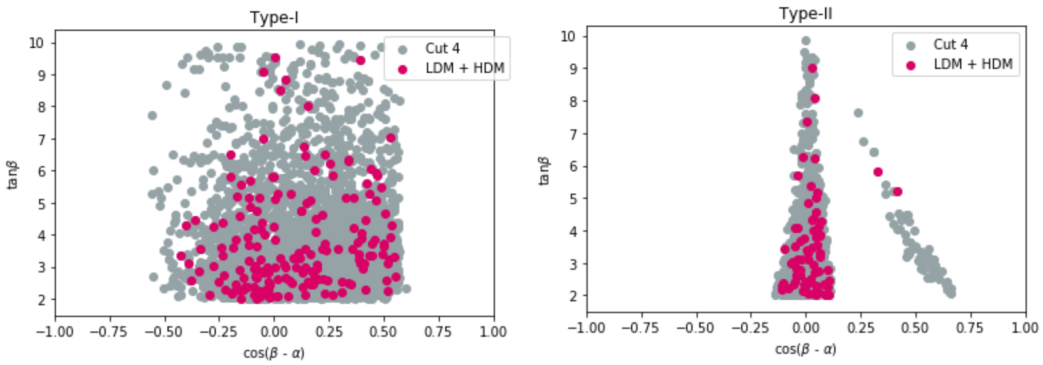

Figure 2.3: Parameter space points in the $\cos(\beta-\alpha)$-$\tan\beta$. All points survived the parameter scan while the pink dots are also compliant with Planck lower limit. Image from [72].

The effects of improved sensitivity of direct detection experiments, e.g. LZ collaboration [113], were also explored. Shown in figure 2.4 are the parameter space points, colored brown, that fall into LDM and HDM and superimposed, color green, are points that survive after imposing the improved LZ upper limits in the $m_\chi - \lambda_{abc}$ plane. The parameter space would be dramatically squeezed into fine tuned regions with $|\lambda_{abc}| \leq 5\times10^{-4}$ (corresponding to $|m_\eta - m_\chi| \leq 0.1$ GeV) in LDM and $|\lambda_{abc}| \leq 0.02$ (corresponding to $|m_\eta - m_\chi| \leq 0.25$ GeV) in HDM.

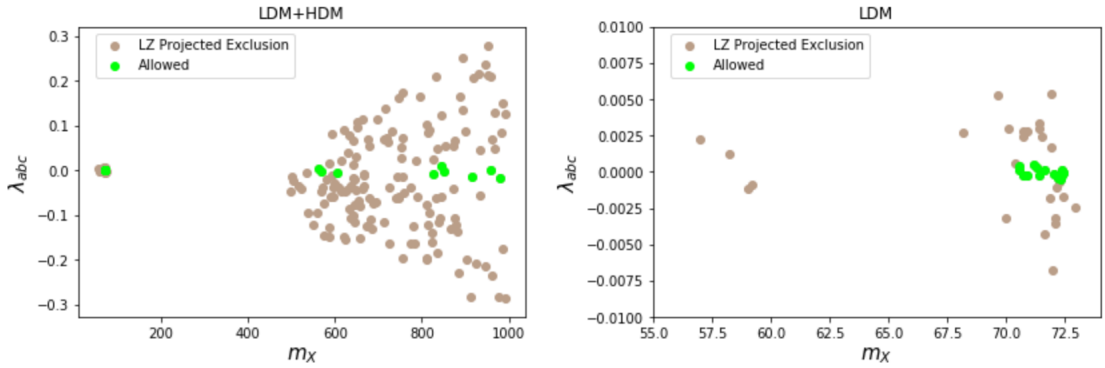

Figure 2.4: LDM+HDM (left) and LDM (right) regions where points colored brown would be excluded by LZ projected upper limits while points colored green would still be allowed. Image from [72].

The I(1+2)HDM serves as a simple extension of the IDM and thus results in the latter can be used as a guidance. For example, indirect detection constraints, e.g. from DM annihilation in the galaxy halo, searched by AMS-02 or Fermi-LAT are much weaker than the LHC and direct detection constraints above, see Refs. [37, 114]. Therefore the constraints coming from indirect detection experiments were not considered.

2.4.2.3 Collider Constraints

The particle nature of the DM candidate in this model can also be tested at particle colliders. Since DM interacts weakly and escapes detection one can look for processes with missing energy in the final state. The predictions for mono object signals plus missing transverse energy were tested against LHC data. In particular production cross sections for proton-proton collisions with 13 TeV center of mass energy were calculated for final states with a jet, a Z boson and a Higgs boson.

It was found that the strongest effect come from the mono-jet process $pp \to j\chi\chi$ with a cross section of about a few pb for DM mass in the range $50 \leq m_\chi \leq 70$ GeV. These predictions were assessed against LHC data using the CheckMATE 2 [115–121] software package. A grid search for different benchmark points in the plane of λ_{abc} and m_χ in the range $1 \leq \lambda_{abc} \leq 5$ and $50 \leq m_\chi \leq 100$ GeV were implemented . For each point in the

grid partonic events using CalcHEP [122] were generated.

Parton showering and hadronization using Pythia 8 [121] was performed within CheckMATE 2. The program then performs a fast detector simulation using DELPHES 3 [116]. All points in the grid were found to be allowed at 95% CL with the most sensitive analysis given in Ref. [123] which corresponds to an ATLAS search for DM using 36.1 fb^{-1} of data at 13 TeV center of mass energy.

This implies that, using mono-jet final states, current LHC data or at least the analyses currently implemented within CheckMATE 2 cannot rule out the I(1+2)HDM even for maximal values of λ_{abc} allowed by theoretical and experimental constraints. The LDM and HDM regions are trivially allowed as they lead to very small cross sections either due to very small λ_{abc} in LDM or very high mass in HDM. This effect can be better appreciated in figure 2.4 (left) where the region in the λ_{abc}, m_χ plane is shown. On the right of that figure the zoomed LDM region is shown where the points colored brown are excluded by the projected bounds from LZ collaboration.

These results agree with those of the IDM, see Ref. [79]. In that reference the authors obtained upper limits for current and projected luminosities by doing a shape analysis of the missing transverse momentum distribution. Only by combining the final states $j\chi\chi + j\chi\chi_a$ for small mass separation $m_{\chi_a} = m_\chi + 1$ GeV, they found that DM masses very close to the Higgs threshold $m_h/2$ could be excluded with 30 fb^{-1} of integrated luminosity. Further with 3000 fb^{-1} all the region with $m_\chi < m_h/2$ could be excluded for maximal Higgs-DM coupling.

The I(1+2)HDM stands as a simple extension of the IDM with more parameters that can weaken the limits coming from mono-jet searches at the LHC.

2.5 Conclusions

This chapter has been devoted to study extensions of the electroweak sector with three Higgs doublets. We have presented to concrete examples where the imposition of appro-

priate discrete Z_2 symmetries allows one to explain hints of new physics signals or account for the DM relic density of our universe.

In section 2.4.1 our lepton specific 3HDM of Ref. [71] was discussed. This model can accommodate the hinted lepton flavor violating signal $h \to \mu\tau$ while remaining consistent with the most stringent FCNC constraints in the quark sector. The phenomenology of the charged scalar was studied taking into account the constraints from B decays. The most remarkable prediction of this scenario is the significant branching fraction of the charged Higgs into $\mu\nu_\tau$ without needing large mixing angles that could jeopardize unitarity. No significant experimental upper limit on this process is known to date but the disappearing $h \to \mu\tau$ signal puts this model in to the ruled out list.

The inert 3HDM that we implemented in Ref. [72] was explored in section 2.4.2. A study of its parameter space taking into account theoretical and experimental constraints was performed. The model has a viable DM candidate that can account for the relic density for two regions of the DM mass. There is a low mass region we called LDM with $m_\chi \in [57, 73]$ GeV and a high mass region HDM with $m_\chi \in [500, 1000]$ GeV. For a given value of m_χ, the Higgs coupling to DM is controlled by the inert sector mass squared parameter as shown in equation 2.28.

The maximum deviation from the alignment limit in LDM and HDM regions was found to be in agreement with the overall shape of the parameter space of mixing angles of type-I and type-II models [112]. This demonstrates that relic density constraints are only dependent on the quartic λ_{abc} as is evident from figure 2.3.

Predictions of the model for mono-jet, mono Z and mono Higgs final states have been studied. For well motivated benchmarks it has been shown that the most competitive signal is given by $pp \to j\chi\chi$ with cross sections of about $\mathcal{O}(1)$ pb for DM mass in the range $50 < m_\chi < 70$ GeV and a Higgs DM interaction of about $\lambda_{abc} \approx 0.2$. The model has been tested using CheckMATE 2 and it was found allowed at 95 % CL by the LHC analyses implemented in this package.

It was shown that searches for DM at the LHC in final states with a jet offer a difficult

way to test this model however future direct detection experiments will be able to challenge this scenario as a model that can account for all the DM in the universe. As is the case in the IDM, the current LHC bounds on mono-particle processes are not sufficient to test the model, but the HL-LHC will, after 3000 fb^{-1}, be able to probe a substantial part of the parameter space.

Chapter 3

The Randall-Sundrum Model

3.1 Introduction

As we discussed in the first chapter of this thesis, the mass of the SM Higgs boson suffers a hierarchy problem with respect to the UV cutoff of the theory, usually taken to be the scale at which quantum gravity effects become relevent, i.e. the Planck scale $M_{\rm Pl} = 10^{19}$ GeV. The fact that the mass parameter of the Higgs potential is not technically natural demonstrates that its experimental value is in gross violation with our naturalness expectations.

Randall and Sundrum [124] (RS) proposed a solution to the hierarchy problem in which the cutoff of the theory is lowered down to the electroweak scale, making the hierarchy problem vanish. They considered an extra dimensional scenario with the extra dimension being spatial in nature and compactified into a S_1/Z_2 orbifold. The size of the extra dimension is finite $y_c = \pi r_c$ and at its boundaries there are 4D slices, also called "3-branes". The brane at $y = y_c$ is called the TeV-brane or IR-brane and the brane at $y = 0$ is usually called the UV- or Planck brane. A fine tuning is required between the negative $5D$ cosmological constant and the brane tensions in order to achieve a static flat solution which corresponds to a vanishing effective $4D$ cosmological constant. This fine tuning is not related to the electroweak hierarchy problem and is merely the same fine tuning that

one has to accept regarding the cosmological constant.

The solution to Einstein equations gives the $5D$ bulk metric

$$ds^2 = e^{-2A}\eta_{\mu\nu}dx^\mu dx^\nu - dy^2, \tag{3.1}$$

where $A = k|y|$ is the warp factor and k is the curvature scale. This solution corresponds to a slice of anti-de-Sitter (AdS_5) space between the two branes.

In this scenario the electroweak scale is generated from the fundamental scale by an exponential hierarchy, which is induced by the background metric. To see more explicitly how the weak scale can be generated without fine tuning lets consider the model in its original incarnation and take the Higgs field to be embedded in the visible brane. We can write its action

$$S_{vis} \supset \int d^4x\sqrt{|g_{vis}|}\{g^{\mu\nu}_{vis}D_\mu H^\dagger D_\nu H - \lambda(|H|^2 - v_0^2)^2\}, \tag{3.2}$$

where the metric corresponds to the visible brane, i.e. $g^{vis}_{\mu\nu} = e^{-2ky_c}\eta_{\mu\nu}$ and the Higgs vev is of order the fundamental scale $v_0 \sim M_{\rm Pl}$. By substituting this form of the metric into the action above one obtains

$$S_{vis} \supset \int d^4x e^{-4ky_c}\{\eta^{\mu\nu}e^{2ky_c}D_\mu H^\dagger D_\nu H - \lambda(|H|^2 - v_0^2)^2\}, \tag{3.3}$$

Performing a canonical normalization $H \to e^{ky_c}H$, we obtain

$$S_{eff} \supset \int d^4x\{\eta^{\mu\nu}D_\mu H^\dagger D_\nu H - \lambda(|H|^2 - e^{-2ky_c}v_0^2)^2\}. \tag{3.4}$$

From this expression we notice that the symmetry breaking scale is fixed by

$$v \equiv e^{-ky_c}v_0. \tag{3.5}$$

This result is completely general for any mass parameter located in the visible brane. It will be "warped" down by a geometric factor coming from the metric and which is exponential. Thus e.g. if we take $ky_c \approx 37$ the electroweak scale is generated without any fine tunings.

In the original RS model only gravity propagates in the bulk of the extra dimension [124, 125]. It was later shown [126–128] that allowing the SM fermions and gauge bosons to propagate in the bulk could offer a natural explanation of the flavor hierarchy.

3.1.1 The radion

For the background metric solution in the RS model, given by equation (3.1), any value of the radius dimension y_c is equally acceptable. Therefore a mechanism is needed to fix the value $y_c \sim 37/k$ so that the EW hierarchy is explained and this must be accomplished without severe fine tuning of parameters.

The original RS model has the theoretical shortcoming that the value of the brane separation, y_c, is not fixed by any dynamical mechanism and in the 4D effective field theory gives rise [129] to a massless scalar field. This scalar field, associated with fluctuations in the size of the extra dimension is called the radion or, by its ADS/CFT dual [130], the dilaton. A stabilization mechanism that gives mass to the radion was devised by Goldberger and Wise (GW) [131] by introducing a bulk scalar field with appropriate bulk and brane potentials. Taking the quartic interactions of the scalar on the brane to be large, the dynamics of this scalar generate an effective potential for the radion and the global minimum of the potential fixes the size of the extra dimension without fine tuning of the parameters.

In the GW mechanism the authors did not take into account the backreaction of the bulk scalar on the background geometry. A superpotential technique for generating solutions to the coupled scalar-gravity Einstein equations by choosing appropriate bulk and brane potentials was presented in [132]. This method has the advantage of reducing the coupled non-linear second order Einstein equations to simple ordinary differential equations for a simple choice of superpotential. The backreaction of the background metric

due to the scalar can be solved directly using this method. A full account of these effects together with a perturbative calculation for the radion mass and couplings is given in the paper of Csaki et al. [133]. Here we will only present the most relevant results while we reserve the superpotential method for the next section.

After the extra dimension is stabilized the radion field arises from the scalar fluctuations of the metric given by the general ansatz [133, 134]

$$ds^2 = e^{-2A-2F(x,y)}\eta_{\mu\nu}dx^\mu dx^\nu - (1+G(x,y))^2 dy^2, \tag{3.6}$$

and since the background VEV for the bulk scalar also depends on the extra dimension one also has to include the fluctuations in the GW scalar namely: $\phi(x,y) = \phi_0(y) + \varphi(x,y)$ where ϕ_0 is the background VEV and φ denotes the fluctuation. By evaluating the linearized Einstein equations one is able to derive $G = 2F$. To solve the system one linearizes the Einstein and scalar field equations to obtain coupled relations for φ and F. In particular, by integrating the $(\mu, 5)$ component of the linearized Einstein equations $\delta R_{\mu 5} = \kappa^2 \delta T_{\mu 5}$ with $\kappa^2 = 1/2M^3$, one obtains

$$\phi_0' \varphi = \frac{3}{\kappa^2}(F' - 2A'F) \tag{3.7}$$

where the prime indicates d/dy and this equation implies that the fluctuations φ and F will have the same KK eigenstates but with different profiles. Using the Einstein equations together with (3.7) a single differential equation in the bulk for F can be obtained [133]:

$$F'' - 2A'F' - 4A''F - 2\frac{\phi_0''}{\phi_0'}F' + 4A'\frac{\phi_0''}{\phi_0'}F = e^{2A}\Box F \tag{3.8}$$

supplemented by the boundary conditions

$$(F' - 2A'F)|_{y=0,y_c} = 0, \tag{3.9}$$

where the boundary conditions are simplified in the limit of stiff boundary potentials of the bulk stabilizer $\partial^2 V_i/\partial\phi^2 \gg 1$ implying $\varphi|_{y=y_i} = 0$. In the system there are two integration constants and one mass eigenvalue $\Box F_n(x,y) = -m_n^2 F_n(x,y)$. One integration constant corresponds to an overall normalization while the other constant and the mass eigenvalue are determined by the boundary conditions. In Ref [133] this differential equation was solved in a perturbative approach in the limit of small backreaction of the metric due to the stabilizing scalar, and it was found to zero-order in the backreaction that the KK zero-mode can be approximated by

$$F_0(x,y) \approx e^{2k|y|} R(x) + \mathcal{O}(l^2), \tag{3.10}$$

where $R(x)$ is the radion field. Using the boundary conditions the radion mass is [133]

$$m_r \approx 0.1 \; l \; k e^{-ky_c} \tag{3.11}$$

where $l^2 \equiv \phi_P^2/4M^3$ is the backreaction and ϕ_P is the VEV of the bulk stabilizer field on the Planck brane. It should be noted that generically, the radion mass is always proportional to the backreaction independently of the stabilization mechanism. From the expression above, the radion mass is expected to be of $\mathcal{O}$(TeV) scale. The canonical normalization of the radion comes from integrating out the extra dimension in the Einstein-Hilbert action

$$M^3 \int dy \sqrt{g} \mathcal{R}(\bar{g}) \supseteq \frac{6M^3}{k} e^{2ky_c} (\partial_\mu R(x))^2 \tag{3.12}$$

therefore a canonically normalized radion is obtained by writing

$$R(x) = r(x) \frac{e^{-ky_c}}{\sqrt{6} M_{Pl}}. \tag{3.13}$$

It is explicitly proved in [133] that the normalization is dominated by the gravitational contribution coming from the Einstein-Hilbert action against that coming from the kinetic

term of the bulk stabilizer.

3.2 Bulk Higgs Models

The scenario of a bulk Higgs was discussed in [135–137]. In those references the authors assumed that the $5D$ bulk Higgs was responsible for inducing EWSB by a constant VEV. This scenario required an extreme fine-tuning of parameters in order to generate $\mathcal{O}$(TeV) gauge boson masses, a problem that the RS model was purported to resolve. Thus it was concluded that the Higgs had to remain on the TeV brane in order to avoid the hierarchy problem.

Later on, in Ref. [138], the authors did a careful treatment of EWSB by a $5D$ bulk Higgs and derived the conditions necessary for the appearance of a tachyonic zero-mode such that a realistic $4D$ picture of EWSB can be achieved. The Higgs KK zero-mode develops a non-trivial profile function and is no longer a constant. This is different from the two references above which assumed a constant VEV. The authors showed that no fine-tuning is necessary and provided a phenomenologically acceptable scenario of a universal extra dimension (UED). Models with a bulk Higgs have been studied extensively after that, see Ref. [139–144].

Several studies motivated by the question of whether the SM Higgs can be the GW radion of the RS model have appeared in the literature. In [145] the authors studied the profile function $\phi(y)$ of a bulk scalar field under general boundary conditions (BCs) and showed that a bulk scalar with non-zero Dirichlet BCs (D, D) on the branes and without brane potentials is equivalent to the GW mechanism and can therefore stabilize the radius. They concluded that a bulk SM Higgs cannot be the GW stabilizer unless one assumes unnaturally small values of its bulk mass, but that a Higgs triplet under the $SU(2)_R$ gauge group of the custodial model in [146] can provide stabilization.

It was later shown by Geller, Bar-Shalom and Soni (GBS) [147] that the GW mechanism, as it is, cannot be applied to an $SU(2)_L$ doublet stabilizer since (D, D) BCs yield

a phenomenologically unacceptable value of the EW scale and therefore one has to adopt a different choice for applying the BCs. They showed that the condition $\phi(0) \ll M_{\rm Pl}$ necessary to generate the correct value of the EW scale does not add to the level of fine tuning already required in order to have a vanishing cosmological constant. They solved the coupled scalar-gravity system of equations by assuming a small backreaction of the $SU(2)_L$ doublet stabilizer on the metric. In [148] a complete account of the backreaction was calculated using the superpotential method of Ref. [132]. A similar calculation was presented in [149].

In Ref. [150] it was argued that the stabilization of the extra dimension by a bulk Higgs is possible, provided the $5D$ bulk mass satisfies the Breitenlohner-Freedman bound, which corresponds to $m^2 = -4k^2$. And as we will see this is consistent with the GBS condition $\nu \sim 1$. In this reference the author provides a qualitative analysis of the stabilization mechanism from the CFT side of the correspondence.

The work of GBS provided an alternative to the GW mechanism. They considered a bulk doublet, with different boundary conditions than GW, and showed that this single doublet could both stabilize the extra dimension and break the electroweak symmetry. Thus, in this model the Higgs and radion are one and the same (which they refer to as a "Higgs-radion"). Since the couplings of the radion to gluons and photons are enhanced, one has the couplings of the Higgs to gluons and photons enhanced. At that time of their work, not only were these enhancements phenomenologically acceptable, but there did appear to be an enhancement in the diphoton decay of the Higgs.

In Ref. [151] we showed that most current LHC data on the Higgs boson couplings rule out the GBS model as it is. Thus they considered a version in which fermions are allowed to propagate in the bulk and found that for any choice of parameters, the model remains in conflict with experimental results. They also consider a substantial expansion of the parameter-space by looking at a Two Higgs Doublet Model, and find that the model will contain a physical, zero-mass scalar, which is phenomenologically excluded. The presence of such zero modes in multiple bulk scalar models had previously been demonstrated for

soft-wall models by George [152], but it appears that the result applies to GBS-type models as well. Thus, it appears that the attractive idea of having the same field responsible for radius stabilization and electroweak symmetry breaking appears to be excluded

In the following subsections we will look at more detail into our paper [151] by presenting the GBS model and the extensions implemented in that reference.

3.2.1 Higgs-radion Unification

In the model of Geller, Bar-Shalom and Soni [147], the possibility of a bulk scalar $SU(2)_L$ doublet which can stabilize the radius of the warped RS model and provide the source of electroweak symmetry breaking leading to a unified Higgs-radion state was presented. This Higgs-radion serves as an intriguing alternative to the usual radius stabilization via the GW mechanism. However, as we will see, some of the phenomenological signatures predicted by this model are now at odds with recent LHC data, particularly the combined ATLAS and CMS measurement [153, 154] of $BR(H_{\rm SM} \to \gamma\gamma)/BR(H_{\rm SM} \to ZZ)$.

The model is the standard RS framework with two branes located at the orbifold fixed points $y = 0$ and $y = y_c$. The $5D$ metric is

$$ds^2 = e^{-2A}\eta_{\mu\nu}dx^\mu dx^\nu - dy^2, \tag{3.14}$$

where A is a function of the extra dimension that is determined by solving Einstein equations. As in the GW mechanism, the bulk scalar has both a bulk potential and potentials sourced on each of the two branes. The actions of the bulk-brane system are,

$$S_{\rm Bulk} = \frac{1}{2}\int d^4x \int dy\sqrt{g}\left(g^{MN}\partial_M\Phi\partial_N\Phi - V(\Phi) + 6\frac{k^2}{\kappa^2}\right), \tag{3.15}$$

$$S_{\rm Brane} = -\int d^4x\sqrt{g_4}\; V_i^{\rm Brane}(\Phi), \tag{3.16}$$

where

$$V(\Phi) = m^2\Phi^2, \tag{3.17}$$

$$V_i^{\text{Brane}}(\Phi) = \lambda_i \Phi^4 + m_i^2 \Phi^2 + \Lambda_i, \tag{3.18}$$

$$\kappa^2 = \frac{1}{2M^3}. \tag{3.19}$$

Here the subscript i =Planck, TeV is used to denote each of the two branes, g^{MN} represents the $5D$ metric tensor and $g_i^{\mu\nu}$ are the induced metrics on each brane. From the Einstein and Euler-Lagrange equations one obtains the following

$$4A'^2 - A'' = 4k^2 - \frac{2\kappa^2}{3} V(\phi_0) - \frac{\kappa^2}{3} V_i^{\text{Brane}}(\phi_0)\delta(y - y_i), \tag{3.20}$$

$$A'^2 = k^2 + \frac{\kappa^2 \phi_0'^2}{12} - \frac{\kappa^2}{6} V(\phi_0), \tag{3.21}$$

$$\phi_0'' = 4A'\phi_0' + \frac{\partial V(\phi_0)}{\partial \phi_0} + \frac{\partial V_i^{\text{Brane}}(\phi_0)}{\partial \phi_0}\delta(y - y_i), \tag{3.22}$$

where primes denote derivatives with respect to y and it is assumed that VEV profile of the bulk field depends only on the extra dimension. By matching the singular terms in the previous equations, the following boundary conditions may be obtained:

$$[A']_i = \frac{\kappa^2}{3} V_i^{\text{Brane}}(\phi_0), \quad [\phi_0']_i = \frac{\partial V_i^{\text{Brane}}(\phi_0)}{\partial \phi_0}. \tag{3.23}$$

There are three relevant integration constants in this set of equations, two for ϕ_0 and one for A. However the constant in A is completely irrelevant by scale invariance of the metric. The last constant is the separation between the branes y_c. With the four boundary conditions above one can determine three of the integration constant leaving one of the conditions to be tuned. This fine-tuning is the inescapable one due to the cosmological constant. In the GBS model the authors considered the small backreaction ($l^2 \ll 1$) approximation, such that $A = ky + \mathcal{O}(l^2)$ and the Euler-Lagrange equations for the background VEV simplifify to

$$\phi_0'' = 4k\phi_0' + \frac{\partial V(\phi_0)}{\phi_0}, \tag{3.24}$$

which has the most general solution

$$\phi_0 = e^{2k(y-y_c)}\left(C_1 e^{\nu k(y-yc)} + C_2 e^{-\nu k(y-y_c)}\right), \tag{3.25}$$

where $\nu = \sqrt{4 + m^2/k^2}$, similar to the GW mechanism and C_1 and C_2 are integration constants. If one is going to identify the bulk doublet with a $5D$ Higgs field that is responsible for EWSB and to give the electroweak gauge bosons their masses one has to impose that the effective $4D$ VEV, given by

$$v_{eff}^2 = \int dy\ \phi_0^2\ e^{-2A}, \tag{3.26}$$

is of order the EW scale. This implies that one must tune the value of the Higgs profile at the Planck brane to be $\phi_0(0) \ll M_{\rm Pl}^{3/2}$. One can achieve this by requiring $\nu < 1$ so that $\phi_0 \approx C_2 e^{(2-\nu)k(y-y_c)}$ is near the Planck brane leading to a small value as desired. This is one of the key differences from the GW scenario where $\nu \sim 2$ giving order Planck values for the VEV on both branes which, as was argued, cannot work for a $SU(2)_L$ stabilizer. The condition $\nu < 1$ implies $m^2 \approx -4k^2$ which corresponds to the Breitenlohner-Freedman bound, consistent with Ref. [150]. The condition $\phi_0(0) \ll M_{\rm Pl}^{3/2}$ forces one to choose different boundary conditions from those used in the GW stabilization. In this case one chooses the two conditions in (3.23) for the values of ϕ_0' at the two branes, together with the condition of the value of A' at the TeV brane to solve for C_1, C_2 and y_c. No additional fine tunings, beyond that needed to fine-tune the cosmological constant, have been introduced to stabilize the extra dimension.

Once the solutions for the background equations are found one has to consider the scalar perturbations of the metric and the bulk doublet and solve the linearized Einstein equations to find the spectrum of physical fields. These perturbations are parametrized as [134]

$$\Phi_i(x,y) = \begin{pmatrix} 0 \\ \phi_0(y) + \varphi(x,y) \end{pmatrix}, \tag{3.27}$$

$$ds^2 = e^{-2A-2F(x,y)}\eta_{\mu\nu}dx^\mu dx^\nu - (1+2F(x,y))^2 dy^2. \tag{3.28}$$

and the linearized Einstein equations are given [133]

$$F'' - 2A'F' - 4A''F - 2\frac{\phi_0''}{\phi_0'}F' + 4A'\frac{\phi_0''}{\phi_0'}F = e^{2A}\Box F, \tag{3.29}$$

$$\phi_0'\varphi = \frac{3}{\kappa^2}\left(F' - 2A'F\right), \tag{3.30}$$

where the second equations imply that the scalar perturbations can be KK decomposed as

$$\varphi(x,y) = \sum \varphi_n(y)h_n(x)\ , \tag{3.31}$$

$$F(x,y) = \sum F_n(y)h_n(x)\ . \tag{3.32}$$

The boundary conditions are given by

$$\left[\varphi'\right]_i = \frac{\partial^2 V_i^{Brane}(\phi_0)}{\partial\phi^2}\varphi + 2\frac{\partial V_i^{Brane}(\phi_0)}{\partial\phi}F\ , \tag{3.33}$$

and the stiff boundary potential assumption cannot be made here. This is different from the GW case where one takes the quartic coupling to be infinitely large in order to simplify the boundary conditions. The resulting mass and effective VEV of the so called "Higgs-radion" field were found to be given to the lowest order in the backreaction by

$$m_{h_r}^2 = l^2\frac{52k^2}{15ky_c}e^{2ky_c}, \tag{3.34}$$

$$v_{eff}^2 = l^2\frac{2}{5k\kappa^2}e^{2ky_c}. \tag{3.35}$$

The solutions for the scalar fluctuations can be written in terms of the canonically nor-

malized Higgs-radion field and to the lowest order are

$$F(x,y) = h_r \frac{e^{2k(y-y_c)}}{\Lambda_r} , \tag{3.36}$$

$$\varphi(x,y) \approx h_r \frac{1}{\Lambda_r e^{2ky_c}} \left(2\sqrt{5} e^{4ky} \sqrt{\frac{1}{\kappa^2}} - \frac{13 e^{2ky+2ky_c} \sqrt{\frac{1}{\kappa^2}} y}{\sqrt{5} y_c} \right) \ell , \tag{3.37}$$

$$l^2 \equiv \frac{1}{4} e^{-2(2-\nu)ky_c} \kappa^2 \phi_{TeV}^2 (20 - 4\nu - 3\nu^2) \tag{3.38}$$

where l^2 parametrizes the backreaction and $\Lambda_r \equiv \sqrt{6} M_{\rm Pl} e^{-ky_c}$ is the canonical normalization.

Another important parameter in the study of RS models with bulk gauge bosons is the KK scale defined to be the mass of the first excited state of the gauge bosons. This parameter is independent of the gauge symmetry and gauge couplings and is universal for all gauge bosons that satisfy the same BCs. In particular, for gauge bosons satisfying Neumann BCs at both branes it is given by [155]

$$m_{KK} = 2.45 \frac{k}{\sqrt{6} M_{Pl}} \Lambda_r, \tag{3.39}$$

so any bound on the KK scale will directly affect the allowed values of the curvature scale k and Λ.

Since the Higgs-radion field arises from the massive zero mode of both the metric and scalar perturbations, its couplings to the SM matter fields are different from those of the GW pure radion state. Thus one has to add the contributions coming from the $5D$ Higgs couplings to those coming from the conformal couplings of the radion. In paticular, due to the trace anomaly, the radion has couplings to photons proportional to the QED beta function in addition to the usual momentum dependent effective couplings coming from fermions and the W gauge boson running around loops. The Higgs scalar only has the latter contributions. A table with the most relevant couplings is given in table 3.1. These couplings were calculated by GBS, we refer the reader to section IV of Ref. [147]. The

somewhat surprising perfect integers of 3 and 9 in the couplings to fermions and gauge bosons arise after expanding the Higgs kinetic term and integrating the product of profiles for the vev function and scalar perturbation. To lowest order in the backreaction, the gauge bosons have a constant profile $V_\mu(x,y) = 1/\sqrt{y_c}V_\mu^{(0)}(x)$, see Appendix A and its mass scales quadratically with the backreaction l, allowing us to express the coupling in terms of the gauge boson masses, as it is usually the case. Corrections to these formulas are order $\mathcal{O}(l^4)$ and will be neglected here.

	h_r Couplings
$h_r tt$	$4\frac{m_t}{\Lambda_r}$
$h_r \bar{f} f$ for $f \neq t$	$\frac{9m_f}{\Lambda_r}$
$h_r VV$	$-\frac{9m_V^2}{\Lambda_r}$
$h_r gg/\gamma\gamma$	$\frac{1}{\Lambda_r}\frac{\beta_{QCD/QED}}{2g}$

Table 3.1: Couplings of h_r to gauge bosons and fermions

In the GBS model the top quark profile was assumed to be a delta function peaked at the TeV brane while the lighter fermions profiles were approximated to be flat. Setting the Higgs-radion mass to $m_{h_r} = 126$ GeV and using the three level couplings of table 3.1, the branching fractions to different decay channels may be calculated, see their Table II in [147] where they compared with the SM Higgs values.

The most significant differences between the Higgs-radion and the SM Higgs come from the branching fractions to photons and gluons. Recent ATLAS measurements of the Higgs production and decay modes at 80 fb^{-1} of luminosity [154], obtained $BR(H \to \gamma\gamma)/BR(H \to ZZ) = 0.076^{+0.013}_{-0.011}$ for which the corresponding values in Table II in [147] yield the ratio $BR(h_r \to \gamma\gamma)/BR(h_r \to ZZ) = 0.147$. However, as GBS mentioned, this is a leading order calculation that does not take into account the effects of summing over the one-loop contributions of the KK towers. In Ref. [140], the effect of including these corrections from the KK towers of fermions were investigated and it was shown that for a

low KK scale, $M_{KK} \approx 3.3$ TeV there is a sizable suppression in the $h \to \gamma\gamma$ decay width relative to the SM Higgs decay width, see their figure 8.

From fitting the Higgs-radion normalization Λ_r to the Higgs signal strengths data, the GBS authors found that the KK scale must lie in the range 4.48 TeV $< M_{KK} <$ 5.44 TeV. In Ref [140] the authors calculated the decay rate $H \to \gamma\gamma$ for a bulk Higgs including the corrections coming from the KK towers of fermions, charged scalars and gauge bosons. They found that the most significant deviation from the SM came from KK quarks and leptons effects unless one assumes unnaturally small values for the Yukawa couplings. As can be seen from their figure 8 (bottom-left) the deviations from the SM are less than 5% for Yukawa couplings $y = 1, 2$ in the range of KK scales that are allowed in the GBS model. Also in the same reference, it was found that the one-loop corrections from KK towers on $h \to WW^*$ would correspond to a less than 1% supression.

In the GBS model the Higgs-radion is expected to have significant deviation in its couplings to fermions relative to the bulk Higgs of Ref. [140] so that KK towers effects might be more pronounced. Even then it would be challenging to accommodate the Higgs branching fraction within experimental levels.

3.2.2 Bulk Fermions

In this section we relax the assumption made in the GBS paper that the light fermions have a constant profile along the extra dimension and we will find the parameter space of the fermion bulk mass parameters $c = m/k$ that reproduce the flavor mass hierarchies. The hope would be that the expanded parameter space might allow a viable model.

For simplicity we present the results for the quarks only. A similar analysis can be carried out for leptons. The $5D$ Yukawa interactions are given by

$$S_{\text{Yukawa}} = -\int d^5x\sqrt{g}\left[y^{(5)}_{u_{ij}}\bar{Q}^i\tilde{\Phi}\ u^j + y^{(5)}_{d_{ij}}\bar{Q}^i\Phi\ d^j + h.c.\right] \tag{3.40}$$

where the $y^{(5)}_{ij}$ are the Yukawa parameters and have mass dimenion $-1/2$. The fermion

masses and interactions of the Higgs-radion h_r are found by expanding the doublet as in equation (3.27), where the VEV profile is given by [147]

$$\phi_0(y) = \phi_{TeV} e^{(2-\nu)k(y-y_c)}. \tag{3.41}$$

Since fermions propagate in the bulk, the 5D Yukawa couplings can give rise to mixing between different modes and could lead to potentially dangerous FCNC's mediated by the Higgs-radion or its higher dimensional excitations. These effects can impose tight lower bounds on the KK scale [127,157]. However we will show below that these constraints will not be necessary for our purposes and we will assume diagonal 5D Yukawa couplings.

The fermion masses are given by the integral expression

$$m_{u/d} = y^{(5)}_{u/d} \int_0^{y_c} \phi_0(y) \chi^{(0)}_Q(y) \chi^{(0)}_{u/d}(y) dy \tag{3.42}$$

where the zero-mode profiles where derived in Ref. [126] (see also appendix B for a short review), to be

$$\chi^{(0)}_Q(y) = \chi^{(0)}_Q(0) e^{m_Q y}, \quad \chi^{(0)}_u(y) = \chi^{(0)}_u(0) e^{-m_u y} \tag{3.43}$$

with normalization $\int_0^{y_c} dy e^{\sigma} \chi^{(m)}_\psi(y) \chi^{(n)}_\psi(y) = \delta_{mn}$ and we assumed the Yukawa constants are diagonal. The fermion masses are then given by

$$m_{u,d} = y^{(5)}_{u,d}\ \phi_{TeV} e^{-(2-\nu)ky_c} \left\{ \frac{(1+2c^i_L)}{(e^{ky_c(1+2c^i_L)}-1)} \frac{(1-2c^{u,d}_R)}{(e^{ky_c(1-2c^{u,d}_R)}-1)} \right\}^{1/2} \frac{e^{Aky_c}-1}{A} \tag{3.44}$$

where we defined A and the bulk mass parameters as

$$A \equiv 2 - \nu + c^i_L - c^{u,d}_R, \quad c^i_L \equiv \frac{m_{Q_i}}{k}, \quad c^{u,d}_R \equiv \frac{m_{u,d}}{k}. \tag{3.45}$$

From the requirement of $v_{\text{eff}} \approx 246$ GeV and assuming natural values for the Yukawa constants it is straightforward to find $y^{(5)}\phi_{TeV} = \sqrt{k/M_{\text{Pl}}}\ v_{\text{eff}} e^{ky_c}$. The relation $k/M_{\text{Pl}} \approx 1.6$ is fixed by the ratio of the Higgs-radion mass to its VEV. Also the stabilization of the

extra dimension is obtained when $\frac{1}{2\nu} \sim 37$, thus we can neglect the parameter ν above. Note that for each generation, there are three mass parameters (c_Q, c_u, c_d) and two masses leaving more flexibility in studying the phenomenology. The mass hierarchy of the quark sector can be explained by the profile values given in the table 3.2, although other choices are also viable.

	c_L^i	$c_R^{u_i}$	$c_R^{d_i}$
$i=1$	-0.51	0.77	0.74
$i=2$	0.63	0.62	0.7
$i=3$	0.53	0.03	0.58

Table 3.2: A set of bulk mass parameters that reproduces the quark spectrum. Since each generation has three parameters and two masses, many other choices can be made. The predictions made in this section are only weakly sensitive to the specific choices; we have scanned the entire set of parameters and our conclusion in this section are unaffected.

Similarly the Yukawa couplings of the Higgs-radion are given by

$$y_u^{(4)} = y_u^{(5)} \int_0^{y_c} dy \chi_u^{(0)}(y) \chi_Q^{(0)}(y) \varphi_0(y), \tag{3.46}$$

where the expression for $\varphi_0(y)$ was presented in (3.37). After evaluating the integral the Yukawa Lagrangian is

$$-\mathcal{L}_{\text{Yukawa}} = \frac{h_r}{\Lambda_r} \left(\tilde{y}_Y m_f \bar{f}_L f_R + (KK, n > 0) \right). \tag{3.47}$$

To this couplings we have to add the gravitational contribution coming from the scalar perturbation of the metric. One finds

$$-\mathcal{L}_{\text{Metric}} = -\frac{h_r}{\Lambda_r} \left(\tilde{y}_G m_f \bar{f}_L f_R + (KK, n > 0) \right). \tag{3.48}$$

and the numerical factors multiplying the masses are given in terms of the bulk mass

parameters by

$$\tilde{y}_Y = \frac{ky_cA}{e^{ky_cA}-1}\left\{\frac{10}{ky_c}\frac{e^{ky_cA}-e^{-2ky_c}}{(2+A)} - 13\frac{e^{ky_cA}(ky_cA-1)+1}{(ky_cA)^2}\right\}, \tag{3.49}$$

$$\tilde{y}_G = \left[2e^{-2ky_c}\frac{e^{(2+A)ky_c}-1}{2+A}\frac{A}{e^{Aky_c}-1}\right]. \tag{3.50}$$

The overall couplings to fermions and massive gauge bosons can be written in the following Lagrangian density

$$\mathcal{L} = \frac{h_r}{\Lambda_r}\left(-\sum_f(\tilde{y}_Y-\tilde{y}_G)m_f\bar{f}f - 9m_V^2V_\mu V^\mu\right), \tag{3.51}$$

where the sum is over quarks and leptons and $V_\mu V^\mu = 2W^+_\mu W^{\mu-}, Z_\mu Z^\mu$.

The couplings of the Higgs radion to the massless gauge bosons is zero at tree level, however, there is a loop contribution coming from the trace anomaly term

$$T^\mu_\mu = \sum_a \frac{\beta_a(g_a)}{2g_a}F^a_{\mu\nu}F^{a\mu\nu}. \tag{3.52}$$

The list of branching ratios for both the SM Higgs and the Higgs radion are given in table 3.3 where we set $\Lambda_r = 4$ TeV

$BR(h_r \to XX)$	SM $m_h = 126$ GeV	Higgs radion ($m_{h_r} = 126$GeV)
WW^*	0.231	0.207
ZZ^*	0.0289	0.0260
gg	0.0848	0.183
$\gamma\gamma$	2.28×10^{-3}	2.47×10^{-3}
$b\bar{b}$	0.561	0.501
$\tau\bar{\tau}$	0.0615	0.054
$c\bar{c}$	0.0283	0.024
Total width (GeV)	4.21×10^{-3}	1.36×10^{-3}

Table 3.3: Branching fractions to different decay channels of the SM Higgs boson and the Higgs-radion. The values of the c parameters corresponds to those in table 3.2.

From table 3.3 we can see that the predictions for the Higgs-radion branching fractions

lie very close to the SM Higgs boson expectation. We scanned the parameter space of the bulk mass parameters $c = m/k$ and checked that the ratios $\frac{BR(h_r \to \gamma\gamma)}{BR(h_r \to ZZ)}$, $\frac{BR(h_r \to WW)}{BR(h_r \to ZZ)}$, $\frac{BR(h_r \to \tau\tau)}{BR(h_r \to ZZ)}$ and $\frac{BR(h_r \to bb)}{BR(h_r \to ZZ)}$ are within at least 2σ of the experimentally allowed region presented by the CMS and ATLAS collaborations [153, 154].

The fact that the radion has a narrow width allows us to correlate its production cross section with the partial width [158] and simply rescale by the SM Higgs cross section, i.e., $\sigma(gg \to h_r)\Gamma(H_{SM} \to gg) = \sigma(gg \to H_{SM})\Gamma(h_r \to gg)$. The effects of both the trace anomaly and the top quark loop were included in the partial width calculation. The formula for the $h_r \to gg$ decay rate is quoted in the GBS paper. We just inserted the appropriate quark and gauge boson couplings.

The prediction for the production cross section via gluon-gluon fusion (ggF) of a Higgs-radion gives

$$\sigma(gg \to h_r) \geq 140 \text{ pb} \tag{3.53}$$

for a bulk mass parameter in the region $-2 \leq c_L^3 \leq 2$ (we determine c_R^t and c_R^b by the quark masses) which is more than 5 σ away from the measured central value $\sigma_{ggF} = 47.8 \pm 4.0$ pb [154]. We do not consider higher absolute values of the bulk mass parameters as they would appear unnatural.

The reason why such a large production cross section was obtained is that the top Yukawa coupling, presented as $\tilde{y}_Y - \tilde{y}_G$ in eq. (3.51) of the Higgs-radion is more than 5 times the top Yukawa coupling of the SM Higgs boson for the range $-2 \leq c_L^3 \leq 2$ and its contribution adds constructively with that from the trace anomaly. The model, within this bulk mass parameter range is phenomenologically excluded.

3.2.3 2HDM in the bulk

In this section we will extend the GBS scenario by adding an extra Higgs doublet in the bulk. The spacetime configuration is the same as in section 3.2.1, with the metric given by equation (3.14). The action contains two scalar doublets coupled with gravity and $5D$

bulk and brane potentials. It can be written generically as

$$S = \int d^5x\sqrt{g}\left(-M^3R + \frac{1}{2}g^{MN}D_M\Phi_i^\dagger D_N\Phi_i - V(\Phi_1,\Phi_2)\right) - \sum_{i=UV,IR}\int d^4x\sqrt{g_4}\,\lambda_i(\Phi_1,\Phi_2), \tag{3.54}$$

with g is the determinant of the $5D$ metric, M is the cutoff of the theory and R is the Ricci scalar and where D_M is the covariant derivative containing the gauge fields.

The radius stabilization by a Higgs doublet has been done in [147, 149], here we will closely follow their calculations while taking care of the extra Higgs in the bulk. Electroweak symmetry breaking occurs when the Higgs doublets acquire y-dependent $5D$ VEVs

$$\Phi_1 = \begin{pmatrix} 0 \\ \phi_1(y) \end{pmatrix}, \quad \Phi_2 = \begin{pmatrix} 0 \\ \phi_2(y) \end{pmatrix}. \tag{3.55}$$

These VEV profiles together with the metric field $A(y)$ are determined by solving the Einstein equations

$$R_{MN} = \kappa^2\left(T_{MN} - \frac{1}{3}g_{MN}g^{AB}T_{AB}\right), \tag{3.56}$$

where $\kappa^2 = 1/2M^3$ is the $5D$ Newton constant. This set of equations together with the Euler-Lagrange equations for the doublets yield the following Higgs-gravity coupled equations [133]

$$4A'^2 - A'' = -\frac{2\kappa^2}{3}V(\phi_1,\phi_2) - \frac{\kappa^2}{3}\lambda_{Pl}(\phi_1,\phi_2)\delta(y) - \frac{\kappa^2}{3}\lambda_{IR}(\phi_1,\phi_2)\delta(y-y_c), \tag{3.57}$$

$$\phi_i'' = 4A'\phi_i' + \frac{\partial V(\phi_1,\phi_2)}{\partial\phi_i} + \frac{\partial\lambda_{UV}(\phi_1,\phi_2)}{\partial\phi_i}\delta(y) + \frac{\partial\lambda_{IR}(\phi_1,\phi_2)}{\partial\phi_i}\delta(y-y_c), \tag{3.58}$$

$$A'^2 = \frac{\kappa^2(\phi_1'^2+\phi_2'^2)}{12} - \frac{\kappa^2}{6}V(\phi_1,\phi_2). \tag{3.59}$$

Here primes denote derivative with respect to the extra dimension and the last equation is the zero-energy condition which, after differentiating with respect to y, automatically vanishes provided the other three equations are satisfied in the bulk. The boundary conditions

are obtained by matching the delta functions

$$A'\Big|_{y_i} = \pm\frac{\kappa^2}{6}\lambda_{UV,IR}(\phi_1,\phi_2)\Big|_{y_i}, \quad \phi_i'\Big|_{y_i} = \pm\frac{1}{2}\frac{\partial\lambda_{UV,IR}(\phi_1,\phi_2)}{\partial\phi_i}\Big|_{y_i} \tag{3.60}$$

with the + (−) sign for the UV (IR) boundary and orbifolding was taken into account. There is one more constraint coming from the generation of the correct gauge boson masses. Assuming the gauge boson zero modes are flat the effective VEV is given by

$$v_{eff}^2 = \int_0^{y_c} dy\,\left(\phi_1^2+\phi_2^2\right)e^{-2A}, \tag{3.61}$$

where $v_{eff} = 246$ GeV.

Now, we count the parameters and constraints. From the scalar-gravity coupled system, eqns. (3.65)-(3.67), we have 5 integration constants, namely $\phi_1(0)$, $\phi_1'(0)$, $\phi_2(0)$, $\phi_2'(0)$ and $A(0)$ and there is one additional parameter, the inter brane distance y_c. But $A(0)$ is an irrelevant additive constant that can be absorbed by rescaling of the metric and therefore we are left with an overall of 5 relevant parameters and 6 jump conditions. Thus we expect one of the boundary conditions to be fine tuned as is general in any RS-type model and this fine tuning is associated with a vanishing effective $4D$ cosmological constant. We shall discuss this counting of parameters and constraints again in the next section in the context of the superpotential generating solution.

In this section we will extend the GBS scenario by adding an extra Higgs doublet in the bulk. The spacetime configuration is the same as in section 3.2.1, with the metric given by equation (3.14). The action contains two scalar doublets coupled with gravity and $5D$ bulk and brane potentials. It can be written generically as

$$S = \int d^5x\sqrt{g}\left(-M^3R + \frac{1}{2}g^{MN}D_M\Phi_i^\dagger D_N\Phi_i - V(\Phi_1,\Phi_2)\right) - \sum_{i=UV,IR}\int d^4x\sqrt{g_4}\,\lambda_i(\Phi_1,\Phi_2), \tag{3.62}$$

with g is the determinant of the $5D$ metric, M is the cutoff of the theory and R is the

Ricci scalar and where D_M is the covariant derivative containing the gauge fields.

The radius stabilization by a Higgs doublet has been done in [147, 149], here we will closely follow their calculations while taking care of the extra Higgs in the bulk. Electroweak symmetry breaking occurs when the Higgs doublets acquire y-dependent $5D$ VEVs

$$\Phi_1 = \begin{pmatrix} 0 \\ \phi_1(y) \end{pmatrix}, \quad \Phi_2 = \begin{pmatrix} 0 \\ \phi_2(y) \end{pmatrix}. \tag{3.63}$$

These VEV profiles together with the metric field $A(y)$ are determined by solving the Einstein equations

$$R_{MN} = \kappa^2 \left(T_{MN} - \frac{1}{3} g_{MN} g^{AB} T_{AB} \right), \tag{3.64}$$

where $\kappa^2 = 1/2M^3$ is the $5D$ Newton constant. This set of equations together with the Euler-Lagrange equations for the doublets yield the following Higgs-gravity coupled equations [133]

$$4A'^2 - A'' = -\frac{2\kappa^2}{3} V(\phi_1, \phi_2) - \frac{\kappa^2}{3} \lambda_{Pl}(\phi_1, \phi_2)\delta(y) - \frac{\kappa^2}{3} \lambda_{IR}(\phi_1, \phi_2)\delta(y - y_c), \tag{3.65}$$

$$\phi_i'' = 4A'\phi_i' + \frac{\partial V(\phi_1, \phi_2)}{\partial \phi_i} + \frac{\partial \lambda_{UV}(\phi_1, \phi_2)}{\partial \phi_i}\delta(y) + \frac{\partial \lambda_{IR}(\phi_1, \phi_2)}{\partial \phi_i}\delta(y - y_c), \tag{3.66}$$

$$A'^2 = \frac{\kappa^2(\phi_1'^2 + \phi_2'^2)}{12} - \frac{\kappa^2}{6} V(\phi_1, \phi_2). \tag{3.67}$$

Here primes denote derivative with respect to the extra dimension and the last equation is the zero-energy condition which, after differentiating with respect to y, automatically vanishes provided the other three equations are satisfied in the bulk. The boundary conditions are obtained by matching the delta functions

$$A'\Big|_{y_i} = \pm \frac{\kappa^2}{6} \lambda_{UV,IR}(\phi_1, \phi_2)\Big|_{y_i}, \quad \phi_i'\Big|_{y_i} = \pm \frac{1}{2} \frac{\partial \lambda_{UV,IR}(\phi_1, \phi_2)}{\partial \phi_i}\Big|_{y_i} \tag{3.68}$$

with the $+$ $(-)$ sign for the UV (IR) boundary and orbifolding was taken into account. There is one more constraint coming from the generation of the correct gauge boson masses.

Assuming the gauge boson zero modes are flat the effective VEV is given by

$$v_{eff}^2 = \int_0^{y_c} dy \left(\phi_1^2 + \phi_2^2\right) e^{-2A}, \tag{3.69}$$

where $v_{eff} = 246$ GeV.

Now, we count the parameters and constraints. From the scalar-gravity coupled system, eqns. (3.65)-(3.67), we have 5 integration constants, namely $\phi_1(0)$, $\phi_1'(0)$, $\phi_2(0)$, $\phi_2'(0)$ and $A(0)$ and there is one additional parameter, the inter brane distance y_c. But $A(0)$ is an irrelevant additive constant that can be absorbed by rescaling of the metric and therefore we are left with an overall of 5 relevant parameters and 6 jump conditions. Thus we expect one of the boundary conditions to be fine tuned as is general in any RS-type model and this fine tuning is associated with a vanishing effective $4D$ cosmological constant. We shall discuss this counting of parameters and constraints again in the next section in the context of the superpotential generating solution.

3.2.3.1 Superpotential

The Einstein field equations (3.65)-(3.67) are automatically satisfied in the bulk if we express the potential in terms of a superpotential as

$$V(\phi_1, \phi_2) = \frac{1}{8}\left[\left(\frac{\partial W(\phi_1,\phi_2)}{\partial \phi_1}\right)^2 + \left(\frac{\partial W(\phi_1,\phi_2)}{\partial \phi_2}\right)^2\right] - \frac{\kappa^2}{6} W(\phi_1,\phi_2)^2, \tag{3.70}$$

provided we have

$$A' = \frac{\kappa^2}{6} W(\phi_1,\phi_2), \quad \phi_i' = \frac{1}{2}\frac{\partial W(\phi_1,\phi_2)}{\partial \phi_i} \tag{3.71}$$

and once the appropriate boundary conditions are imposed. Another condition for (3.70) to solve the system is that the Hessian matrix of the function $W(\phi_1, \phi_2)$ is symmetric, or in other words that the second partial derivatives acting on the superpotential commute. The advantage of using this method is that one can find a simple form for $W(\phi_1, \phi_2)$ and solve for the backreaction of the background VEVs on the metric without the assumption

of small backreaction as in GBS where they used the form $A' = k + \mathcal{O}(l^2)$ in order to solve for the VEV profile.

Since the bulk Higgs doublets are fundamentals of $SU(2)_L$ we must consider a super-potential function that is bi-linear in the two doublets. For simplicity we consider the following

$$W(\Phi_1, \Phi_2) = 6\frac{k}{\kappa^2} + ku_{11}\Phi_1^\dagger\Phi_1 + ku_{22}\Phi_2^\dagger\Phi_2 + ku_{12}\left(\Phi_1^\dagger\Phi_2 + \Phi_2^\dagger\Phi_1\right), \tag{3.72}$$

where the parameters u_{ij} are dimensionless numbers assumed to be of $\mathcal{O}(1)$. By plugging (3.72) into (3.70) we find that the bulk potential is given by

$$\begin{aligned} V(\Phi_1, \Phi_2) = &- 6\frac{k^2}{\kappa^2} + \bar{m}_{11}^2\Phi_1^\dagger\Phi_1 + \bar{m}_{22}^2\Phi_2^\dagger\Phi_2 + \bar{m}_{12}^2\left(\Phi_1^\dagger\Phi_2 + H.c.\right) \\ &+ \lambda_1(\Phi_1^\dagger\Phi_1)^2 + \lambda_2(\Phi_2^\dagger\Phi_2)^2 + \lambda_3(\Phi_1^\dagger\Phi_1)(\Phi_2^\dagger\Phi_2) + \lambda_4(\Phi_1^\dagger\Phi_2 + \Phi_2^\dagger\Phi_1)^2 \\ &+ \lambda_6\Phi_1^\dagger\Phi_1(\Phi_1^\dagger\Phi_2 + \Phi_2^\dagger\Phi_1) + \lambda_7\Phi_2^\dagger\Phi_2(\Phi_1^\dagger\Phi_2 + \Phi_2^\dagger\Phi_1), \end{aligned} \tag{3.73}$$

where, with a little abuse of notation, we denote the quartic terms by λ_i, but it should be obvious that these are not the brane potentials which are defined below.

The potentials on each brane are given by

$$\lambda_{UV}(\Phi_1, \Phi_2) = W(\Phi_1, \Phi_2) + V_{UV}^{2HDM}(\Phi_1, \Phi_2), \tag{3.74}$$

$$\lambda_{IR}(\Phi_1, \Phi_2) = - W(\Phi_1, \Phi_2) + V_{IR}^{2HDM}(\Phi_1, \Phi_2), \tag{3.75}$$

where

$$
\begin{aligned}
V_i^{2HDM}(\Phi_1,\Phi_2) =& \gamma_1^i \left(\Phi_1^\dagger\Phi_1 - \phi_1(y_i)^2\right)^2 + \gamma_2^i \left(\Phi_2^\dagger\Phi_2 - \phi_2(y_i)^2\right)^2 \\
&+ \gamma_3^i \left(\Phi_1^\dagger\Phi_1 + \Phi_2^\dagger\Phi_2 - \phi_1(y_i)^2 - \phi_2(y_i)^2\right)^2 \\
&+ \gamma_4^i \left(\Phi_1^\dagger\Phi_1\Phi_2^\dagger\Phi_2 - \Phi_1^\dagger\Phi_2\Phi_2^\dagger\Phi_1\right) + \gamma_5^i \left(\mathrm{Re}(\Phi_1^\dagger\Phi_2) - \phi_1(y_i)\phi_2(y_i)\right)^2 \\
&+ \gamma_6^i \left(\mathrm{Im}\ \ \Phi_1^\dagger\Phi_2\right)^2, \qquad (3.76)
\end{aligned}
$$

with $i =$UV, IR. Notice that in the boundary conditions, the brane potentials have to be evaluated at the background $\Phi_i = \phi_i$ first, and then taken derivative with respect to the profile. It is remarkable that looking at solutions that have a potential of the form (3.70) immediately gives us general 2HDM in the branes and on the bulk.

With the superpotential chosen above, the equations for the VEV profiles (3.71) become a system of homogeneous linear differential equations with constant coefficients

$$
\begin{pmatrix} \phi_1' \\ \phi_2' \end{pmatrix} = k \begin{pmatrix} u_{11} & u_{12} \\ u_{12} & u_{22} \end{pmatrix} \begin{pmatrix} \phi_1 \\ \phi_2 \end{pmatrix}, \qquad (3.77)
$$

where the solutions, satisfying the boundary conditions $\phi_i(y_c) = v_i$ can be found in Appendix C . The warp function can be solved and written as

$$
A(y) = ky + \frac{\kappa^2}{12}\left[\phi_i(y)\phi_i(y) - \phi_i(0)\phi_i(0)\right], \qquad (3.78)
$$

where the irrelevant additive constant was chosen such that $A(0) = 0$ and the sum over i is implicit. The backreaction of the bulk scalars on the AdS background is associated with the second term in the warp function and is proportional to the square of the background vevs.

In models with the Higgs propagating in the bulk of AdS, the localization of the Higgs profile towards the IR brane is an extra condition that needs to be fine tuned in order to generate the correct values for the electroweak gauge bosons. Therefore for the effective

VEV to be $\mathcal{O}$(TeV) we need to impose $\phi_i(0)\phi_i(0) \ll M_{Pl}^3$, see equation (3.69). Assuming $u > 0$ (the case $u < 0$ yields $\phi_i(0)\phi_i(0) \approx M_{Pl}^3$ and is excluded), one finds

$$4u_{12}^2 = 9 + 4u_{11}u_{22} - 6(u_{11} + u_{22}) \tag{3.79}$$

has to be tuned in order to generate a phenomenologically acceptable VEV and therefore reducing the number of free parameters. This is not surprising at all since the radius stabilization by a single $SU(2)$ doublet required the VEV profile at the Planck brane to be less than $\mathcal{O}$(TeV) [147] and that condition doesn't add to the level of fine-tuning related to the cosmological constant. This is one of the fundamental differences between the Goldberger-Wise mechanism and a Higgs-doublet stabilizer.

The hierarchy problem is resolved if we can generate the TeV scale by redshifting the Planck scale, i.e., $M_{\text{TeV}} = M_{Pl}e^{-A(y_c)}$. Solving for the warp function neglecting the term $\phi_i(0)\phi_i(0)$, we obtain, even if we assume natural values for the parameters, i.e., $v_i^2 \approx M_{Pl}^3$, that the contribution coming from the backreaction term above is negligible compared to that of the curvature term for the generation of the exponential hierarchy. Therefore in this model, the small backreaction approximation corresponds to

$$l^2 \equiv \frac{\kappa^2(v_1^2 + v_2^2)}{12} \ll 1 \tag{3.80}$$

where $\phi_i(y_c) = v_i$.

3.2.3.2 Scalar Perturbations

In order to study the radion field we need to add the scalar perturbations about the background solution and then find the coupled Higgs-gravity Einstein equations for this fields. Following the reasoning of [133] we consider the following perturbations

$$\Phi_i(x, y) = \begin{pmatrix} 0 \\ \phi_i(y) + \varphi_i(x, y) \end{pmatrix}, \tag{3.81}$$

$$ds^2 = e^{-2A-2F(x,y)}\eta_{\mu\nu}dx^\mu dx^\nu - (1+2F(x,y))^2 dy^2. \tag{3.82}$$

The linearized Einstein equations for one scalar coupled to gravity were presented in [133]. For the most general case of N scalars coupled minimally to gravity, see Refs. [152, 159] where the authors derived general conditions for the existence of zero-mode (massless) solutions in models with definite parity and used for particular applications of their results examples of domain- and soft-wall models.

Here we concentrate on the $N = 2$ case. The equations can be brought into a simpler form by writing the combination $e^{2A}\delta\mathcal{R}_{\mu\nu} + \delta\mathcal{R}_{55}$ in the bulk and integrating the $\mu 5$ equation directly. Together with the linearized Euler-Lagrange equations, the system that has to be solved in the bulk is given by

$$e^{2A}\Box F + F'' - 2A'F' = \frac{2}{3}\kappa^2\left(\phi_1'\varphi_1' + \phi_2'\varphi_2'\right), \tag{3.83}$$

$$\phi_1'\varphi_1 + \phi_2'\varphi_2 = \frac{3}{\kappa^2}(F' - 2A'F), \tag{3.84}$$

$$e^{2A}\Box\varphi_i - \varphi_i'' + 4A'\varphi_i' + \frac{\partial^2 V}{\partial\phi_i\partial\phi_j}\varphi_j = -6\phi_i'F' - 4F\frac{\partial V}{\partial\phi_i}, \tag{3.85}$$

where we used the background equations (3.65)-(3.67) to simplify. The second relation above is a constraint equation and tells us that the KK expansions of $F(x,y)$, $\varphi_1(x,y)$ and $\varphi_2(x,y)$ correspond to the same $4D$ state at each KK level so that we can write

$$F(x,y) = \sum F_n(y)h_n(x), \quad \varphi_i(x,y) = \sum \varphi_{i,n}(y)h_n(x). \tag{3.86}$$

The boundary conditions are obtained by matching the delta functions in the linearized equations. Naively, the (μ,ν) and $(5,5)$ linearized Einstein equations yield 4 BCs but as discussed in [133], they are equivalent to each other and therefore only 2 BC arise from this equations. However this 2 boundary conditions are trivially satisfied by (3.84) and the background equations, so the Einstein equations do not provide any relevant boundary conditions. On the other hand, the Euler-Lagrange equations give 2 separate boundary

conditions for each scalar fluctuations. These are given by

$$[\varphi_i']|_{y=y_i} = \left[\frac{\partial^2 \lambda_{UV,IR}}{\partial\phi_i \partial\phi_j}\varphi_j + 2F\frac{\partial\lambda_{UV,IR}}{\partial\phi_i}\right]\Bigg|_{y=y_i} \tag{3.87}$$

where we omit the mode subindex n for simplicity. As we can see, the Euler-Lagrange and Einstein equations yield a set of 4 differential equations for 3 functions of the extra dimension, namely F, φ_1 and φ_2. These equations are supplemented with the boundary conditions of equations (3.87). There are 4 integration constants and one mass eigenvalue. One integration constant corresponds to an overall normalization and the three remaining constants and the mass, together, are determined by the four boundary conditions.

The zero-mode (with $m^2 = 0$) solutions of the system were calculated in Ref. [152]. In that reference the authors found that in domain- and soft-wall models with $N = 2$ scalars and with a bulk potential generated by a superpotential, the zero-mode solutions generally survive after imposing finite normalization and vanishing of the surface terms. Therefore they correspond to physical fields and these models are phenomenologically unacceptable. They commented that the inclusion of fundamental branes would modify the boundary conditions and could possibly render the zero-modes unphysical, making the model viable.

In this scenario, with two bulk Higgs doublets coupled to gravity, the only possible form of the bulk and brane potentials, that is consistent with $SU(2)_L$ gauge invariance, is if they are given as combinations of field bi-linears $\Phi_a^\dagger\Phi_b$, just as in (3.73), (3.74) and (3.75). More complicated expressions for the supepotential could be considered by adding terms quadratic in the fields bi-linears, i.e., $W \propto (\Phi_a^\dagger\Phi_b)^2$ but this choice of superpotential would generate non-linear ODE's for the background fields which would be more harder to solve.

For the superpotential we considered in the previous section, eq. (3.72), the boundary conditions for the scalar perturbations, eq. (3.87) can be written very simply as

$$\varphi_i'\Big|_{y=y_i} = ku_{ij}\varphi_j\Big|_{y=y_i} + 2ku_{ij}\phi_j F\Big|_{y=y_i}, \tag{3.88}$$

and it is straightforward to show, by using (3.77), that the zero-mode solution $F = e^{2A}A'$, $\varphi_i = e^{2A}\phi_i'$ satisfies this conditions trivially. It should be emphasized that the derivatives of the brane potentials are taken after first evaluating at the background, that is by substituting $\Phi_a = \phi_a$ in which case the second term in (3.74) and (3.75) vanishes trivially.

By inspection of the background solutions (C.15) and (C.16), it can be seen that this functions remain finite in the interval $0 < y < y_c$ and thus the normalization

$$N = \int dy e^{-2A} \left(\frac{2}{\kappa^2} F^2 + \varphi_i' \varphi_i' \right), \tag{3.89}$$

would also be finite rendering the zero-mode physical and making this scenario unviable. Factorizing the profiles as

$$F = e^{2A}\tilde{F}, \quad \varphi_i = e^{2A}\tilde{\varphi}_i, \tag{3.90}$$

one can rewrite the bulk equations in a more compact form as

$$-\begin{pmatrix} \tilde{F}'' \\ \tilde{\varphi}_i'' \end{pmatrix} + \begin{pmatrix} 2A'' & 2\frac{\kappa^2}{3}(\phi_j'' - A'\phi_j') \\ 4(\phi_i'' - A'\phi_i') & (4A'^2 - 2A'')\delta_{ij} + V_{ij} + 2\kappa^2 \phi_i'\phi_j' \end{pmatrix} \begin{pmatrix} \tilde{F} \\ \tilde{\varphi}_j \end{pmatrix} = m^2 e^{2A} \begin{pmatrix} \tilde{F} \\ \tilde{\varphi}_i \end{pmatrix}, \tag{3.91}$$

with the constraint equation (3.84) given by

$$\tilde{F}' = \frac{\kappa^2}{3} \phi_i' \tilde{\varphi}_i. \tag{3.92}$$

We thus find that the argument of Ref. [152], which applied to domain-wall and soft-wall models also applies here, leading to an unacceptable massless scalar.

Within the present model one could consider an inert 2HDM where a discrete Z_2 symmetry is imposed such that only one of the scalars gets a vev profile. This case would correspond to setting the superpotential parameter $u_{12} = 0$ and consequently $\tilde{m}_{12}^2 = \lambda_4 = \lambda_6 = \lambda_7 = 0$, see the Appendix. Nonetheless the conclusion of this section, namely the appearance of the zero-mode, still applies and this model is ruled out. An interesting possibility would be to consider the Higgs-radion scenario and adding an extra Higgs on

the TeV brane. This might avoid the appearance of a massless scalar, however generally a second doublet would increase the diphoton decay rate of the SM Higgs boson [50], this would make the deviation of the original GBS model even worse. Nonetheless a full investigation of the parameter space would be interesting. Furthermore a model with 2HDM and one or more singlets would have a much more complicated potential and it is not certain that there will be a physical massless scalar in that case.

3.3 2HDM-radion mixing

As we have discussed in the previous section, in the RS model the radion field emerges as the lightest new state and the possibility of its experimental discovery must be evaluated. Particular attention has been placed on the curvature-Higgs term $\xi\mathcal{R}\ \Phi^\dagger\Phi$ since after expanding about the radion field VEV this term induces kinetic mixing between the radion field and the Higgs, therefore requiring a non-unitary transformation to obtain the canonically normalized degrees of freedom. After diagonalization the physical fields become mixtures of the original non-mixed radion and Higgs boson. The phenomenological consequences of a non-zero mixing have been studied extensively in the literature [133, 155, 158, 160–169]

The radion interacts with matter via the trace of the energy-momentum tensor and the form of these interactions is very similar to those of the SM Higgs boson but are multiplied by v/Λ where $\Lambda \sim \mathcal{O}(\text{TeV})$ is a normalization factor. In the case $\xi = 0$, there is no Higgs-radion mixing and the branching ratios of the radion become very similar to those of the SM in the heavy mass region, being dominated by vector bosons while for the low mass region the gg mode is dominant. Due to its large, anomaly induced, coupling to two gluons a radion can be produced through gluon fusion.

The parameter space coming from the curvature-Higgs mixing scenario consists of four parameters, viz., the bare mass terms m_h and m_r, the mixing parameter ξ and the normalization scale Λ. However in some of the above references, the Higgs boson had been discovered [1, 2] and their parameter space is reduced to (m_r, ξ, Λ). The $\xi - m_r$ parameter

space is very constrained by direct searches for additional scalars at the LHC [168] leaving only small experimentally and theoretically allowed windows for $\Lambda = 3$ TeV and these windows open up as one increases Λ. The bounds on the parameter Λ are dependent on the mass the first KK excitation m_{KK} and the curvature scale k as was shown in [169].

Despite the model differences in the analyses that have appeared on Higgs-radion mixing, the overall conclusion is that there is possibility that the measured Higgs boson could be in fact a mixture of the radion with the Higgs doublet that is consistent with experimental data. However the constraints mentioned in the previous paragraph will be pushed further if a radion signal is not seen in the coming future and it would be interesting to look at possible ways to relax these constraints.

In this section we will study how some of the constraints on the minimal Higgs-radion mixing may be relaxed or modified by adding a second Higgs doublet on the visible brane as we did in Ref. [170]. In this case one generally have curvature scalar couplings of the form $\mathcal{L} \supseteq \xi_{ab}\mathcal{R}(g_{ind})\ \Phi_a^\dagger \Phi_b$ where $a, b = 1, 2$. We will investigate in detail how the radion couples to the SM fields and present the predictions of this model assuming CP conservation. The constraints from LHC Higgs measurements, collider signals and expectations from heavy Higgs searches are discussed.

3.3.1 Custodialy Symmetric 2HDM

In RS models with gauge and matter fields propagating in the bulk there are large contributions to electroweak precision observables (EWPO) [171] that push the KK scale far beyond the reach of accelerators. A possible cure can be implemented by imposing a gauge $SU(2)_L \times SU(2)_R \times U(1)_X$ symmetry in the bulk that is spontaneously broken to provide custodial protection [146] for the S and T parameters and this reduces the bound on the KK scale to $m_{KK} \gtrsim$ 3 TeV. This custodial protection also protects the $Zb\bar{b}$ vertex from large corrections [172].

In the absence of mixing $\xi = 0$, a custodialy symmetric 2HDM potential has vanishing contributions to the T parameter [173] and the contributions of the radion are also small

(see Csaki et al. [133]). However when one includes mixing, the radion and Higgs scalar couplings are modified and could result in large corrections depending on the values of the mixing parameters and masses.

In Ref. [170] we implemented a custodialy protected 2HDM in the visible brane by promoting the Higgs doublets to bi-doublets transforming under the $SU(2)_L \times SU(2)_R$ gauge group. It was shown in that paper that that by imposing the custodial symmetry the number of free parameters in the scalar potential is reduced. From [174] it was also shown that custodial protection implies CP is automatically conserved in the potential.

Furthermore to avoid FCNCs at tree level a softly broken Z_2 symmetry is imposed. As a direct consequence of the custodial symmetry and the discrete symmetry the quartic couplings in the most general potential of equation (2.1) must satisfy

$$\lambda_4 = \lambda_5, \quad \lambda_6 = \lambda_7 = 0, \tag{3.93}$$

which implies the pseudoscalar is degenerate with the charged Higgs bosons. For zero mixing the couplings of the scalar eigenstates in the Higgs sector are identical to the usual 2HDM formulas with the only difference being that the fermions and gauge bosons correspond to the zero modes of their $5D$ bulk fields. Non-zero KK modes are presumed to be sufficiently heavy that they don't have a phenomenological impact.

In Ref. [170] we found that the model can easily satisfy EWPO even under the simplifying assumptions mentioned above and without including the effects from non-renormalizable contributions, which are arbitrary at the cutoff scale. We will not delve into more detail about the contributions to EWPO in this thesis.

3.3.2 Radion interactions

Stabilization of the extra dimension by a GW bulk scalar (not a $SU(2)_L$ Higgs doublet) is taken for granted in this model.

We now proceed to present the radion interactions with the SM fields. The induced

metric on the TeV brane is given by

$$\bar{g}^{ind}_{\mu\nu}(x) = e^{-2A(y_c)} e^{-2e^{2ky_c}R(x)} \eta_{\mu\nu} \equiv e^{-2ky_c}\Omega(r)^2 \eta_{\mu\nu}, \tag{3.94}$$

where we use $\bar{g}_{MN}$ to denote the metric with scalar perturbations included. After rescaling of the doublets $\Phi_a \to e^{ky_c}\Phi_a$, the radion couplings to the Higgs sector are obtained from

$$S_H = \int d^4x \left[\sum_{a=1,2} \eta^{\mu\nu} (D_\mu \Phi_a)^\dagger D_\nu \Phi_a \Omega(r)^2 - V(\Phi_1, \Phi_2)\Omega(r)^4 \right], \tag{3.95}$$

and all mass terms are redshifted accordingly. Expanding to linear order in the radion field $\Omega(r) \approx 1 - r\frac{\gamma}{v}$, with $\gamma \equiv v/\Lambda$ and $\Lambda \equiv \sqrt{6} M_{Pl} e^{-ky_c}$, a straightforward calculation yields the coupling of the radion with the trace of the energy-momentum tensor

$$\frac{\gamma}{v} r \; T^\mu_\mu \supseteq - \sum \frac{\gamma}{v} r \left[(\partial_\mu \phi)^2 - 2m_\phi^2 \phi^2 \right], \tag{3.96}$$

with the sum performed over all physical scalars.

The couplings to the EW gauge sector are obtained from the kinetic terms of the Higgs doublets expanding to linear order in the perturbations

$$S_H \supseteq - \int d^4x \; \frac{\gamma}{v} r(x) \; \eta^{\mu\nu} \left\{ 2m_W^2 W^{(0)+}_\mu(x) W^{(0)-}_\nu(x) + m_Z^2 Z^{(0)}_\mu(x) Z^{(0)}_\nu(x) + ... \right\} \tag{3.97}$$

where the dots represent higher KK excitations. In addition to the boundary terms there are tree level couplings of the radion coming from the kinetic term of the bulk gauge bosons [175]

$$S_{gauge} \supseteq - \int d^4x \frac{\gamma}{v} r(x) \left\{ \frac{1}{ky_c} \frac{1}{4} \eta^{\mu\nu} \eta^{\alpha\beta} V^{(0)}_{\mu\alpha}(x) V^{(0)}_{\nu\beta}(x) + \frac{m_V^4}{2k^2} e^{2ky_c} k y_c \eta^{\mu\nu} V^{(0)}_\mu(x) V^{(0)}_\nu(x) \right\}. \tag{3.98}$$

where $V_{MN} = \partial_M V_N - \partial_N V_M$ is the usual field strength and $V = \{\sqrt{2}W^\pm, Z, A\}$ and $m_V = \{m_W, m_Z, 0\}$. The coupling to the field strengths above becomes significant for

momentum transfer much larger than the EW scale and the second term constitutes a correction of about 20% to the dominant TeV-boundary coupling. In the case of the photon only the first term is present. A similar expression for gluons should be included.

Overall we can write

$$\mathcal{L}_r^{WW,ZZ} = \frac{\gamma}{v} r \left\{ 2m_W^2 \left(1 - \frac{3m_W^2 k y_c}{\Lambda^2} \right) W_\mu^+ W^{\mu -} + m_Z^2 \left(1 - \frac{3m_Z^2 k y_c}{\Lambda^2} \right) Z_\mu Z^\mu \right\}. \quad (3.99)$$

For massless gauge bosons we have to include the contributions coming from the localized trace anomaly and from loop triangle diagrams in which the W gauge boson and fermions in the case of the photon and only fermions in case of the gluons that induce couplings to the radion.

All these contributions can be written as [158, 164, 168, 175] [1]

$$\mathcal{L}_r^{gg,\gamma\gamma} = -\frac{\gamma}{4v} r \left\{ \left(\frac{1}{k y_c} + \frac{\alpha_s b_{QCD}^r}{2\pi} \right) G_{\mu\nu} G^{\mu\nu} + \left(\frac{1}{k y_c} + \frac{\alpha_{EM} b_{EM}^r}{2\pi} \right) F_{\mu\nu} F^{\mu\nu} \right\}, \quad (3.100)$$

with $\alpha_s(\alpha_{EM})$ being the strong (electroweak) coupling constant and

$$b_{QCD}^r = 7 + F_f, \quad (3.101)$$

$$b_{EM}^r = -\frac{11}{3} + \frac{8}{3} F_f - F_W, \quad (3.102)$$

$$F_f = \tau_f \left(1 + (1 - \tau_f) f(\tau_f) \right), \quad (3.103)$$

$$F_W = 2 + 3\tau_W + 3\tau_W (2 - \tau_W) f(\tau_W), \quad (3.104)$$

$$f(\tau) = Arcsin^2 (\frac{1}{\sqrt{\tau}}) \quad \tau \geq 1, \quad (3.105)$$

$$f(\tau) = -\frac{1}{4} \left(\log \frac{1 + \sqrt{1 - \tau}}{1 - \sqrt{1 - \tau}} - i\pi \right)^2, \quad \tau < 1, \quad (3.106)$$

[1] The Lagrangian takes into account only the leading order mass effects for the radion coupling to exactly two gauge bosons.

and $\tau_i = (\frac{2m_i}{m_r})^2$, m_i is the mass of the particle going around the loop. An important property of the kinematic functions is their saturation $F_f \to 2/3$, $F_W \to 7$, $\tau f(\tau) \to 1$ for $\tau > 1$ and $F_{f,W} \to 0$ for $\tau < 1$.

The corrections to the couplings coming from excited KK modes of the top and W boson in the loop and simply were not considered and it was assumed that the above contributions are dominant.

Fermions propagating in the bulk are characterized by a bulk mass parameter $c = m/k$ which specifies their location in the bulk. In addition, the boundary conditions of their profiles at the location of the branes force either the left- or the right-handed zero modes to be zero [126]. Therefore for each SM fermion we need to introduce two different bulk fermions, one with bulk mass parameter c_L and for which the right-handed zero mode vanishes and the other with a bulk mass parameter c_R and for which the left-handed zero mode vanishes.

The couplings of the radion to SM fermions can be simpliffied as [168]

$$S \supseteq \int d^4x \sum_{f=u,d,e} \frac{\gamma}{v} r(x) m_f \bar{f} f \times \begin{cases} 1 & \text{Planck} \\ (c_L - c_R) & \text{TeV.} \end{cases} \tag{3.107}$$

with the lower option if the zero-mode profile is peaked towards the TeV brane $c_L < 1/2$, $c_R > -1/2$ otherwise the localization is in the Planck brane and the upper option applies. Besides this couplings it seems that the boundary Yukawa couplings will have a direct contribution to the radion couplings to fermions. However, as shown in [175], these contributions get cancelled by induced wave function discontinuities obtained by carefully treating the boundary conditions.

3.3.3 Mass Eigenstates

The most general term that will give rise to kinetic mixing between the Higgs doublets and the radion field is given by

$$\mathcal{L}_\xi = \sqrt{\bar{g}_{ind}}\xi_{ab}\mathcal{R}(\bar{g}_{ind})\Phi_a^\dagger\Phi_b \tag{3.108}$$

where the indices $a, b = 1, 2$ are summed so that we have, in principle, four different mixing parameters. However the assumption of CP invariance forces $\xi_{12} = \xi_{21}$ and thus the pseudoscalar does not mix with the radion. Evaluation of the Ricci scalar is straightforward and yields the following expression [133]

$$\mathcal{L}_\xi = -6\xi_{ab}\Omega^2\left[\Box \ln\Omega + (\nabla \ln\Omega)^2\right]\Phi_a^\dagger\Phi_b \tag{3.109}$$

The warp factor disappears after we make the rescaling of the Higgs doublets. Using the expression for the Higgs mass eigenstates eq. (2.4) and expanding to linear order in the fields we can write

$$\mathcal{L}_\xi \supseteq -6\left[-\frac{\gamma}{v}\Box r + \frac{\gamma^2}{v^2}r\Box r\right]\left[\frac{v^2}{2}K_r + \frac{v}{2}K_h h + \frac{v}{2}K_H H\right], \tag{3.110}$$

where $\gamma \equiv v/\Lambda$ and we define the mixing parameters by

$$K_r = \xi_{11}c_\beta^2 + \xi_{22}s_\beta^2 + 2\xi_{21}s_\beta c_\beta, \tag{3.111}$$

$$K_h = 2(\xi_{22}s_\beta c_\alpha - \xi_{11}c_\beta s_\alpha) + 2\xi_{12}\cos(\alpha+\beta), \tag{3.112}$$

$$K_H = 2(\xi_{11}c_\beta c_\alpha + \xi_{22}s_\beta s_\alpha) + 2\xi_{12}\sin(\alpha+\beta). \tag{3.113}$$

Adding the kinetic and mass terms of each field, the mixing Lagrangian can be expressed as

$$\mathcal{L} = -\frac{1}{2}(1+6\gamma^2 K_r) r \Box r - \frac{1}{2} m_r^2 r^2 + \sum_{\phi=h,H} \left\{ 3\gamma K_\phi \phi \Box r - \frac{1}{2}\phi(\Box + m_\phi^2)\phi \right\} \tag{3.114}$$

The kinetic terms can be diagonalized by performing the transformation

$$r \to \frac{r'}{Z}, \quad \phi \to \phi' + \frac{3\gamma K_\phi}{Z} r' \tag{3.115}$$

with $\phi = h, H$ and

$$Z^2 = 1 + 6\gamma^2 K_r - 9\gamma^2 (K_h^2 + K_H^2), \tag{3.116}$$

is the determinant of the kinetic mixing matrix and therefore should always satisfy $Z^2 > 0$ to avoid the presence of ghosts fields. This condition allows us to impose our first theoretical constraint on the mixing parameters after choosing appropriate values for α, β and γ. This transformation induces mixing in the mass terms. The mass matrix obtained can be written as

$$M = \begin{pmatrix} \omega_{rr}^2 & \omega_{rh}^2 & \omega_{rH}^2 \\ \omega_{rh}^2 & m_h^2 & 0 \\ \omega_{rH}^2 & 0 & m_H^2 \end{pmatrix}, \tag{3.117}$$

where

$$\omega_{rr}^2 = \frac{m_r^2}{Z^2} + \frac{9\gamma^2}{Z^2}\left(K_h^2 m_h^2 + K_H^2 m_H^2\right), \tag{3.118}$$

$$\omega_{r\phi}^2 = \frac{3\gamma}{Z} K_\phi m_\phi^2. \tag{3.119}$$

The physical eigenstates are obtained by performing a three dimensional rotation

$$\begin{pmatrix} r' \\ h' \\ H' \end{pmatrix} = U \begin{pmatrix} r_D \\ h_D \\ H_D \end{pmatrix}. \tag{3.120}$$

The relation between the gauge eigenstates and the mass eigenstates can be written as

$$r = \frac{U_{11}}{Z} r_D + \frac{U_{12}}{Z} h_D + \frac{U_{13}}{Z} H_D, \tag{3.121}$$

$$h = \left(U_{21} + 3\gamma\frac{K_h}{Z}U_{11}\right) r_D + \left(U_{22} + 3\gamma\frac{K_h}{Z}U_{12}\right) h_D + \left(U_{23} + 3\gamma\frac{K_h}{Z}U_{13}\right) H_D, \quad (3.122)$$

$$H = \left(U_{31} + 3\gamma\frac{K_H}{Z}U_{11}\right) r_D + \left(U_{32} + 3\gamma\frac{K_H}{Z}U_{12}\right) h_D + \left(U_{33} + 3\gamma\frac{K_H}{Z}U_{13}\right) H_D. \quad (3.123)$$

For later convenience we name the coefficients of this transformation as

$$U_{rr} = \frac{U_{11}}{Z}, \qquad U_{rh} = \frac{U_{12}}{Z}, \qquad U_{rH} = \frac{U_{13}}{Z}, \quad (3.124)$$

$$U_{hr} = U_{21} + 3\gamma K_h\frac{U_{11}}{Z}, \qquad U_{hh} = U_{22} + 3\gamma K_h\frac{U_{12}}{Z}, \qquad U_{hH} = U_{23} + 3\gamma K_h\frac{U_{13}}{Z}, \quad (3.125)$$

$$U_{Hr} = U_{31} + 3\gamma K_H\frac{U_{11}}{Z}, \qquad U_{Hh} = U_{32} + 3\gamma K_H\frac{U_{12}}{Z}, \qquad U_{HH} = U_{33} + 3\gamma K_H\frac{U_{13}}{Z}, \quad (3.126)$$

which will be used in the next section for the predictions of the electroweak precision observables.

The Higgs scalars-radion system is determined by the three mixing parameters of equation (3.108), the two mixing angles of the Higgs sector, the scale γ and the three scalar masses, giving a total of nine parameters. However one of the physical masses will be set to the Higgs mass value and only the set $(\xi_{11}, \xi_{12}, \xi_{22}, \alpha, \beta, \gamma, \lambda_r, \lambda_H)$ needs to be specified.

Another important parameter in the study of RS models with bulk gauge bosons is the KK scale defined to be the mass of the first excited state of the gauge bosons. Recall that this parameter is given by [155]

$$m_{KK} = 2.45\frac{k}{\sqrt{6}M_{Pl}}\Lambda, \quad (3.127)$$

so any bound on the KK scale will directly affect the allowed values of the curvature scale k and Λ.

In Higgs-radion mixing scenarios there is a particular point in the parameter space called the "conformal point" [156, 158, 168], usually around $\xi = 1/6$ where the conformal symmetry is minimally violated by the Higgs VEV. At this point the tree-level couplings of the radion to the massive fermions and gauge bosons are very suppressed and the gg

decay mode dominates even in the large radion mass limit. In this work we do not attempt to calculate a conformal point due to the large number of parameters.

In what follows we will sometimes reduce the parameter space by assuming that the diagonal elements of the curvature-scalar mixing matrix are equal to each other, $\xi_{11} = \xi_{22} \equiv \xi_1$ and for simplicity we will refer to the off diagonal as $\xi_{12} \equiv \xi_2$. Relaxing this constraint will not radically alter the numerical results in the following sections. However, we will primarily focus on K_r, K_h, K_H, which is independent of this assumption.

From now on we will drop the subindex D for the diagonal eigenstates and simply write them as r, h and H. Whenever we need to distinguish between the non-diagonal and physical states a clarification will be made.

3.3.4 Model Predictions

3.3.4.1 Constraints From Current LHC Higgs Data

In the 2HDM the interactions of all the scalars to the SM fields are completely determined by the two mixing angles of the scalar sector β and α. In addition, the alignment limit is defined to be the limit in which one of the CP-even scalars has exactly the same interactions as the SM Higgs and corresponds to $\cos(\beta - \alpha) = 0$.

In this section we perform an analysis on the effects Higgs-radion mixing has on the 2HDM parameter space, $\cos(\beta - \alpha)$ and $\tan\beta$. We use a chi-square test to fit the model to the data presented in Appendix D and find the region in the 2HDM parameter space allowed by current LHC data on the SM-like Higgs boson, h. By definition the chi-square function to be minimized is written as

$$\chi^2 = \sum_i \frac{(R_i^p - R_i^m)^2}{(\sigma_i)^2}, \tag{3.128}$$

where R_i^P is the signal strength predicted by the model, R_i^m is the measured signal strength and σ_i is the corresponding standard deviation of the measured signal strength and not to be confused with the scattering cross section. Asymmetric uncertainties are averaged

in quadrature $\sigma = \sqrt{\frac{\sigma_+^2+\sigma_-^2}{2}}$. The expected signal strengths are defined as the production cross section times branching ratio of a particular decay channel ff normalized to the standard model prediction, i.e.,

$$R_f^p \equiv \frac{\sigma(pp \to h)BR(h \to ff)}{\sigma(pp \to h_{SM})BR(h_{SM} \to ff)}. \tag{3.129}$$

Directly obtaining analytical expressions for the mass eigenstates is challenging therefore numerical techniques were used. The analysis was carried out using two benchmarks for the radion vev, $\Lambda = 3, 5$ TeV. Random values were generated for the 2HDM mixing angles, (α, β), the curvature scalar couplings (ξ_1, ξ_2) and the scalar mass parameters before radion mixing (m_h, m_H, m_r) amounting to seven degrees of freedom. By imposing the field h has a mass of 125.09 ± 0.5 GeV one degree of freedom is removed leaving us with six degrees of freedom in our chi-square analysis. We also constrained the radion and heavy Higgs physical masses to lie in the range $[200, 1000]$ GeV. We plot the points allowed by the LHC data in Fig. 3.1 at a 95% confidence level for the type-I and type-II models.

No significant difference can be observed between the $\Lambda = 3$ TeV and $\Lambda = 5$ TeV plots for each type of model. Therefore it seems that a curvature-scalar mixing has no significant effect on the 2HDM parameter space. One can understand this by looking at the off-diagonal elements of the mass matrix, equation (3.117), which are $3\gamma K_\phi/Z \sim 1/1000$ times the diagonal elements. This is a reasonable approximation since we assume natural values for the curvature-scalar mixing parameters, $\xi \sim \mathcal{O}(1)$ and therefore the unitary matrix that diagonalizes (3.117) is nearly diagonal which implies that the couplings of the SM-like Higgs to a pair of gauge bosons and fermions receive very small corrections and are nearly given by the corresponding couplings in the 2HDM, i.e.,

$$g_{hVV} = U_{hh}\sin(\beta-\alpha) + U_{Hh}\cos(\beta-\alpha) + U_{rh}\gamma(1 - 3\frac{m_V^2 k y_c}{\Lambda^2}) \approx \sin(\beta-\alpha), \tag{3.130}$$

$$g_{hff} = U_{hh}\xi_h^f + U_{Hh}\xi_h^f + U_{rh}\gamma(c_L - c_R) \approx \xi_h^f, \tag{3.131}$$

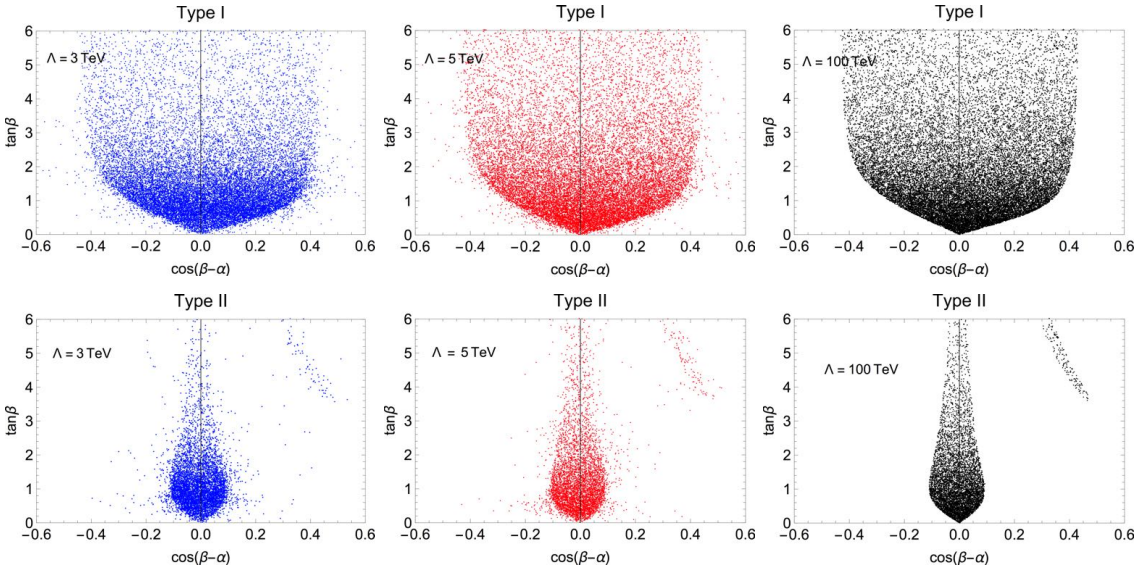

Figure 3.1: The top plots show the allowed regions for the type-I model and the bottom plots show the allowed regions in the type-II model. The blue (red, black) points shown are used for the $\Lambda = 3(5, 100)$ TeV cases. Values of the curvature scalar couplings, ξ_1, ξ_2 were allowed to range between $[-4, 4]$. We have varied the radion and heavy Higgs masses over the range 200 to 1000 GeV. Image from [170].

where U_{ij} are the elements of the non-unitary transformation. The general shape of the regions is understood by looking at the behavior of the couplings. In the type-I model $\xi_h^t = \cos\alpha/\sin\beta$ and in the large $\tan\beta$ limit the production cross section is suppressed, allowing the parameter space to grow. For type-II model the coupling to a pair of b quarks is $\xi_h^b = -\sin\alpha/\cos\beta$ and therefore the production cross section is enhanced by the b quark loop squeezing the parameter space.

The allowed region of the curvature-scalar parameter space is constrained by the requirement that the determinant of the kinetic mixing matrix, Eq. (3.116), be positive. This condition was discussed in the last section. We can examine the constraint in the $\xi_2 - \xi_1$ plane. This depends only on $\tan\beta$ and γ and is given, for $\Lambda = 3, 5$ TeV, in Figure 3.2. However, large values of the ξ_i can require some fine-tuning, and we have found that the density of points in a scatterplot drops substantially once ξ_i is greater than 4 and less than -4. As a result, restricting the mixing parameters to the range between $-4 \leq \xi_i \leq 4$ will not substantially affect our scatterplots below. In that range, the region

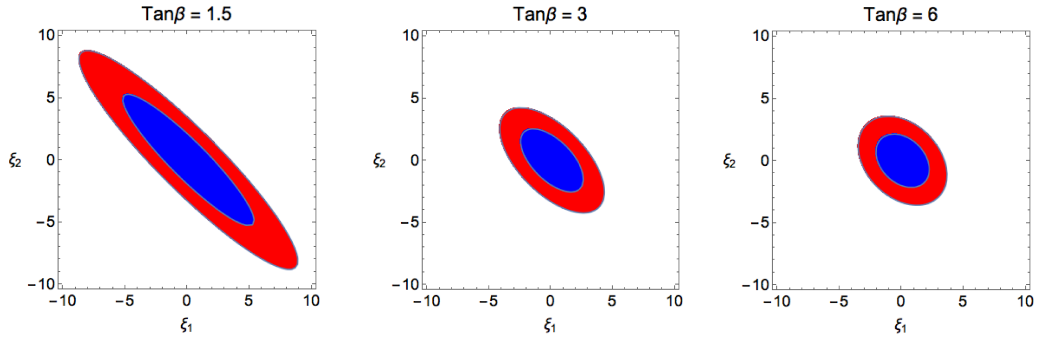

Figure 3.2: Theoretically allowed ξ_1-ξ_2 parameter space for different values of $\tan\beta$. The blue (red) region is for $\Lambda = 3(5)$TeV. Image from [170].

of the curvature-scalar parameter space allowed by the chi-square test is shown in Fig. 3.3. The region shrinks by reducing the value of Λ.

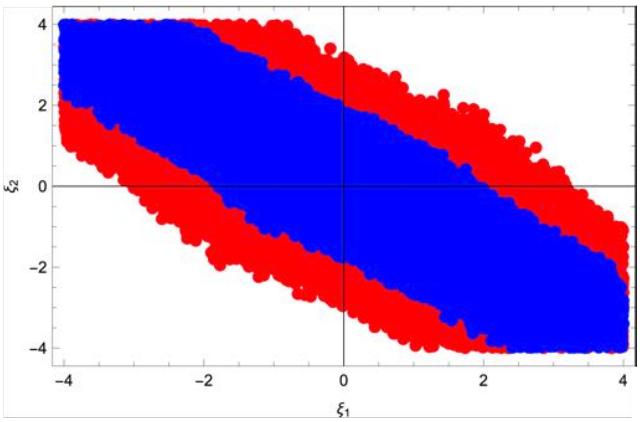

Figure 3.3: The parameter space of ξ_1 and ξ_2 allowed by the chi-square goodness of fit. The blue and red points correspond to $\Lambda = 3$ TeV and $\Lambda = 5$ TeV respectively. Image from [170].

3.3.4.2 Collider Signals

Let us now consider some predictions of this model accessible to the LHC and how one may distinguish this model from some other multi-Higgs model. One feature of a multi-Higgs model is that the sum of the CP-even scalar couplings to Z bosons in quadrature should

total to the square of the SM Higgs coupling to the Z bosons, namely

$$g_{h_{SM}ZZ}^{-2} \sum_{i}^{n} g_{\phi_i ZZ}^2 = 1. \tag{3.132}$$

Due to the bulk couplings of the radion to the bulk gauge bosons we find that the sum of the neutral scalar couplings in quadrature normalized to the $h_{SM}ZZ$ coupling gives $1 + \gamma^2(1 - 3m_Z^2 k y_c/\Lambda^2)^2$ being bounded from below by 1 and setting it apart from other multi-Higgs models. However, this deviation from unity may be quite small. For $\Lambda_\phi = 3$ TeV one finds Eq. 3.132 gives 1.0054 and the deviation from unity vanishes in the limit $\Lambda_\phi \to \infty$. It is unlikely that the LHC will be able to measure such a small deviation, but such a measurement may be possible at the future ILC.

Another strategy to distinguish the heavy scalar state H from a radion is to measure the ratio of the widths of the heavy scalars to $b\bar{b}$ and ZZ pairs,

$$R_{bb/ZZ}^{\Phi} \equiv \frac{\Gamma(\Phi \to \bar{b}b)}{\Gamma(\Phi \to ZZ)}, \text{ for } \Phi = r,\ H. \tag{3.133}$$

The mass eigenstates, H and r are primarily aligned with the unmixed states. This means that couplings of H to the Z boson and b quark should be dominated by the corresponding expressions in a 2HDM . Then for H, $R_{bb/ZZ}^{H}$ should mostly scale like $\left(\frac{\sin\alpha}{\sin\beta}\frac{1}{\cos(\beta-\alpha)}\right)^2$ for the type-I model and $\left(\frac{\cos\alpha}{\cos\beta}\frac{1}{\cos(\beta-\alpha)}\right)^2$ for the type-II model. In either case this ratio becomes quite large in the neighborhood of $\cos(\beta - \alpha) = 0$. For the radion, in the limit that its fully aligned with the unmixed radion, $R_{bb/ZZ}^{r} \propto \frac{(c_L - c_R)^2}{\left(1 - 3\frac{m_Z^2 k y_c}{\Lambda^2}\right)^2} \approx (c_L - c_R)^2$. This is typically less than one and thus measurement of this ratio might distinguish r from H.

As an example, consider the benchmark point with $\tan\beta = 1$, $\cos(\beta - \alpha) = 0.01$, $\Lambda = 5$ TeV and moderate mixing $\xi_1 = 2$ and $\xi_2 = -3$. The values of the masses before mixing are fixed to $m_r = 540$ GeV, $m_h = 125$ GeV and $m_H = 600$ GeV which yield the mass eigenvalues $m_r \approx m_H \approx 600$ GeV, $m_h = 125$ GeV and $R_{bb/ZZ}^{r} \approx 0.4$ and $R_{bb/ZZ}^{H} \approx 5540$. This is a huge, five order of magnitude difference and would be easily detectable.

3.3.4.3 Constraints From Heavy Higgs searches

The radion interactions with the scalar sector come from the following sources:

1 The quartic interactions in the 2HDM potential

$$V(\Phi_1,\Phi_2) \supseteq \frac{\lambda_1}{2}(\Phi_1^\dagger\Phi_1)^2+\frac{\lambda_2}{2}(\Phi_2^\dagger\Phi_2)^2+\lambda_3\Phi_1^\dagger\Phi_1\Phi_2^\dagger\Phi_2+\frac{\lambda_4}{2}(\Phi_1^\dagger\Phi_2+\Phi_2^\dagger\Phi_1)^2. \quad (3.134)$$

2 The coupling of the radion with the trace of the energy momentum tensor

$$\mathcal{L} \supseteq -\frac{r}{\Lambda}((\partial_\mu h)^2-2m_h^2h^2+...). \quad (3.135)$$

3 The curvature-scalar mixing term $\mathcal{L}=-\xi_{ab}\mathcal{R}\Phi_a^\dagger\Phi_b$, where we expand the Ricci scalar up to second order in γ:

$$\mathcal{R} \supseteq -\frac{\gamma}{v}\Box r+2\frac{\gamma^2}{v^2}r\Box r+\frac{\gamma^2}{v^2}(\partial_\mu r)^2+\mathcal{O}(\gamma^3). \quad (3.136)$$

4 There is a model dependent contribution coming from the potential of the GW scalar field that one can consider however we will assume this interaction to be small as it is proven in [155] that addition of this extra term doesn't affect the phenomenology.

5 Non-zero mixing will also induce tree-level interactions of the radion with a gauge field and a scalar, namely $rW^\pm H^\mp$ and rZA coming from a direct expansion of the kinetic terms.

In this model the amount of kinetic mixing between the Higgs field and the radion is parametrized by the parameter K_h of equation (3.112). Similarly the amount of kinetic mixing between the heavy Higgs state and the radion is encoded in the parameter K_H given in equation (3.113). We use the most recent LHC direct searches for a heavy scalar decaying into a pair of SM Higgs bosons [176, 177], into WW bosons [178] and into a pair of ZZ bosons [179] to find bounds on the amount of mixing. The most relevant decay channels,

when kinematically accesible, are $\phi_i \to hh, \phi_j\phi_j, h\phi_j, bb, tt, WW, ZZ, gg, AA, H^+H^-, ZA$, $W^\pm H^\mp$ with $\phi_i = r, H$. The trilinear interactions coming from the 2HDM potential have a dependence on the pseudoscalar mass m_A and on the quartic coupling of the potential λ_4. We scanned over all the parameters and chose as benchmark values $\Lambda = 3,5$ TeV, $m_A = 200, 500, 700$ GeV and fixed $\lambda_4 = 0.1$. Changing the value of the quartic coupling does not affect significantly the results. The results are presented as scattered plots in figures 3.4 and 3.5 where we show the allowed region in m_r-K_h and m_H-K_H parameter space for the type-I 2HDM (for the type-II the results are not dramatically different and therefore we do not show them here). In those figures the background black points correspond to the points that are both theoretically allowed and that survived the chi-square analysis of the previous subsection while the points colored yellow, green and red correspond to regions that are forbidden by LHC searches of a heavy scalar decaying in the WW, ZZ and HH channels respectively. No bounds were found from Higgs resonant production searches in [177]. One can immediately notice that direct searches in the WW and ZZ channel forbid mainly the low mass region $m_r = 200 - 400$ GeV with the bounds from thee WW being weaker than those from the ZZ channel and no bounds at all from the WW channel were found for the heavy Higgs. The di-Higgs search channels put constraints mostly in the intermediate mass region $m_{r/H} = 300 - 800$ GeV.

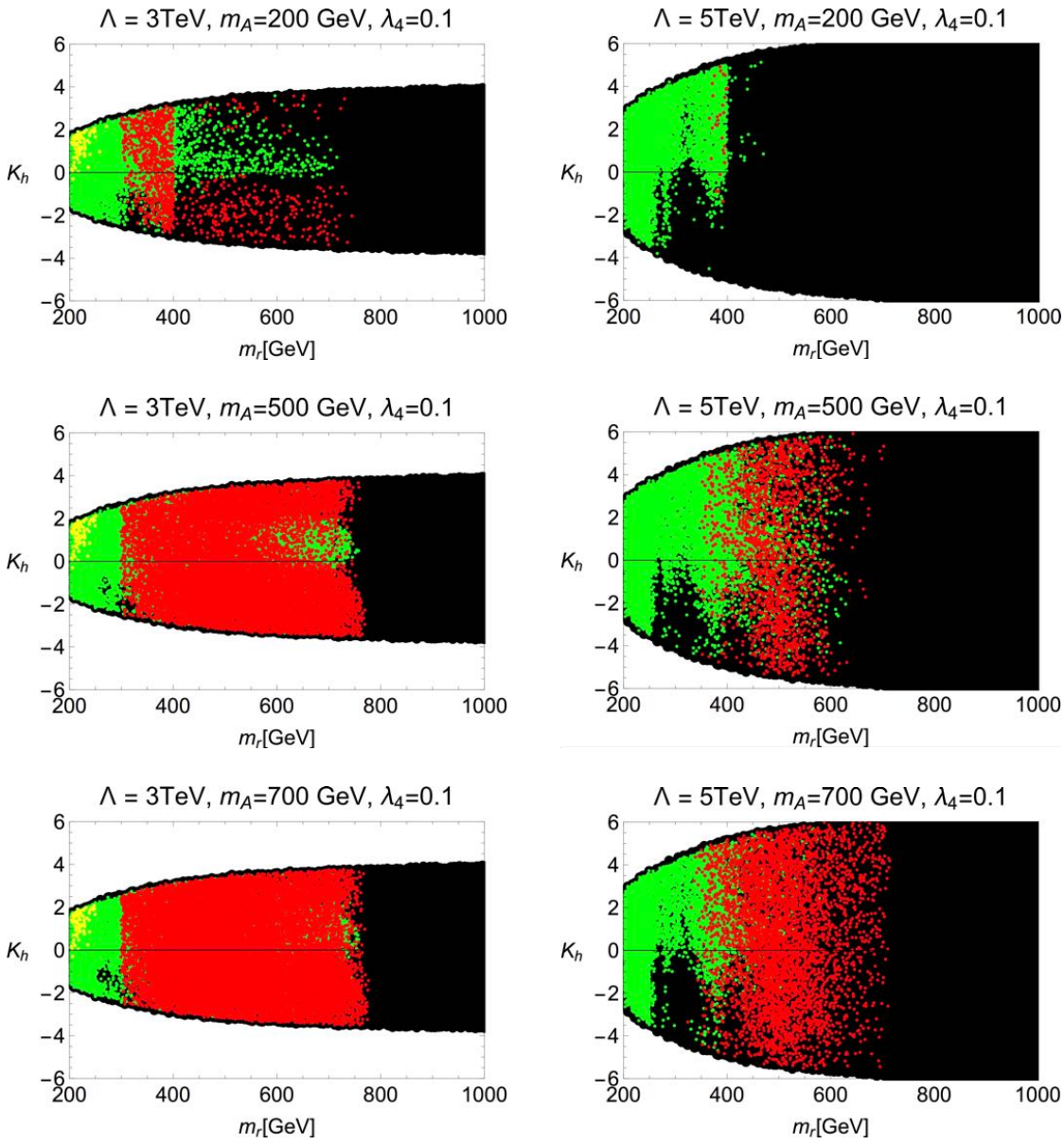

Figure 3.4: Scatter plots of the amount of mixing between the Higgs and the radion, K_h defined in equation (3.112), as function of the radion mass for the type-I 2HDM. The black region is theoretically allowed and the points colored yellow, green and red are forbidden by heavy scalar searches in the WW, ZZ and hh channels respectively. The benchmark point $\Lambda = 3(5)$TeV was used on the left (right). Due to the custodial symmetry, the charged scalar mass is identical to the pseudoscalar mass, whose value is given above each figure. The heavy neutral Higgs mass, m_H, is varied from 200 to 1000 GeV. Image from [170].

From the figure we can notice that as the pseudoscalar mass increases the bounds com-

ing from the di-Higgs boson and ZZ channels become more stringent. This is reasonable since an increase in the pseudoscalar mass corresponds, via the 2HDM potential, to an increase in the trilinear coupling of the radion to a pair of SM Higgs fields and the branching fraction becomes bigger.

The LHC has also searched for a CP-odd Higgs scalar in the processes $pp \to H/A \to ZA/H$ [180–182] where the final state Z boson decays into two oppositely charged electrons or muons and the scalar, either H or A, is assumed to decay into a pair of b quarks. These final states were motivated by the large branching fractions predicted in a 2HDM with type-II Yukawa structure and the benchmark values $\tan\beta = 0.5$-1.5 and $\cos(\beta - \alpha) = 0.01$ are used in those references. In those papers, the charged Higgs boson masses were kept equal to the highest mass involved in the benchmark signal, namely $m^2_{H^\pm} \approx m^2_H$ for $H \to ZA$ or $m^2_{H^\pm} \approx m^2_A$ for $A \to ZH$.

Due to the custodial symmetry imposed in the 2HDM potential we can only account for the latter triplet mass degeneracy but we can consider both decay topologies. To the best of our knowledge there has been no search for the signal $H \to ZA$ with $m_{H^\pm} \approx m_A$.

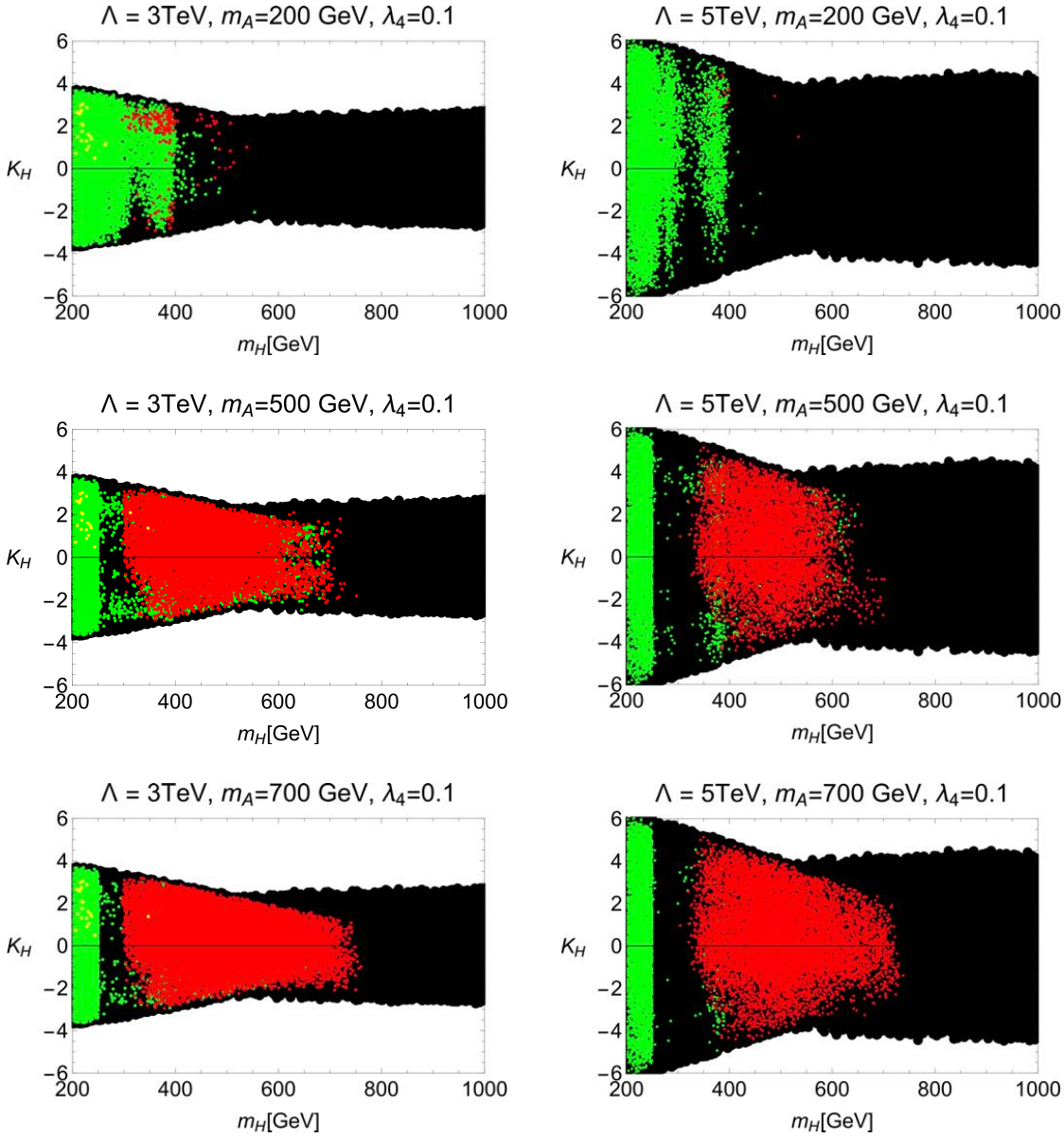

Figure 3.5: Scatter plots of the amount of mixing between the heavy Higgs and the radion, K_H defined in equation (3.113), as function of the heavy Higgs mass for the type-I 2HDM. The black region is theoretically allowed and the points colored yellow, green and red are forbidden by heavy scalar searches in the WW, ZZ and hh channels respectively. The benchmark point $\Lambda = 3(5)$TeV was used on the left (right). Due to the custodial symmetry, the charged scalar mass is identical to the pseudoscalar mass, whose value is given above each figure. The radion mass, m_r, is varied from 200 to 1000 GeV. Image from [170].

In figure 3.6 we show the production cross section, via gluon fusion, for A times the branching fractions $BR(A \to ZX)BR(Z \to l^+l^-)BR(X \to b\bar{b})$ in the type-I (top) and type-II model (bottom) as a function of the mass m_X where $X = H(\text{red}), r(\text{blue})$. The values $m_A = 700$ GeV and $\lambda_4 = 0.1$ were fixed.

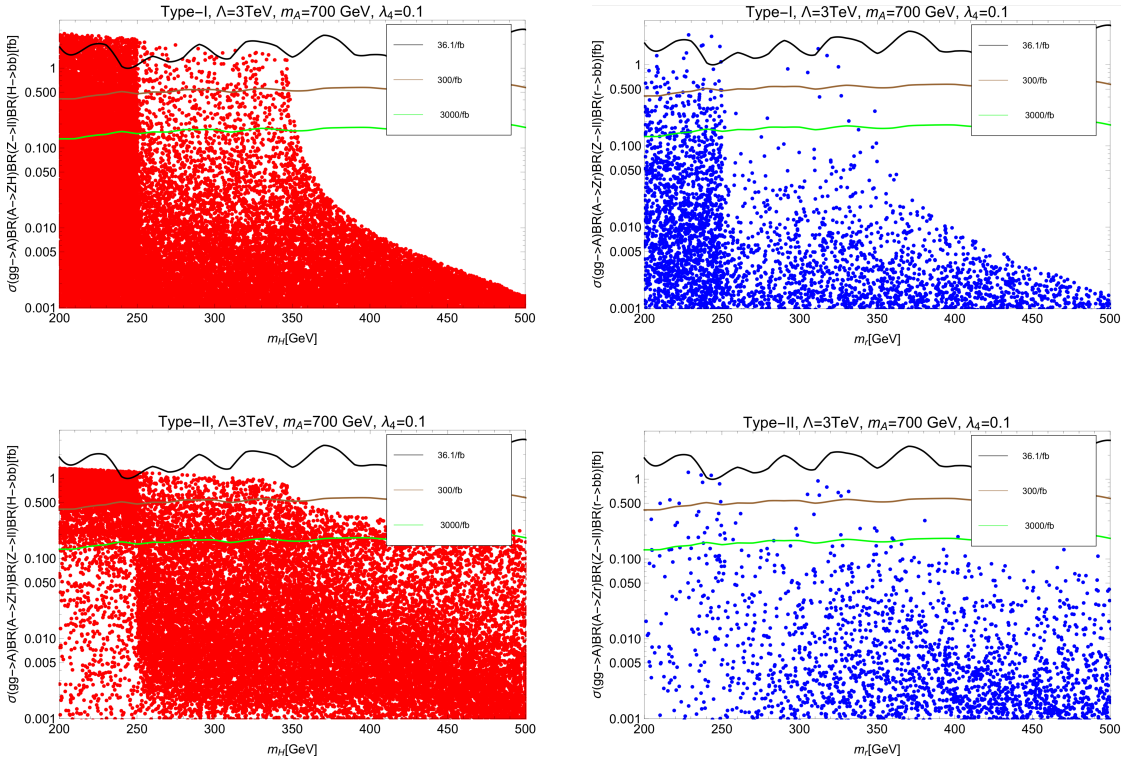

Figure 3.6: The observable $\sigma(gg \to A \to ZX)BR(Z \to l^+l^-)BR(X \to b\bar{b})$ as a function of the resonance mass with $X = H(\text{red}), r(\text{blue})$ for type-I (top) and type-II (bottom) models. We fixed $\Lambda = 3$ TeV, $m_A = 700$ GeV and $\lambda_4 = 0.1$. Due to the custodial symmetry, the charged scalar mass is identical to the pseudoscalar mass, whose value is given above each figure. The heavy neutral Higgs (radion) mass is varied from 200 to 1000 GeV in the right (left) figures and the values of α and β are chosen to be consistent with the constraints of Figure 3.1. The solid lines represent current and future upper bounds at the LHC. Image from [170].

The 95% CL upper limits from ATLAS [182], after multiplying by $BR(Z \to l^+l^-) \approx 0.0336$ [183], for $m_A = 700$ GeV are shown in Fig. 3.6. We have also shown the expected limits for 300 fb^{-1} and 3000 fb^{-1} [2]. It is clear that the LHC will only be able to cover

[2]Since the limits are background limited, we are assuming in Figs. 3.6 and 3.7 that the bounds will scale as $1/\sqrt{N}$.

a small range of parameter space, however discovery of the process for $m_H > 400$ GeV in the near future would rule out the model. In any event the hadronic decay mode ($b\bar{b}$ or $t\bar{t}$) will dominate the pseudoscalar decays.

In figure 3.7 we show the production cross section via gluon fusion of a heavy Higgs boson (red) and a radion (blue) times the branching fractions $BR(X \to ZA)BR(Z \to l^+l^-)BR(A \to b\bar{b})$ as a function of the mass m_X and with $X = H$, r for the type-I (top) and type-II (bottom) models. For type-I model we fixed $m_A = 200$ GeV and in the type-II, due to lower bounds on the charged Higgs [184], we fixed $m_A = 500$ GeV.

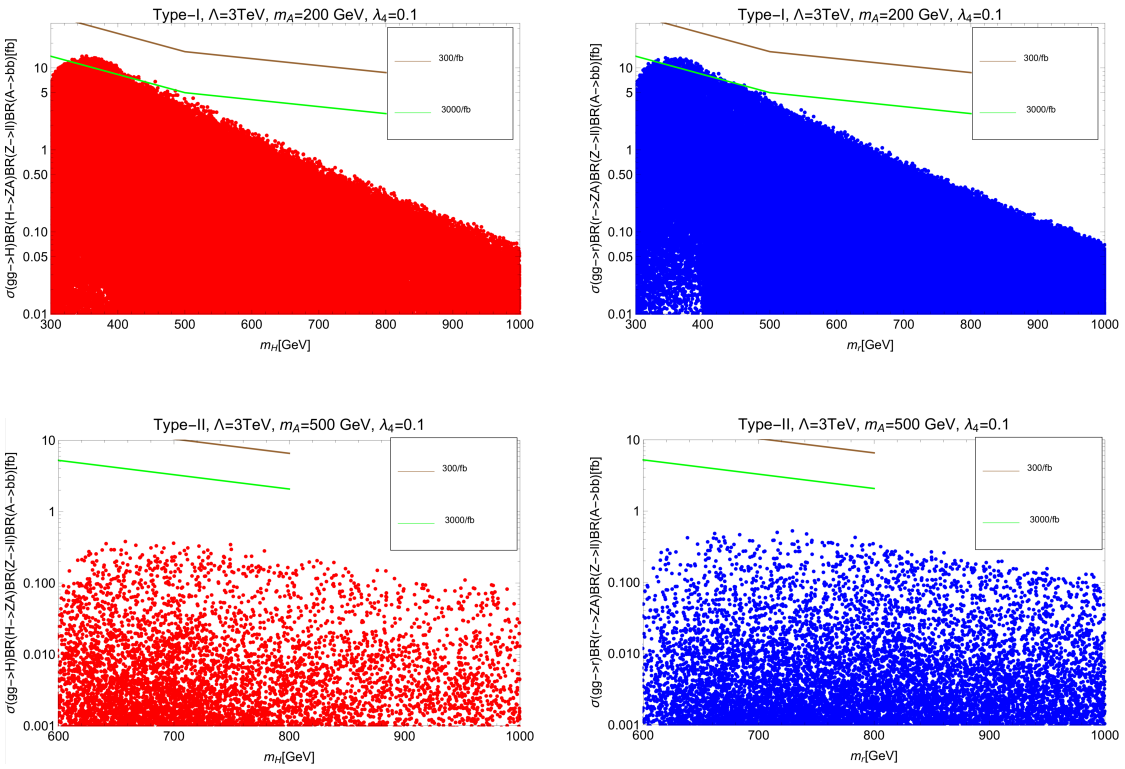

Figure 3.7: The observable $\sigma(gg \to X \to ZA)BR(Z \to l^+l^-)BR(A \to b\bar{b})$ as a function of the resonance mass with $X = H$(red), r(blue) in the type-I (top) and type-II (bottom) models. We fixed $\Lambda = 3$TeV, $m_A = 200$GeV($m_A = 500$GeV) on top (bottom) and $\lambda_4 = 0.1$. Due to the custodial symmetry, the charged scalar mass is identical to the pseudoscalar mass, whose value is given above each figure. The heavy neutral Higgs (radion) mass is varied from 200 to 1000 GeV in the right (left) figures and the values of α and β are chosen to be consistent with the constraints of Figure 3.1. The solid lines represent future upper bounds at the LHC. Image from [170].

Current upper limits from CMS [180, 181] are out of the range of the figures. Extrapolations of the expected reach for 300 fb^{-1} and 3000 fb^{-1} are given by the brown and green lines, respectively, in figure 3.7.

We can see from figure 3.7 that for this decay our predictions are not in reach for the LHC except at the very edge of the parameter space in the type-I 2HDM. Note that discovery of this decay mode in the near future would rule out these models. The primary decays of the radion would be into pairs of Higgs bosons or Z's depending on its mass and scalar trilinear coupling. The decays of H might also be into these final states as well as $b\bar{b}$ and $t\bar{t}$ depending on its mass and scalar trilinear coupling.

3.4 Conclusion

The model of Geller, Bar-Shalom and Soni [147] offers a very appealing alternative to the Goldberger-Wise stablization mechanism, in which the same field that stabilizes the radius of the extra dimension also breaks electroweak symmetry. The model is extremely constrained, since the Higgs boson and radion are the same, and thus predictions were made for Higgs-radion production cross section and branching fractions that conflicted with the Standard Model. Alas, during the years since their model was developed, data from the LHC has ruled out the original form of the model. By adding bulk profiles for fermions, the parameter-space of the model is expanded, but we have shown that there are no values of these extra parameters that bring the model into agreement with LHC data. Finally, we consider expanding the Higgs sector. Although work of George [152] showed that soft-wall models with a potential generated by a superpotential and with more than one bulk scalar have an unacceptable physical massless scalar, we hoped that this might not apply to this model. However, we have found that the zero mode is present and physical. Further extending the Higgs sector would likely not change this result. Thus, models in which the radion is a bulk Higgs doublet appear to be excluded.

We have studied a scenario with two Higgs doublets coupling to the Ricci scalar in the

TeV-brane of an RS model. Assuming CP-conservation, the inclusion of this term causes kinetic mixing between the CP-even scalars of the 2HDM and the radion field of the RS model.

The most up to date LHC measurements of the signal strengths of the SM Higgs boson were used to fit the model and the allowed $\cos(\beta-\alpha)$-$\tan\beta$ parameter space for type-I and type-II 2HDM were presented.

We have discussed two possible ways to differentiate this model from other scenarios with similar scalar states. One possibility is to look at the sum of squared couplings of the scalars to gauge bosons. This model predicts a small deviation of about 0.5% from the SM value which could be measured at a future ILC. The other possibility is to look at the ratio of decay widths to a pair of b quarks and Z bosons for both scalars. Future experiments might distinguish the scalars by determining the value of the mixing angles α and β.

Throughout this work we have taken the mass of the extra scalars to be in the range of 200-1000 GeV and we study the constraints that LHC searches of heavy resonances impose on the amount of mixing. The most stringent bounds arise if we take $\Lambda = 3$ TeV and $m_A = 700$ GeV where a radion is disfavored in the mass range $m_r < 780$ GeV while a heavy Higgs is disfavored in the mass range 300 GeV $< m_H <$ 750 GeV and $m_H < 250$ GeV and kinetic mixing for both, radion and Higgs, is constrained to $-4 < K_h,\ K_H < 4$. These constraints relax significantly by reducing m_A and increasing the value Λ.

Finally we showed how improvements of the experimental analysis for the decay topologies $X \to ZA$ and $A \to ZX$ where $X = r$ or H could further constrain the parameter space of, or possibly eliminate, the model

Chapter 4

The Strong CP Problem and Flavor Symmetry

4.1 Introduction

Within the SM one can write down the following CP violating operator

$$\mathcal{L} \supseteq \theta \frac{g_s^2}{32\pi^2} G^a_{\mu\nu} \tilde{G}^{a\mu\nu} \tag{4.1}$$

where $G^a_{\mu\nu}$ is the gluon field strength and $\tilde{G}^{a\mu\nu} \equiv \epsilon^{\mu\nu\alpha\beta} G^a_{\alpha\beta}$. Although this operator can be written as a total derivative and we can simply ignore it in perturbative calculations, it has non-trivial effects for non-perturbative processes. For example, it induces an electric dipole moment for the neutron [185] which is very constrained by experiments and leads to the upper bound [186]

$$|\bar{\theta}| \leq 10^{-10} \tag{4.2}$$

where $\bar{\theta} \equiv \theta + \text{argdet}((M_q))$ and M_q is the quark mass matrix. This strong upper limit implies there is a fine tuning between the two contributions unless there is a hidden mechanism that can render natural values without violating the experimental bound.

Different explanations have been proposed, e.g. [187,188] however the most popular and

the subject of this chapter is the one originally proposed by Peccei and Quinn (PQ) [17,189].

We now proceed to briefly review the basic ingredients of the PQ solution by considering a toy example, for more complete literature see Refs. [190, 191].

The mechanism postulates a global $U(1)_{PQ}$ symmetry spontaneously broken by a complex scalar sector and quarks transform chirally under this symmetry, thus acquiring masses from Yukawa couplings with the scalar, the Lagrangian can be written as

$$\mathcal{L} \supseteq V(\phi) + y\phi\bar{Q}_L Q_R + \text{h.c.} \tag{4.3}$$

Under the $U(1)_{\text{PQ}}$, the fields transform as

$$\phi \to e^{i\alpha}\phi, \quad Q \to e^{-i\gamma_5\alpha/2}Q, \tag{4.4}$$

and the classical Lagrangian is invariant under this chiral rotation however, the path integral measure transforms non-trivially [192, 193] and after spontaneous symmetry breaking is induced by a non-zero scalar vev, $\langle\phi\rangle = fe^{ia/f}$, obtaining

$$\mathcal{L} \supseteq yfe^{ia/f}\bar{Q}_L Q_R + \text{h.c.} + \alpha\frac{g_s^2}{32\pi^2}G^a_{\mu\nu}\tilde{G}^{a\mu\nu}, \tag{4.5}$$

where the field appearing in the exponential of the mass term is a pseudo Nambu-Goldstone boson of the spontaneously broken symmetry and is called the axion. A spacetime dependent chiral rotation can be performed and the axion will appear accompanied by a $G\tilde{G}$ term. Furthermore non-perturbative QCD effects induce a potential for the axion of the form

$$V(a) = \Lambda^4\left(1 - \cos\left(\alpha - \frac{a}{f}\right)\right), \tag{4.6}$$

for which the minimum of the axion potential is achieved for

$$\frac{\langle a\rangle}{f} = -\alpha, \tag{4.7}$$

cancelling the effective $G\tilde{G}$ in the action. This is essentially how the axion solution works. For a complete treatment within the chiral Lagrangian of QCD we recommend Ref. [194].

Having introduced the axion solution to the strong CP problem we now turn back to the SM where it is an experimental fact that the ratios of fermion masses, namely

$$\frac{m_e}{m_t} \sim 10^{-5}, \qquad \frac{m_\nu}{m_{\rm t}} \sim 10^{-11}, \tag{4.8}$$

exhibit a hierarchical pattern which as we know can be directly translated into hierarchies of their Yukawa couplings.

As we discussed in section 2.3, the Yukawa interactions are technically natural and therefore stable from radiative corrections. This means that the sense of worry of not knowing why these hierarchies arise is on a lower level relative to the strong CP problem and the electroweak hierarchy problem where it is evident that there must be some UV completion that engenders the observed values of parameters at low energies. Nevertheless, as theoretical physicists, we would still like to have a fundamental theory in which all free parameters arise naturally.

This brings us to the topic of flavor symmetries in which additional symmetries in the theory render operators with smaller Yukawa couplings to be non renormalizable and hence to be suppressed by some cut off scale M_F. These type of scenarios come with the name of Froggatt-Nielsen (FN) models [195], after the authors who first introduced them. A few years after the FN model, Wilczek [196] pointed out a possible connection between the PQ mechanism and flavor hierarchies. Since then many models have appeared in the literature.

To illustrate the idea more clearly, lets consider our toy model example from above and add an extra fermion with different quantum numbers but which transforms under $U(1)_{\rm PQ}$ as

$$E \to e^{-in\gamma_5\alpha/2}E, \quad \text{with} \quad n \in \mathbb{Z}^+, \tag{4.9}$$

then the Yukawa Lagrangian, including non renormalizable terms, contains

$$\mathcal{L} \supseteq y_Q \phi \; \bar{Q}_L Q_R + y_E \phi \left(\frac{\phi}{M_F} \right)^n \bar{E}_L E_R + \text{h.c.}, \tag{4.10}$$

where M_F corresponds to the cut off scale of the theory and the complex scalar is also called “flavon" in the literature. In this way we see that when the complex scalar acquires a vev, the fermions masses lead to the ratio

$$\frac{M_E}{M_Q} = \left(\frac{f}{M_F} \right)^n, \tag{4.11}$$

such that for a suitable value of n, a hierarchy $M_E \ll M_Q$ can be naturally explained. This toy model exemplifies how the axion solution to the strong CP problem and the FN mechanism for the flavor hierarchies can be unified in a single framework. Realistic scenarios that extend the SM and incorporate this idea can be found in the literature [197–200] these all come with the name of flavorful axions, flaxions or axiflavons.

For the rest of this chapter we will focus our attention on our flavorful axion model of Ref. [201] which offers a variant of this idea with the addition of a discrete symmetry based on the double tetrahedral group.

4.2 Flavorful Axion from the double Tetrahedral Group

A realistic flavor model is in general more complicated than the flavor toy model we presented above. For example, the symmetry breaking sector can have more complex functional structure with different scalars acquiring vevs at different energy scales thus breaking the flavor symmetry in successive steps. Furthermore the flavor symmetry group can be any combination of gauge or global, continuous or discrete and Abelian or non-Abelian, e.g. [202–208].

In the context of supersymmetric models it was realized that non-Abelian symmetries can be particularly useful to help suppress dangerous FCNC’s [209] and in Refs. [210–212]

supersymmetric flavor models based on a $U(2)$ global symmetry were introduced where besides the flavor hierarchies, these theories were successful in generating the correct values of the CKM matrix.

During the following years after these developments, in Ref. [213], it was proven that the smallest discrete group that can reproduce the successes of the supersymmetric $U(2)$ models was given by the product of $T' \times Z_3$ with T' the double tetrahedral group.

We will not delve into the group theoretic details about the T' group but will simply mention the most relevant properties that are relevant for the discussion of the flavorful axion model we implemented in [201]. For a more complete discussion see Refs. [213, 214]. The double tetrahedral group T' has the following representations: $\mathbf{1}^0$, $\mathbf{1}^{\pm}$, $\mathbf{2}^0$, $\mathbf{2}^{\pm}$, $\mathbf{3}$ where the triality superscript is a short-hand notation for ± 1 and indicates the multiplication rules for representations: trialities add under addition modulo three. The rules for multiplying representations are the following

$$\begin{aligned} &\mathbf{1} \otimes \mathbf{R} = \mathbf{R} \otimes \mathbf{1} = \mathbf{R} \quad \text{for any rep } \mathbf{R}, && \mathbf{2} \otimes \mathbf{2} = \mathbf{3} \oplus \mathbf{1}, \\ &\mathbf{2} \otimes \mathbf{3} = \mathbf{3} \otimes \mathbf{2} = \mathbf{2}^0 \oplus \mathbf{2}^+ \oplus \mathbf{2}^-, && \mathbf{3} \otimes \mathbf{3} = \mathbf{3} \oplus \mathbf{3} \oplus \mathbf{1}^0 \oplus \mathbf{1}^+ \oplus \mathbf{1}^-. \end{aligned} \tag{4.12}$$

Under Hermitian conjugation, trialities flip sign, so e.g. $(\mathbf{2}^+)^\dagger = \mathbf{2}^-$. The Glebsch-Gordan matrices for combining representations are summarized in an appendix in [214].

More recently a non-supersymmetric flavor model with T' symmetry appeared in Ref. [215] where the authors explored the viability of the model by letting the flavor scale M_F to be a free parameter that could vary from a few TeV up to the Planck scale. They also considered lower limits constraints on M_F from FCNCs mediated by the flavons and from their numerical fits they found that lower values of M_F were favored.

We now turn to the core subject of this section, the model we implemented in [201]. Here we went beyond the work of Ref. [215] in a number of ways: (i) they present a simplification of the model involving a smaller number of flavor-symmetry-breaking fields. While simplicity may be desirable by itself, the smaller field content allows a less cumbersome study of the flavon potential that leads to the spontaneous breaking of the flavor

symmetry, so that we can confirm the assumed pattern of symmetry breaking and study the spectrum of scalar states. (*ii*) We address the strong CP problem by promoting an Abelian factor that is required in the model from a Z_3 symmetry to an anomalous U(1) symmetry. This leads to a flavorful axion which leads to more stringent lower bounds on the flavor scale M_F than in [215] (as well as new avenues for discovery). The possibility of flavored axions due to a continuous Abelian factor in a T' flavor model was considered in a supersymmetric model in Ref. [216]; the present work gives a simple, nonsupersymmetric realization of this possibility. (*iii*) they extend the model to include the neutrino sector. As we describe later, one model building difficulty that has to be overcome is to explain how the small symmetry-breaking parameters that lead to pronounced hierarchies in the charged fermion Yukawa matrices lead to much less pronounced hierarchies in the neutrino mass matrix (as indicated, for example, by the two large mixing angles). The model will show how this outcome can be achieved.

4.2.1 The Model

The flavor symmetry is assumed to be given by $G_F = T' \times Z_3 \times U(1)$, where the last factor is anomalous and will allow for the existence of a flavorful axion. The flavor-symmetry-breaking sector consists of three complex scalar fields A, s, and ϕ, in the $\mathbf{1}^{0-}$, $\mathbf{1}^{00}$, and $\mathbf{2}^{0+}$ representations of $T' \times Z_3$, using the notation of Ref. [214]. Notably, the triplet flavon S of Ref. [215] has been omitted; the model is nonetheless viable, as we will discuss below. The complete field content and charge assignments for the model are shown in Table 4.1.

	A	s	ϕ	H	$\overline{Q}_L^a$	$\overline{Q}_L^3$	d_R^a	d_R^3	u_R^a	u_R^3	$\overline{L}^a$	$\overline{L}^3$	e_R^a	e_R^3
$T' \times Z_3$	$\mathbf{1^{0-}}$	$\mathbf{1^{00}}$	$\mathbf{2^{0+}}$	$\mathbf{1^{00}}$	$\mathbf{2^{0-}}$	$\mathbf{1^{00}}$	$\mathbf{2^{0-}}$	$\mathbf{1^{00}}$	$\mathbf{2^{0-}}$	$\mathbf{1^{00}}$	$\mathbf{2^{0-}}$	$\mathbf{1^{00}}$	$\mathbf{2^{0-}}$	$\mathbf{1^{00}}$
$U(1)$	0	1	0	0	0	0	0	-1	0	0	0	-1	0	0

Table 4.1: Charge assignments. The index $a = 1, 2$ is a generation label. The first four columns correspond to complex scalar fields, while the remainder are either right-handed standard model fermion fields or Dirac adjoints of left-handed ones.

Since the standard model fermions are charged under G_F, the Yukawa couplings, aside from that of the top quark, arise via higher-dimension operators involving the flavon fields. These are suppressed by appropriate powers of the flavor scale M_F, the cut off of the low-energy effective theory. When the flavon fields acquire vevs, these operators depend on the ratios

$$\langle\phi\rangle/M_F \equiv \begin{bmatrix} \epsilon \\ 0 \end{bmatrix}, \quad \langle A\rangle/M_F \equiv \epsilon', \quad \text{and} \quad \langle s\rangle/M_F \equiv \rho \ . \tag{4.13}$$

After flavor-symmetry breaking, the following Yukawa textures are generated:

$$Y_U \sim \begin{pmatrix} 0 & u_1\epsilon' & 0 \\ -u_1\epsilon' & u_2\epsilon^2 & u_3\epsilon \\ 0 & u_4\epsilon & u_5 \end{pmatrix}, \tag{4.14}$$

$$Y_D \sim \begin{pmatrix} 0 & d_1\epsilon' & 0 \\ -d_1\epsilon' & d_2\epsilon^2 & d_3\epsilon\,\rho \\ 0 & d_4\epsilon & d_5\rho \end{pmatrix}, \tag{4.15}$$

$$Y_E \sim \begin{pmatrix} 0 & l_1\epsilon' & 0 \\ -l_1\epsilon' & l_2\epsilon^2 & l_3\epsilon \\ 0 & l_4\epsilon\,\rho & l_5\rho \end{pmatrix}. \tag{4.16}$$

Here the u_i, d_i and l_i are (in general complex) $\mathcal{O}(1)$ parameters and only the leading-order expressions are presented. The non-zero entries differ in two ways from the textures of Ref. [215]: the 2-2 entries above are $\mathcal{O}(\epsilon^2)$, rather than $\mathcal{O}(\epsilon)$, due to the absence of the T'-triplet flavon. However, the factors of ρ appear in different locations, so that the end results are qualitatively similar. For example, the suppression of the 1-2 block of Y_u in Ref. [215] by an overall factor of ρ is mimicked here by the higher-order 2-2 entry and the proportionally smaller numerical value of ϵ', as we will see later. We also note that there will be CP violation in the model even if all the operator coefficients defined at the level of the Lagrangian are real, due to imaginary numbers in Clebsch-Gordan coefficients; these would lead, for example, to factors of i in the 2-2 entries of Y_U, Y_D and Y_E. In general, however, all operator coefficients are themselves complex, and the 10 phase degrees of freedom in Y_U and Y_D can be used to obtain the desired CKM phase rather easily. In light

of this, and to simplify our subsequent numerical analysis, we have chosen all the operator phases so that the parameters shown in Eqs. (4.14)-(4.16) are real, and omit the CKM phase from our global fit in Sec. 4.2.3.

4.2.2 The Flavon Potential

In this subsection, we consider the flavon potential, to confirm that the pattern of vevs assumed in Eq. (4.13) can be achieved and to study the spectrum of physical scalar states. We will do this by assuming the desired vev pattern, and imposing the extremization conditions on the potential to fix some of its otherwise free parameters. We then check the second-derivative matrix of the potential for positive definiteness. To simplify the discussion, we exclude the s field, since it is a trivial singlet under the non-Abelian discrete flavor group and it is straightforward to write down a potential involving s alone that provides for its vev. Including terms that couple s to the other fields, *e.g.*, $|s|^2|\phi^2|$, will not qualitatively change our results providing that their couplings are not too large, which is good enough for a proof of principle. We are particularly interested in accidental global symmetries that arise in the potential as a consequence of the $T' \times Z_3$ discrete symmetry. These lead to pseudo-goldstone bosons whose masses arise via higher-dimension operators. We estimate the masses of these states to confirm that they are not so light that their phenomenological consequences need to be taken into account. In this case, the only light state that will have interesting flavor-changing physics will be a single flavorful axion associated with the s field.

The most general scalar potential for a singlet and a doublet transforming as $A \sim \mathbf{1^{0-}}$, $\phi \sim \mathbf{2^{0+}}$ under $T' \times Z_3$, respectively, is given by

$$V = V_A + V_\phi + V_{A\phi}, \tag{4.17}$$

where

$$V_A = m_A^2 |A|^2 + \mu \left(A^3 + A^{*3}\right) + \lambda_A \left|A\right|^4, \tag{4.18}$$

$$V_\phi = m_\phi^2 \left|\phi\right|^2 + \lambda_\phi \left|\phi\right|^4, \tag{4.19}$$

$$V_{A\phi} = \lambda_{A\phi} \left|A\right|^2 |\phi|^2. \tag{4.20}$$

Note that this potential has an accidental $U(2)_\phi$ global symmetry as well as an additional $U(1)_A$ symmetry in the limit $\mu \to 0$. We parametrize the fields in terms of their real degrees of freedom

$$A = \frac{1}{\sqrt{2}}(A_1 + iA_2) \ , \tag{4.21}$$

and

$$\phi = \frac{1}{\sqrt{2}} \begin{pmatrix} \phi_{11} + i\phi_{12} \\ \phi_{21} + i\phi_{22} \end{pmatrix}. \tag{4.22}$$

The Yukawa textures in Eqs. (4.14)-(4.16) are reproduced provided only the following real fields develop vevs:

$$\left\langle \phi_{11} \right\rangle / \sqrt{2} = \epsilon \, M_F \quad \text{and} \ \left\langle A_1 \right\rangle / \sqrt{2} = \epsilon' \, M_F \ . \tag{4.23}$$

The location of a local minimum of the potential is determined by six first-derivative equations, corresponding to the six real scalar fields in Eqs. (4.21) and (4.22). However, for the assumed vev pattern, only two of these equations are non-vanishing,

$$\left.\frac{\partial V}{\partial A_1}\right|_{\text{vev}} = \sqrt{2}\epsilon' M_F (m_A^2 + 2\epsilon'^2 M_F^2 \lambda_A + \epsilon^2 M_F^2 \lambda_{A\phi} + 3\epsilon' M_F \mu) = 0 \ , \tag{4.24}$$

$$\left.\frac{\partial V}{\partial \phi_{11}}\right|_{\text{vev}} = \sqrt{2}\epsilon M_F (m_\phi^2 + \epsilon'^2 M_F^2 \lambda_{A\phi} + 2\epsilon^2 M_F^2 \lambda_\phi) = 0 \ , \tag{4.25}$$

were the subscript “vev" indicates that the fields have been set to their vevs, those shown in Eq (4.23) with all others vanishing. For a given choice of the dimensionless couplings,

Eqs. (4.24) and (4.25) allow us to determine the mass parameters

$$m_A^2 = -2\epsilon'^2 M_F^2 \lambda_A - \epsilon^2 M_F^2 \lambda_{A\phi} - 3\epsilon' M_F \mu \ , \tag{4.26}$$

$$m_\phi^2 = -\epsilon'^2 M_F^2 \lambda_{A\phi} - 2\epsilon^2 M_F^2 \lambda_\phi . \tag{4.27}$$

To obtain the mass spectrum, we construct the second derivative matrix for the potential in terms of the six real scalar fields, evaluated with the assumed vevs, and with mass parameters fixed by Eqs. (4.26) and (4.27). In the basis $(\phi_{11}, A_1, A_2, \phi_{12}, \phi_{21}, \phi_{22})$ we find

$$m^2_{scalar} = \begin{pmatrix} 4\epsilon^2 M_F^2 \lambda_\phi & 2\epsilon\epsilon' M_F^2 \lambda_{A\phi} & 0 & 0 & 0 & 0 \\ 2\epsilon\epsilon' M_F^2 \lambda_{A\phi} & \epsilon' M_F (4\epsilon' M_F \lambda_A + 3\mu) & 0 & 0 & 0 & 0 \\ 0 & 0 & -9\epsilon' M_F \mu & 0 & 0 & 0 \\ 0 & 0 & 0 & 0 & 0 & 0 \\ 0 & 0 & 0 & 0 & 0 & 0 \\ 0 & 0 & 0 & 0 & 0 & 0 \end{pmatrix} \tag{4.28}$$

The three non-vanishing eigenvalues of the mass squared matrix are positive, provided that $\mu < 0$ and (assuming ϵ, ϵ' and λ_ϕ are positive)

$$|\mu| < \frac{\epsilon' M_F}{3\lambda_\phi}(4\lambda_A \lambda_\phi - \lambda_{A\phi}^2) \quad \text{and} \quad |\mu| < \frac{4}{3}\frac{M_F}{\epsilon'}(\epsilon^2 \lambda_\phi + \epsilon'^2 \lambda_A) \ , \tag{4.29}$$

which is easily arranged. The three massless states are expected from Goldstone's Theorem, since the $\mathrm{U}(2)_\phi$ symmetry is spontaneously broken to a residual U(1) symmetry that rotates the second component of the ϕ column vector by a phase. However, these zero eigenvalues are lifted when one takes into account corrections to the potential from higher-dimension operators that break the accidental $\mathrm{U}(2)_\phi$ global symmetry. We find that the lowest-order operators that have this effect occur at dimension 6,

$$V_{hd} = \frac{1}{M_F^2}\left(c_{61}\left[(\phi\,\phi)_{\mathbf{3}}(\phi\,\phi)_{\mathbf{3}}\right]_{\mathbf{3}}(\phi\,\phi)_{\mathbf{3}} + \text{h.c.}\right) + c_{62}\frac{1}{M_F^2}\left[(\phi^*\,\phi^*)_{\mathbf{3}}(\phi\,\phi)_{\mathbf{3}}\right]_{\mathbf{3}}(\phi^*\,\phi)_{\mathbf{3}} + \cdots \ , \tag{4.30}$$

where the subscript indicates the T' representation of the given product, with Clebsch-Gordan factors left implicit. We have studied the eigenvalues of Eq. (4.28) numerically

after including the additional potential terms in V_{hd}, and find that all the eigenvalues are positive and non-vanishing; the masses of the three pseudo-goldstone bosons are of order $\epsilon^2 M_F$. We will see later that the numerical values of our symmetry breaking parameters and our extension to the neutrino sector will imply that this scale corresponds to roughly 10^{12} GeV. We therefore do not expect meaningful phenomenological bounds on the three pseudo-goldstone states. We note that there are also dimension-5 operators that one can write down which correct the potential (*e.g.*, $A^3|\phi|^2$ and $A^3|A|^2$) but these do not break the accidental $\mathrm{U}(2)_\phi$ symmetry and provide higher-order corrections to the eigenvalues that are already non-vanishing at lowest order.

4.2.3 Fit to quarks and charged leptons

In this subsection, we verify that the Yukawa textures in Eqs. (4.14)-(4.16) reproduce the correct masses and mixing angles for the charged fermions, by performing a global fit that takes into account running from a high scale (which we will take to be 4×10^{16} GeV, to be consistent with our later discussion of the neutrino sector) down to the weak scale. This is the same analysis that was performed in Ref. [215] for an arbitrary M_F scale, but is now modified to take into account the textures predicted in the present model. We take the model parameters $\{u_i, d_i, l_i, \epsilon, \epsilon', \rho\}$ to be real as a simplifying assumption since, as discussed earlier, there is no difficulty in accommodating a CKM phase if one allows an arbitrary phase parameter for every operator coefficient. The experimental inputs are the quark and lepton masses and CKM angles, which we associate with the scale m_Z (*i.e.*, we ignore weak scale threshold corrections). We seek solutions in which the order one parameters are in fact not far from one, while predictions for the observables, renormalized at the weak scale, are within two standard deviations of experimental values. Employing the same technique as Refs. [214] and [215], we construct a function $\widetilde{\chi}$ whose minimization

achieves this goal:

$$\widetilde{\chi}^2 = \sum_{i=1}^{9} \left(\frac{m_i^{th} - m_i^{exp}}{\Delta m_i^{exp}} \right)^2 + \left(\frac{|V_{us}^{th}| - |V_{us}^{exp}|}{\Delta V_{us}^{exp}} \right)^2 + \left(\frac{|V_{ub}^{th}| - |V_{ub}^{exp}|}{\Delta V_{ub}^{exp}} \right)^2 + \left(\frac{|V_{cb}^{th}| - |V_{cb}^{exp}|}{\Delta V_{cb}^{exp}} \right)^2 + \sum_{i=1}^{5} \left(\frac{\ln |u_i|}{\ln 3} \right)^2 + \sum_{i=1}^{5} \left(\frac{\ln |d_i|}{\ln 3} \right)^2 + \sum_{i=1}^{5} \left(\frac{\ln |\ell_i|}{\ln 3} \right)^2 \quad . \tag{4.31}$$

The first four terms would be present in a conventional chi-squared function, and place weight on how close the theoretical predictions for observables are to experimental observations, relative to the experimental error. The experimental errors are handled as in Refs. [214,215]: they are inflated to 1% of the central measured value if the error is smaller that this amount. This takes into account theoretical uncertainties (for example, two-loop running effects) that have been omitted. The remaining three terms of Eq. (4.31) place weight on the coefficients having values that are order one, the expectation of naive dimensional analysis. Including these terms is equivalent to assuming that the coefficients are distributed with a log-normal distribution with mean 1 and standard deviation $\sigma = \ln(3)/2$ such that the absolute value of an element drawn from the distribution has a 95% probability to lie in the range $[0.3, 3]$. There are a total of 12 observables (nine masses and three mixing angles) and, given the stated constraints on the model parameters, the only three genuine free parameters, $\{\epsilon, \epsilon', \rho\}$. Thus, we expect a good fit if $\widetilde{\chi}^2 \approx 9$. The best fit values together with the experimental and theoretical predictions are presented in Table 4.2. We note that our successful results might be anticipated from the qualitatively similar Yukawa textures obtained in U(2) flavor models [200, 217], a further example of the similarities between T' models and U(2) models that was the focus of Refs. [213, 214].

Finally, we note that global symmetries are expected to be broken by quantum gravity effects [218], but we can assume that there is an ultraviolet completion which allows the U(1) symmetry to arise as a consequence of the continuous and discrete gauge symmetries that are present in a more complete theory. Another concern in the present framework is that the breaking of discrete symmetries can lead to potential domain-wall problems.

However, these can be rendered harmless it the domain regions are widely separated due to inflation. We will find later in Sec. 4.2.4 that M_F is constrained to be sufficiently high so that any problems with domain walls may be eliminated via this mechanism.

Table 4.2: Fit to the charged fermion masses and mixing angles. All masses are given in GeV. (Note that m_t is the $\overline{MS}$ mass, not the pole mass.) The value of the quantity $\widetilde{\chi}^2$ defined in the text is 12.3. Running from the flavor scale M_F down to the Z mass is taken into account, with $M_F = 4 \times 10^{16}$ GeV, (see Sec. 4.2.6) chosen for the purpose of illustration.

Best Fit Parameters		
$\epsilon = 2.42 \times 10^{-2},\ \epsilon' = 9.75 \times 10^{-5},\ \rho = -1.38 \times 10^{-2}$		
$u_1 = 1.22$	$d_1 = 0.662$	$\ell_1 = 0.612$
$u_2 = -0.671$	$d_2 = 1.29$	$\ell_2 = 0.643$
$u_3 = -2.26$	$d_3 = -1.02$	$\ell_3 = 0.352$
$u_4 = -0.702$	$d_4 = -0.276$	$\ell_4 = 2.40$
$u_5 = 0.384$	$d_5 = 0.376$	$\ell_5 = 0.295$
Observable	Expt. Value from [228]	Fit Value
m_u	$(2.2 \pm 0.45) \times 10^{-3}$	2.30×10^{-3}
m_c	1.275 ± 0.03	1.274
m_t	160 ± 4.5	160.0
m_d	$(4.7 \pm 0.4) \times 10^{-3}$	5.42×10^{-3}
m_s	$(9.5 \pm 0.6) \times 10^{-2}$	9.16×10^{-2}
m_b	4.18 ± 0.035	4.17
m_e	$(5.11 \pm 1\%) \times 10^{-4}$	5.11×10^{-4}
m_μ	$0.106 \pm 1\%$	0.106
m_τ	$1.78 \pm 1\%$	1.78
$\lvert V_{us}\rvert$	$0.225 \pm 1\%$	0.223
$\lvert V_{ub}\rvert$	$(3.65 \pm 0.12) \times 10^{-3}$	3.62×10^{-3}
$\lvert V_{cb}\rvert$	$(4.21 \pm 0.08) \times 10^{-2}$	4.17×10^{-2}

4.2.4 The Flavorful Axion

The model we have presented includes a flavon field s, charged under the U(1) factor of the flavor group, which assures, for example, the correct values of the bottom quark and tau lepton Yukawa couplings. This U(1) also serves as a Peccei-Quinn (PQ) symmetry and its spontaneous breaking leads to a flavorful axion. Only the third generation right-handed down quark and the third generation left-handed lepton doublet have nontrivial charges

under the U(1) symmetry (see Table 4.1), but rotation to the mass eigenstate basis will induce axion couplings to fields of the first two generations. The axion is identified via the non-linear representation

$$s = \frac{v_s + \sigma}{\sqrt{2}} e^{ia/v_s} \quad . \tag{4.32}$$

The radial component σ is a heavy degree of freedom and is integrated out of the low-energy effective field theory. The phase field a is the Goldstone boson of the spontaneously broken U(1)≡U(1)$_{PQ}$ symmetry and is identified with the QCD axion. Non-perturbative QCD effects generate a potential for the axion, with the minimum corresponding to vanishing of the $\overline{\theta}$ parameter of QCD, solving the strong CP problem. For complete reviews on this subject see Refs. [18, 219].

The axiflavon couplings to fermions originate from the following Yukawa couplings

$$\mathcal{L}_{Ya} = -\left[\overline{Q}^i Y^d_{i3} H d^3_R + \overline{L}^3 Y^e_{3j} H e^j_R\right] \frac{s}{M_F} + \text{ h.c.}\,, \tag{4.33}$$

or more explicitly

$$\begin{aligned} \mathcal{L}_{Ya} &= -\left[d_3 \overline{Q}^a \epsilon_{ab} \left(\frac{\langle \phi^b \rangle}{M_F}\right) H d^3_R + d_5 \overline{Q}^3 H d^3_R \right. \\ &+ \left. l_4 \overline{L}^3 \epsilon_{ab} \left(\frac{\langle \phi^b \rangle}{M_F}\right) H e^a_R + l_5 \overline{L}^3 H e^3_R\right] \frac{v_s\, e^{ia/v_s}}{\sqrt{2} M_F} + \text{ h.c.}\,, \end{aligned} \tag{4.34}$$

where ϵ_{ab}, $a, b = 1, 2$ is the Clebsch-Gordan matrix that allows one to combine two $\mathbf{2}^0$ representations of T' into a $\mathbf{1}^0$. Setting the ϕ flavon to its vev, one obtains

$$\mathcal{L}_{Ya} = -\left[-d_3 \epsilon\, \overline{Q}^2 H d^3_R + d_5 \overline{Q}^3 H d^3_R - l_4 \epsilon\, \overline{L}^3 H e^2_R + l_5 \overline{L}^3 H e^3_R\right] \frac{v_s\, e^{ia/v_s}}{\sqrt{2} M_F} + \text{ h.c.} \tag{4.35}$$

Performing the usual non-linear field redefinition of the third generation fermions

$$d^3_R \to e^{-ia/v_s} d^3_R, \quad \overline{L}^3 \to e^{-ia/v_s} \overline{L}^3, \tag{4.36}$$

we remove the axion entirely from the Yukawa sector, but instead induce derivative in-

teractions coming from the original fermion kinetic terms. For the charged fermions, one finds

$$\mathcal{L} \supseteq \frac{\partial_\mu a}{v_s}\left[\bar{d}_i\gamma^\mu(K_d^\dagger)_{i3}(K_d)_{3j}\frac{(1+\gamma_5)}{2}d_j + \bar{e}_i\gamma^\mu(U_e^\dagger)_{i3}(U_e)_{3j}\frac{(1-\gamma_5)}{2}e_j\right] \ . \tag{4.37}$$

Here K_d (U_e) is the right-handed (left-handed) rotation that diagonalize the Yukawa interactions, where in our conventions a generic Yukawa matrix Y would be diagonalized by $Y = U_L Y^{diag} U_R^\dagger$. Notice that the axion interactions with the fermion mass eigenstates are in general not diagonal and therefore induce flavor-changing neutral currents (FCNC) at tree-level. Flavon FCNCs are very well constrained experimentally [220, 221] and we will discuss these constraints in the next subsection. See Refs. [222–224] for other axion models with FCNCs at tree-level.

While our phenomenological bounds will come from the couplings in Eq. (4.37), we give the axion couplings to two gauge fields here for completeness. After the anomalous chiral rotation in Eq. (4.36), the axion reappears in an effective interaction with the gluon field strength and its dual, namely

$$\mathcal{L} = \frac{\alpha_s}{8\pi}\frac{a}{v_s}N_{DW}G^a_{\mu\nu}\widetilde{G}^{a\mu\nu}. \tag{4.38}$$

With the charge assignments of Table 4.1, we obtain the domain-wall number

$$N_{DW} = \left[2\sum_i X_Q^i - \sum_i X_u^i - \sum_i X_d^i\right] = 1 \ , \tag{4.39}$$

where the X_a represent the U(1) charges for left-handed and the right-handed fermion fields. Since $N_{DW} = 1$, there is one minimum of the axion potential. We identify the axion decay constant as

$$f_a = |v_s/N_{DW}| \ . \tag{4.40}$$

The PQ charge assignments give rise to $\mathrm{U}(1)_Y^2$ $\mathrm{U}(1)_{PQ}$ and $\mathrm{SU}(2)^2 U(1)_{PQ}$ anomalies and

therefore axion couplings to hypercharge and electroweak gauge bosons are induced, namely

$$\mathcal{L} \supseteq \frac{g'^2}{32\pi^2}\frac{a}{v_s}(2N_B)B_{\mu\nu}\widetilde{B}^{\mu\nu} + \frac{g^2}{32\pi^2}\frac{a}{v_s}N_W W^a_{\mu\nu}\widetilde{W}^{a\mu\nu}. \tag{4.41}$$

Rewriting this piece of the Lagrangian in the gauge boson mass eigenstate basis one obtains the axion couplings to photons

$$\mathcal{L}_{\gamma a} = \frac{\alpha_{EM}}{8\pi}\frac{a}{v_s}(2N_B + N_W)F_{\mu\nu}\tilde{F}^{\mu\nu} \tag{4.42}$$

where in this model one obtains

$$N_B = 3\left[2\sum_i \left(\frac{1}{6}\right)^2 X_Q^i - \sum_i \left(\frac{2}{3}\right)^2 X_u^i - \sum_i \left(-\frac{1}{3}\right)^2 X_d^i\right] \tag{4.43}$$

$$+\,2\sum_i \left(-\frac{1}{2}\right)^2 X_L^i - \sum_i (-1)^2 X_e^i = \frac{5}{6}, \tag{4.44}$$

$$N_W = \sum_i X_L^i + 3\sum_i X_Q^i = 1, \tag{4.45}$$

and thus the ratio of the electromagnetic to color anomalies is

$$\frac{2N_B + N_W}{N_{DW}} = \frac{8}{3}. \tag{4.46}$$

As noted in other flavored axion models that make the same prediction for this ratio [199], this is consistent with the predictions of the simplest DFSZ axion models [18, 219].

4.2.5 Constraints from meson decays

As can be seen from the axion couplings to fermions in Eq. (4.37), our model predicts flavor violating processes, *e.g.*, heavy meson decays like $K^+ \to \pi^+ a$. The branching fraction for a generic meson two-body decay $P \to P'\, a$ is given by [197]

$$BR(P \to P' a) = \frac{1}{64\pi\Gamma(P)}\frac{|(K_d)^\dagger_{i3}(K_d)_{3j}|^2}{f_a^2} m_P^3 \left(1 - \frac{m_{P'}^2}{m_P^2}\right)^3 |f_+(0)|^2 \tag{4.47}$$

where $P = (\bar{q}_i q)$, $P' = (\bar{q}_j q)$ and the indices ij denote the constituent quarks. The function $f_+(q^2)$ is the form factor from hadronic physics calculations and $q = q_P - q_{P'}$ is the momentum transfer to the axion; one may take $q^2 \approx 0$ as the axion is very light. The axion mass is the same as a QCD axion, $m_a \approx 6 \times 10^{-6} \cdot (10^{12}\ \text{GeV}/f_a)\ \text{eV}$ [197]; we will see that the strongest bounds presented later in this section imply $m_a \times 10^{-4}$eV, while the neutrino model discussed in the next section corresponds to $m_a \approx 7 \times 10^{-9}$eV.

Experimental bounds on different heavy mesons decays are summarized in Ref. [197]. In Table 4.3, we quote the most relevant of these constraints and indicate the relevant experimental references. The precise numerical bounds that follow from the fit presented in Sec. 4.2.3 are displayed in the last column of this table.

To understand our results qualitatively, it is useful to parameterize the rotation matrices that correspond to the fit in Table 4.2 in terms of powers of the Cabibbo angle $\lambda \approx 0.22$. We find numerically that K_d and U_e have the qualitative form

$$K_d \sim \begin{pmatrix} 1 & \lambda & \lambda^5 \\ \lambda & 1 & 1 \\ \lambda & 1 & 1 \end{pmatrix} \quad \text{and} \quad U_e \sim \begin{pmatrix} 1 & \lambda & \lambda^5 \\ \lambda^2 & 1 & 1 \\ \lambda^2 & 1 & 1 \end{pmatrix} \ . \tag{4.48}$$

The relevant combinations that determine the results in Tables 4.3 are

$$(K_d^\dagger)_{i3}(K_d)_{3j} \sim \begin{pmatrix} \lambda^2 & \lambda & \lambda \\ \lambda & 1 & 1 \\ \lambda & 1 & 1 \end{pmatrix} \quad \text{and} \quad (U_e^\dagger)_{i3}(U_e)_{3j} \sim \begin{pmatrix} \lambda^3 & \lambda^2 & \lambda^2 \\ \lambda^2 & 1 & \lambda \\ \lambda^2 & \lambda & 1 \end{pmatrix} . \tag{4.49}$$

Table 4.3: Experimental constraints on the branching fractions of heavy mesons decays (second column), derived bounds on the axion decay constant times flavor rotation matrix elements from Ref. [197] (third column) and lower bound on the axion decay constant using the numerical value of the matrix element from the fit presented in Sec. 4.2.3 (fourth column).

Decay	Branching Ratio	Bound (f_a/GeV)	Bound from fit
$K^+ \to \pi^+ a$	$< 0.73 \times 10^{-10}$ [225]	$> 3.45 \times 10^{11} \lvert(K_d^\dagger)_{23}(K_d)_{31}\rvert$	$f_a > 6.3 \times 10^{10}$ GeV
$K_L^0 \to \pi^0 a$	$< 5 \times 10^{-8}$ [226]	$> 1.35 \times 10^{10} \lvert(K_d^\dagger)_{23}(K_d)_{31}\rvert$	$f_a > 2.5 \times 10^{9}$ GeV
$B^\pm \to \pi^\pm a$	$< 4.9 \times 10^{-5}$ [227]	$> 5.0 \times 10^{7} \lvert(K_d^\dagger)_{33}(K_d)_{31}\rvert$	$f_a > 7.4 \times 10^{6}$ GeV
$B^\pm \to K^\pm a$	$< 4.9 \times 10^{-5}$ [227]	$> 6.0 \times 10^{7} \lvert(K_d^\dagger)_{33}(K_d)_{32}\rvert$	$f_a > 2.8 \times 10^{7}$ GeV

The strongest bound in this model comes from the heavy meson decay $K^+ \to \pi^+ a$

giving

$$f_a > 6.3 \times 10^{10} \text{ GeV}. \tag{4.50}$$

Given the identification $f_a = |v_s/N_{DW}| = \sqrt{2}|\rho|M_F$, we can translate this to a bound on the flavor scale

$$M_F > 3.2 \times 10^{12} \text{ GeV}. \tag{4.51}$$

Axion mixing with neutral hadronic mesons does not lead to competitive bounds and will not be discussed here. See Ref. [197] for a treatment of these effects.

The authors also found lower bounds from lepton decays but these turn out to be less stringent and will not be presented in this dissertation.

4.2.6 Neutrino Sector

In this section, we consider how our model may be extended to explain the observed neutrino masses and mixing angles. In doing so, we face an immediate challenge: how can we explain two large neutrino mixing angles in a theory where symmetry breaking is achieved through two small parameters, ϵ and ϵ', that are of order 10^{-2} and 10^{-4}, respectively? A similar problem presents itself when one considers the neutrino mass squared differences. The smallness of the overall neutrino mass scale can be explained via the see-saw mechanism; we will implement a type-I see-saw mechanism below, involving three right-handed neutrinos. Choice of the right-handed neutrino mass scale allows us to fix one of the observed neutrino mass squared differences, for example, Δm^2_{32}; what is then determined by the symmetry breaking parameters is the ratio $\Delta m^2_{32}/\Delta m^2_{21}$, which is found experimentally to be 33.3 ± 1.03 [228], assuming a normal, rather than inverted, neutrino mass hierarchy (which is the case on our model). One would expect that the theoretical prediction for $\Delta m^2_{32}/\Delta m^2_{21}$ is proportional to ratios of powers of ϵ and ϵ'; if this quantity is not $\mathcal{O}(1)$, then one finds typically that the predicted value is either much too large or too small to account for the experimental value. This is a consequence of the small and distinctly hierarchical values of ϵ and ϵ'. On the other hand, if the ratio $\Delta m^2_{32}/\Delta m^2_{21}$ is

approximately independent of ϵ and ϵ', then it is a function of the order one coefficients in the theory alone. In this case, a value of 33.3 can be obtained for a rather mundane reason: The see-saw formula tells us that the mass matrix of the light, left-handed neutrino mass eigenstates is given by

$$M_{LL} \approx M_{LR} M_{RR}^{-1} M_{LR}^{\dagger} \ , \tag{4.52}$$

which implies that the eigenvalues of M_{LL} will typically be of cubic order in quantities of $\mathcal{O}(1)$, either operator coefficients or their inverse. Here, M_{LR} represents the neutrino Dirac mass matrix, while M_{RR} is the Majorana mass matrix for the right-handed neutrinos. The numerator and denominator of $\Delta m^2_{32}/\Delta m^2_{21}$ then each depend on terms that are of *sixth* order in quantities that are $\mathcal{O}(1)$, with each typically falling somewhere between 1/3 and 3 in absolute value, given our earlier assumptions. Noting that $1.8^6 \approx 34$, one can understand how easy it is to take input matrices with coefficients that are of $\mathcal{O}(1)$ and still obtain a mass-squared-difference ratio that is consistent with the experimental value. This observation is relevant to our solution below.

We introduce three right-handed neutrinos that are uncharged under the Peccei-Quinn symmetry and have $T' \times Z_3$ charges

$$\nu_R^1 \sim \mathbf{1}^{0-}, \quad \text{and} \quad \nu_R^{2,3} \sim \mathbf{1^{00}} \ . \tag{4.53}$$

The Dirac and Majorana mass matrices have the following $T' \times Z_3 \times U(1)$ transformation properties

$$M_{LR} \sim \left(\begin{array}{cc|c} \mathbf{2}^{0-} & \mathbf{2}^{0+} & \mathbf{2}^{0+} \\ \hline \mathbf{1}^{0+}_{+1} & \mathbf{1}^{00}_{+1} & \mathbf{1}^{00}_{+1} \end{array}\right) \quad \text{and} \quad M_{RR} \sim \left(\begin{array}{cc|c} \mathbf{1}^{0-} & \mathbf{1}^{0+} & \mathbf{1}^{0+} \\ \mathbf{1}^{0+} & \mathbf{1}^{00} & \mathbf{1}^{00} \\ \hline \mathbf{1}^{0+} & \mathbf{1}^{00} & \mathbf{1}^{00} \end{array}\right) \ , \tag{4.54}$$

where we have indicated U(1) charges with a subscript. This leads to the textures

$$M_{LR} = \frac{v}{\sqrt{2}} \begin{pmatrix} b_1\epsilon & 0 & 0 \\ 0 & b_2\epsilon & b_3\epsilon \\ b_4\rho\,\epsilon' & b_5\rho & b_6\rho \end{pmatrix}, \quad \text{and} \quad M_{RR} = \begin{pmatrix} c_1\epsilon' M_F & c_2\epsilon' M_F & c_3\epsilon' M_F \\ c_2\epsilon' M_F & M_{22} & M_{23} \\ c_3\epsilon' M_F & M_{23} & M_{33} \end{pmatrix}. \tag{4.55}$$

Here the b_i and c_i are $\mathcal{O}(1)$ coefficients. Since the elements labelled M_{22}, M_{23} and M_{33} in M_{RR} are each flavor-group invariant, they don't necessarily have to be at the same scale as M_F, or as each other. For the purposes of demonstrating the viability of the neutrino sector, we will take these elements to be at the scale $\epsilon' M_F$, so that M_{RR} takes the form

$$M_{RR} = \epsilon' M_F \begin{pmatrix} c_1 & c_2 & c_3 \\ c_2 & c_4 & c_5 \\ c_3 & c_5 & c_6 \end{pmatrix} \equiv \epsilon' M_F \widetilde{M}_{RR}. \tag{4.56}$$

In other words, with this choice, the right-handed Majorana matrix is a complete arbitrary matrix with $\mathcal{O}(1)$ entries, $\widetilde{M}_{RR}$, times the scale $\epsilon' M_F$. The Dirac mass matrix also has considerable freedom. Noting that our earlier fits indicated $\rho \approx \mathcal{O}(\epsilon)$, we can redefine the coefficients b_5 and b_6, and drop the 13 entry, which is higher order. Then we see that M_{LR} is approximately of the form

$$M_{LR} \approx \frac{v\,\epsilon}{\sqrt{2}} \begin{pmatrix} b_1 & 0 & 0 \\ 0 & b_2 & b_3 \\ 0 & b_5 & b_6 \end{pmatrix} \equiv \frac{v\,\epsilon}{\sqrt{2}} \begin{pmatrix} b_1 & 0 \\ 0 & \widetilde{Y}_{LR} \end{pmatrix} \ , \tag{4.57}$$

where $\widetilde{Y}_{LR}$ is an arbitrary, two-by-two matrix with $\mathcal{O}(1)$ entries. The 10 free parameters in Eqs. (4.56) and the approximation shown in (4.57) are more than sufficient to obtain the desired values of $\Delta m^2_{32}/\Delta m^2_{21}$, as well as $\sin^2\theta_{12}$, $\sin^2\theta_{13}$ and $\sin^2\theta_{23}$, while maintaining $\mathcal{O}(1)$ operator coefficients. The dependence of the output on products of the coefficients allows numerical values like 33 (the experimental value of $\Delta m^2_{32}/\Delta m^2_{21}$) or 1/33 (very close to θ^2_{13}) to arise without fine tunings. We note that the form of Eq. (4.57), with a non-vanishing 1-1 entry, is a consequence of the different charge assignment for the first-generation right-handed neutrino field. This entry of M_{LR} originates from a charge conjugated $\mathbf{2}^{0+}$ flavon; in T', as in SU(2), $\mathbf{2} \sim i\sigma^2\mathbf{2}^*$, which flips the relative location of the doublet vev in the first two columns of M_{LR}.

An example of a viable parameter set for the neutrino sector is shown in Table 4.4. The neutrino mixing angles are defined via a standard parametrization of the PMNS matrix,

Table 4.4: Example of a viable parameter choice for the neutrino sector.

Parameters		
$\epsilon = 2.42 \times 10^{-2},\ \epsilon' = 9.75 \times 10^{-5},\ \rho = -1.38 \times 10^{-2}$		
$b_1 = 1.66$	$b_2 = 1.07$	$b_3 = 2.10$
$b_4 = 1.11$	$b_5 = -0.891$	$b_6 = 1.61$
$c_1 = 2.91$	$c_2 = 1.04$	$c_3 = 0.662$
$c_4 = 1.21$	$c_5 = 1.37$	$c_6 = 1.44$
Observable	Expt. Value from [228]	Fit Value
$\frac{\triangle m^2_{32}}{\triangle m^2_{21}}$	33.3 ± 1.03	33.8
$\sin^2\theta_{12}$	0.307 ± 0.013	0.307
$\sin^2\theta_{23}$	0.417 ± 0.025	0.444
$\sin^2\theta_{13}$	$(2.12 \pm 0.08) \times 10^{-2}$	2.11×10^{-2}

which we call U below,

$$U = U_e^\dagger U_\nu, \tag{4.58}$$

where U_e (U_ν) is a unitary matrix that diagonalizes the charged lepton (left-handed Majorana) matrix following our earlier convention, *i.e.*, $M_{LL} = U_\nu M_{LL}^{diag} U_\nu^\dagger$. We can extract the mixing angles via the relations

$$\sin^2\theta_{13} = U_{13}^2 \quad , \quad \sin^2\theta_{23} = U_{23}^2/(1-U_{13}^2) \quad \text{and} \quad \sin^2\theta_{12} = U_{12}^2/(1-U_{13}^2) \ . \tag{4.59}$$

For the purpose of illustration, we fix ϵ, ϵ' and ρ, as well as the coefficients l_i appearing in the charged lepton Yukawa matrix, to the values that were obtained in our previous global fit of the charged fermions, Table 4.2. A viable choice of neutrino sector parameters b_i and c_i is presented in Table 4.4. These were obtained by defining a $\widetilde{\chi}^2_\nu$ for the neutrino sector that takes into account the neutrino observables listed in the table and also places weight on the neutrino-sector coefficients being $\mathcal{O}(1)$, in analogy to our approach in the charged fermions. This function can be used to diagnose when a good-enough parameter choice has been obtained.

Since the right-handed neutrino mass scale is set by $\epsilon' M_F$, the neutrino mass squared differences (rather than the ratio) can be used to determine the flavor scale. Using either

experimental value [228]

$$\triangle m^2_{21} = (7.53 \pm 0.18) \times 10^{-5}\text{eV}^2 \quad \text{or} \quad \triangle m^2_{32} = (2.51 \pm 0.05) \times 10^{-3}\text{eV}^2, \tag{4.60}$$

we find that the solution in Table 4.4 corresponds to

$$M_F = 4.6 \times 10^{16} \text{ GeV} \quad . \tag{4.61}$$

This is consistent with our axiflavon constraint in Eq. (4.51).

4.3 High Quality Flaxion

It is widely believed that global symmetries are not respected by quantum gravity [229] and several mechanisms for this to happen have been discussed in the literature [230–232]. Thus it is expected that in the low energy effective theory these global symmetry violating effects manifest themselves as higher dimensional operators suppressed by the Planck scale.

As we have seen the PQ mechanism relies on a global symmetry that is imposed by hand so one expects it to be susceptible to gravitational effects. Generically, PQ violating operators suppressed by M_{Pl} shift the minimum of the axion potential away from $\bar{\theta} = 0$ spoiling the solution to the strong CP problem unless there is a mechanism that forbids operators with dimension $D \leq 10$ [233, 234].

This is called the axion quality problem and solutions to it have been put forward, e.g. composite axion models in [235–238], discrete gauge symmetries [239], supersymmetric models in [240, 241] and relating the PQ symmetry to a gauged $U(1)$ in [242–244].

In this section we explore how we can render the flavorful axion of the last section of high quality by using an approach similar to the one used in [243]

The Abelian $U(1)_F$ flavor symmetry is gauged and extra vector-like fermions are introduced to enforce anomaly cancellation. The full theory has an accidental $\text{U}(1)\times\text{U}(1)'$ global symmetry, anomalous with respect to QCD; $\text{U}(1)_{\text{PQ}}$ emerges as a linear combination. The

gauged flavor symmetry restricts the possible PQ symmetry-breaking higher-dimension operators so that sufficient axion quality is preserved. We provide a model of the quark sector, as a proof of principle, and then a model which incorporates the standard model charged leptons as well. In both cases, the charge assignments that lead to acceptable axion quality also lead to a multiplicity of some of the heavy sector states; we check that the Landau pole for hypercharge remains above the cut off of the effective theory. We consider relevant phenomenological constraints on these models including those on the predicted axion couplings.

4.3.1 Quark Sector Model

We focus in this section on a $T' \times Z_3 \times \mathrm{U}(1)_F$ model of quark flavor, corresponding to the quark sector of the model of Ref. [201]. An extension to the lepton sector that assumes the same flavor group is presented in Sec. 4.3.2. The quark-sector model presented in this section exemplifies our approach more directly, and is compatible with models of lepton flavor that may assume a different lepton flavor group structure.

The $\mathrm{U}(1)_F$ in Ref. [201] was a global flavor symmetry whose spontaneous breaking at the flavor scale provided an origin for a flavored axion. This breaking was accomplished by a single flavon field s, whose flavor charge was normalized to $+1$. Of the quark fields, only the right-handed bottom quark carried a flavor charge, -1, so that Yukawa matrix entries that multiply d_R^3 acquire a suppression factor given by $\langle s \rangle / M_F \equiv \rho$, where M_F was the flavor scale. This factor, taken in addition to those related to the breaking of the T' symmetry, provides for the successful Yukawa textures that were summarized in the previous section. Since the $\mathrm{U}(1)_F$ symmetry is anomalous with respect to color, the flavored goldstone boson that emerges from spontaneous symmetry breaking serves as a viable flavored axion.

To implement the "gauged" Peccei-Quinn idea of Fukuda, *et al.* [243], we introduce another flavon field s', with $\mathrm{U}(1)_F$ charge $-1/N$, with N an integer to be determined later. This field will couple to N heavy colored states D_R^j and D_L^j, for $j = 1 \ldots N$. We

promote this symmetry to a gauged flavor symmetry. We will see that at leading order in a $1/M_F$ expansion, the theory including the heavy sector fields has an enlarged global symmetry, U(1)$\times$ U(1)$'$, corresponding to separate phase rotations on the s and s' fields. Gauging the U(1)$_F$ flavor symmetry leaves the full theory with a residual U(1) global symmetry that is both anomalous and spontaneously broken, assuring the presence of a flavorful axion. However, a consequence of the gauged flavor symmetry is that the set of operators that break the residual global symmetry explicitly occur only at very high order, so that the flavored axion evades the axion quality problem. In this section we assume the simplest possibility, that the flavor scale is identified with the reduced Planck scale, $M_F = M_*$, which provides the cut off for the low-energy effective theory. We will see that heavy particles needed to cancel anomalies associated with the gauged U(1)$_F$ flavor symmetry appear at two intermediate scales associated with the expectation values of the s and s' fields.

The gauge quantum numbers of the relevant fields are shown in the first two rows of Table 4.5. Aside from the two scalars, s and s', and the right-handed bottom quark, d_R^3, all other fields shown are heavy fermions that are chiral under U(1)$_F$ and vector-like under the standard model gauge group; they become massive when the U(1)$_F$ symmetry is spontaneously broken. It is straightforward to check that all the gauge and gravitational anomalies are cancelled, with the parameters N and x unspecified.

	s	s'	d_R^3	D_R^i	$\overline{D_L^i}$
$\mathrm{U}(1)_F$	1	$-\frac{1}{N}$	-1	$\frac{1}{N}+x$	$-x$
$\mathrm{SU}(3)_C\times\mathrm{SU}(2)_W\times\mathrm{U}(1)_Y$	$(1,1,0)$	$(1,1,0)$	$(3,1,-1/3)$	$(3,1,-1/3)$	$(\overline{3},1,+1/3)$
$\mathrm{U}(1)\times\mathrm{U}(1)'$	$(1,0)$	$(0,1)$	(-1,0)	$(0,-1)$	$(0,0)$

	E_R	$\overline{E_L}$	$\overline{E_L'^i}$	$E_R'^i$	N_R^j	$\overline{N_L^j}$
$\mathrm{U}(1)_F$	0	$+1$	$-\frac{1}{N}-x$	x	$-\frac{1}{N}-x$	x
$\mathrm{SU}(3)_C\times\mathrm{SU}(2)_W\times\mathrm{U}(1)_Y$	$(1,1,-1)$	$(1,1,+1)$	$(1,1,+1)$	$(1,1,-1)$	$(1,1,0)$	$(1,1,0)$
$\mathrm{U}(1)\times\mathrm{U}(1)'$	$(0,0)$	$(1,0)$	(0,1)	$(0,0)$	$(0,1)$	$(0,0)$

	$N_R'^k$	$\overline{N_L'^k}$
$\mathrm{U}(1)_F$	1	0
$\mathrm{SU}(3)_C\times\mathrm{SU}(2)_W\times\mathrm{U}(1)_Y$	$(1,1,0)$	$(1,1,0)$
$\mathrm{U}(1)\times\mathrm{U}(1)'$	$(1,0)$	$(0,0)$

Table 4.5: Charge assignments under the gauged flavor symmetry, $\mathrm{U}(1)_F$, the standard model gauge group, $\mathrm{SU}(3)_C\times\mathrm{SU}(2)_W\times\mathrm{U}(1)_Y$, and the accidental global $\mathrm{U}(1)\times\mathrm{U}(1)'$ symmetries discussed in the text. Indices range from $i=1\ldots N$, $j=1\ldots 2N$ and $k=1\ldots 2$. Aside from d_R^3, all other standard model fields are $\mathrm{U}(1)_F$ singlets. The parameters N and x are determined later by phenomenological constraints.

Note that x indicates a vectorial gauge rotation on the heavy fields D, E' and N', in addition to what is implied by the other charges shown.

Let $V_0(s,s')$ represent the scalar potential including only the renormalizable terms. For $N>3$, V_0 is only a function of s^*s and s'^*s', leading to an accidental $\mathrm{U}(1)\times\mathrm{U}(1)'$ global symmetry corresponding to separate phase rotations on the two flavon fields. We will normalize the global charges to be $(1,0)$ and $(0,1)$ for the s and s' fields, respectively.

Using notation similar to Ref. [243], we adopt the nonlinear representation

$$s = \frac{1}{\sqrt{2}} f_a e^{i\tilde{a}/f_a} \quad \text{and} \quad s' = \frac{1}{\sqrt{2}} f_b e^{i\tilde{b}/f_b} \ , \tag{4.62}$$

where $\langle s \rangle = f_a/\sqrt{2}$, and $\langle s' \rangle = f_b/\sqrt{2}$. Since V_0 is independent of the phases of s and s', $\tilde{a}$ and $\tilde{b}$ are absent from the potential. When the $\mathrm{U}(1)_F$ symmetry is gauged, however, one linear combination becomes the longitudinal component of the massive flavor gauge boson, while the remaining massless degree of freedom represents the goldstone boson of a residual U(1) global symmetry. This linear combination becomes evident from studying the kinetic terms for s and s':

$$|D_\mu s|^2 + |D_\mu s'|^2 = \frac{1}{2}(\partial_\mu \widetilde{a})^2 + \frac{1}{2}(\partial_\mu \widetilde{b})^2 - g_F A^\mu \partial_\mu (q f_a \widetilde{a} + q' f_b \widetilde{b}) + \frac{g_F^2}{2}(q^2 f_a^2 + q'^2 f_b^2) A_\mu A^\mu \ , \tag{4.63}$$

where g_F is the flavor gauge coupling, the gauge charges of the s and s' fields are q and q', respectively, with $q = +1$ and $q' = -1/N$ for the model defined in Table 4.5. We immediately identify the eaten linear combination

$$b = \frac{1}{\sqrt{q^2 f_a^2 + q'^2 f_b^2}} (q f_a \widetilde{a} + q' f_b \widetilde{b}) \ . \tag{4.64}$$

The orthogonal linear combination is the physical massless degree of freedom, the flavored axion

$$a = \frac{1}{\sqrt{q^2 f_a^2 + q'^2 f_b^2}} (q' f_b \widetilde{a} - q f_a \widetilde{b}) \ , \tag{4.65}$$

or inverting

$$\begin{pmatrix} \widetilde{a} \\ \widetilde{b} \end{pmatrix} = \frac{1}{\sqrt{q^2 f_a^2 + q'^2 f_b^2}} \begin{pmatrix} q' f_b & q f_a \\ -q f_a & q' f_b \end{pmatrix} \begin{pmatrix} a \\ b \end{pmatrix} \ . \tag{4.66}$$

Under a $\mathrm{U}(1)_F$ gauge transformation, the exponentiated fields shift $\widetilde{a}/f_a \to \widetilde{a}/f_a + q\,\alpha$ and $\widetilde{b}/f_b \to \widetilde{b}/f_b + q'\alpha$. It is shown in Ref. [243] that a shift of the axion field a/F by 2π

connects two gauge equivalent points in $\widetilde{a}$-$\widetilde{b}$ space provided that

$$F \equiv \frac{f_a f_b}{\sqrt{q^2 f_a^2 + q'^2 f_b^2}} \ . \tag{4.67}$$

We omit a repetition of that discussion here, but use the quantity F in our discussion below.

We next consider constraints on the parameters N and x. The coupling of the $\widetilde{a}$ and $\widetilde{b}$ fields to gluons and photons is determined by the U(1)×U(1)′ color and electromagnetic anomalies, respectively,

$$\mathcal{L} = \frac{\alpha_s}{8\pi}\left(2N_a\frac{\widetilde{a}}{f_a} + 2N_b\frac{\widetilde{b}}{f_b}\right) G_{\mu\nu}\widetilde{G}^{\mu\nu} + \frac{\alpha_{em}}{8\pi}\left(2E_a\frac{\widetilde{a}}{f_a} + 2E_b\frac{\widetilde{b}}{f_b}\right) F_{\mu\nu}\widetilde{F}^{\mu\nu} \ , \tag{4.68}$$

where $G_{\mu\nu}$ and $F_{\mu\nu}$ are the gluon and photon field strength tensors. The color anomaly factors are given by

$$2N_a = 1 \quad \text{and} \quad 2N_b = N \ , \tag{4.69}$$

and the electromagnetic by

$$2E_a = -4/3 \quad \text{and} \quad 2E_b = -4/3\,N \ . \tag{4.70}$$

Using Eqs. (4.65) and (4.67), we may rewrite Eq. (4.68) as

$$\mathcal{L} = -\frac{\alpha_s}{8\pi}\frac{a}{f_A}G_{\mu\nu}\widetilde{G}^{\mu\nu} + \frac{4}{3}\frac{\alpha_{em}}{8\pi}\frac{a}{f_A}F_{\mu\nu}\widetilde{F}^{\mu\nu} \ , \tag{4.71}$$

where $f_A \equiv F/N$. The quantity f_A is what should be compared to bounds on the decay constant in conventional axion models. For example, the cosmological bound on the axion relic abundance $f_A < 10^{12}$ GeV places a bound on the combination of f_a and f_b that appears in Eq. (4.67). We identify the s field with the flavon in the model of Ref. [201], where a global fit gave

$$f_a \approx 10^{-2} M_F \ . \tag{4.72}$$

We fix f_a to this value with $M_F = M_*$, so that $f_a \approx 2 \times 10^{16}$ GeV; one then finds that $f_A < 10^{12}$ GeV implies, for example that $f_b < 10^{13}$ GeV when $N = 10$. Note that for f_b at this upper limit, we can compute the location of the Landau pole for hypercharge, which we expect to be drastically reduced by the multiplicity of heavy charged particles; we find this scale $\Lambda_{LP} \approx 3 \times 10^{18}$ GeV, which nonetheless remains above the cutoff of our effective theory. We discuss this computation more explicitly below.

We next turn to the issue of axion quality. The accidental global symmetry of the potential is broken by terms that are not functions of $s^* s$ and $s'^* s'$ alone. The lowest order $\mathrm{U}(1)_F$ gauge-invariant term of this form is

$$\mathcal{L}_{bad} = \frac{\xi}{M_*^{N-3}} \, s \, s'^N + \text{h.c.} \ , \tag{4.73}$$

where ξ is an order-one coupling that is generally complex. This contributes both to the axion mass as well as to a linear term in the axion potential:

$$V(a) = -\frac{\text{Im } \xi}{\text{Re } \xi} f_A \Delta m^2 \, a + \frac{1}{2}(m_0^2 + \Delta m^2) \, a^2 \ , \tag{4.74}$$

where m_0 is the standard QCD contribution to the axion mass, and

$$\Delta m^2 = \frac{\text{Re } \xi}{2^{(N-1)/2}} \frac{f_a f_b^N}{f_A^2 M_*^{N-3}} \ . \tag{4.75}$$

The linear term will shift the minimum of the axion potential away from the origin, reintroducing a non-vanishing value of the $\overline{\theta}$ parameter,

$$\overline{\theta} = \langle a \rangle / f_A = \frac{\text{Im } \xi}{\text{Re } \xi} \frac{\Delta m^2}{m_0^2 + \Delta m^2} \ . \tag{4.76}$$

Applying the phenomenological bound $\overline{\theta} < 10^{-10}$ [228], and assuming that the real and imaginary parts of ξ are of order unity, one concludes that $\Delta m^2 / m_0^2 < 10^{-10}$. Using the

following estimate for the QCD contribution [228]

$$m_0 = 5.691 \left(\frac{10^9 \text{ GeV}}{f_A}\right) 10^{-3} \text{ eV} \ , \tag{4.77}$$

as well as our previous choice of $f_a = 10^{-2} M_*$, we find that this bound implies

$$f_b < \left[3.2387 \times 10^{-13} \text{ GeV}^4\right]^{1/N} (\sqrt{2})^{1-\frac{1}{N}} M_*^{1-\frac{4}{N}} \ . \tag{4.78}$$

If we saturate this bound with f_a fixed as previously noted, the mass scales of the heavy particles that carry standard model charges are fixed, since these are determined via the $\mathrm{U}(1)_F$-invariant Yukawa couplings

$$\mathcal{L}_{mass} = \lambda_D s' \overline{D^i}_L D^i_R + \lambda_E s \overline{E}_R E_L + \lambda'_E s' \overline{E'^i}_R E'^i_L + \text{ h.c. } , \tag{4.79}$$

with the sum on $i = 1 \ldots N$ implied. These will contribute significantly to the running of hypercharge so we must check that the associated Landau pole remains above the cut off of our effective theory. To do so, we evaluate the one-loop renormalization group equations between each threshold

$$\alpha_Y^{-1}(m_b) = \alpha_Y^{-1}(m_Z) + \frac{b_{SM}}{2\pi} \ln\left(\frac{m_b}{m_Z}\right) \ , \tag{4.80}$$

$$\alpha_Y^{-1}(m_a) = \alpha_Y^{-1}(m_b) + \frac{b_{SM} + \Delta b_b}{2\pi} \ln\left(\frac{m_a}{m_b}\right) \ , \tag{4.81}$$

$$\alpha_Y^{-1}(\Lambda_{LP}) = \alpha_Y^{-1}(m_a) + \frac{b_{SM} + \Delta b_b + \Delta b_a}{2\pi} \ln\left(\frac{\Lambda_{LP}}{m_a}\right) \ , \tag{4.82}$$

where we define the location of the Landau pole by $\alpha_Y^{-1}(\Lambda_{LP}) = 0$ using the standard model normalization of hypercharge[1], and where the particle content of Table 4.5 gives the

[1]Of course, α_Y will become nonperturbative before this point. However the difference between defining the Landau pole scale by some large perturbative value of the coupling versus $\alpha_Y^{-1} = 0$ is not significant given the rapid increase in the coupling around its blow-up point.

beta functions

$$b_{SM} = -\frac{41}{6} \ , \tag{4.83}$$

$$\Delta b_b = -\frac{16}{9} N \ , \tag{4.84}$$

$$\Delta b_a = -\frac{4}{3} \ . \tag{4.85}$$

Taking the heavy particle thresholds to be $m_a \approx f_a$ and $m_b \approx f_b$ and $\alpha_Y^{-1}(m_Z) = 98.43$, we find the Landau pole locations shown in Table 4.6.

N	f_b	Λ_{LP}		N	f_b	Λ_{LP}
6	1.4×10^4 GeV	2.98×10^{19} GeV		11	4.4×10^{10} GeV	2.93×10^{18} GeV
7	1.5×10^6 GeV	2.97×10^{18} GeV		12	2.0×10^{11} GeV	2.92×10^{18} GeV
8	5.3×10^7 GeV	2.96×10^{18} GeV		13	7.0×10^{11} GeV	2.92×10^{18} GeV
9	8.2×10^8 GeV	2.95×10^{18} GeV		14	2.1×10^{12} GeV	2.91×10^{18} GeV
10	7.4×10^9 GeV	2.94×10^{18} GeV		15	5.4×10^{12} GeV	2.91×10^{18} GeV

Table 4.6: Values of f_b that saturate the bound on axion quality given in Eq. (4.78) as a function of N, with the associated Landau pole scale for standard model hypercharge.

We see that the Landau pole remains above the cut off of our effective theory, M_*, for a wide range in N; the value for this scale remains roughly constant, with the accelerated running caused by the greater particle multiplicity compensated by the heavier particle thresholds, which also increase with N, as given by the axion quality bound in Eq. (4.78). We don't have similar worries for the $\mathrm{U}(1)_H$ gauge coupling since its value at low energies is not fixed phenomenologically and can be taken small enough to keep its Landau pole safely above the cut off.

Bounds on the axion-photon coupling, defined by $g_{a\gamma\gamma} \equiv -\frac{\alpha_{em}}{2\pi}\frac{4}{3}\frac{1}{f_A}$, are summarized by [251]

$$\begin{array}{lll} |g_{a\gamma\gamma}| \lesssim 7 \times 10^{-11}\ \text{GeV}^{-1} & \text{for} & m_a \lesssim 10\ \text{meV} \\ |g_{a\gamma\gamma}| \lesssim 10^{-10}\ \text{GeV}^{-1} & \text{for} & 10\ \text{meV} \lesssim m_a \lesssim 10\ \text{eV}, \\ |g_{a\gamma\gamma}| \ll 10^{-12}\ \text{GeV}^{-1} & \text{for} & 10\ \text{eV} \lesssim m_a \lesssim 0.1\ \text{GeV}, \\ |g_{a\gamma\gamma}| \lesssim 10^{-3}\ \text{GeV}^{-1} & \text{for} & 0.1\ \text{GeV} \lesssim m_a \lesssim 1\ \text{TeV}\ . \end{array} \tag{4.86}$$

Using the values of f_A shown in Table 4.6, as well as the estimate for the axion mass in Eq. (4.77), these bounds eliminate $N \leq 8$, so that $N \geq 9$ is necessary for a viable model.

Finally we consider the value of the parameter x. This is not determined by any of the issues discussed thus far since its value does not contribute to the anomalies of any global symmetries (it parameterizes a vector rather than axial vector phase rotation) and does not affect any of the mass terms in Eq. (4.79). It does, however, determine the dimensions of operators that contribute to mass mixing between the heavy and light fermion fields. For example, in the colored sector and for the choice $x = -2/N$, we can write the following mass mixing terms

$$\mathcal{L}_{mix} = h_i \frac{s s'^2}{M_*^2} \overline{D^i}_L d_R^3 + g_i \frac{s'^*}{M_*} \overline{Q^3}_L H D_R + \text{ h.c. }, \tag{4.87}$$

which lead to small mixing between the heavy and light down-type quarks[2]. Treating the interactions in Eq. (4.87) as perturbations, the second one provides a decay channel for the heavy D fermion via $D \to d\, h^0$, where h^0 is the standard model Higgs boson. For the choice $N = 10$, the results in Table 4.6 tell us that $\langle s'^* \rangle / M_* \approx 2.6 \times 10^{-9}$, from which we can estimate the partial lifetime

$$\tau(D \to d h^0) \approx 10^{-15}\ \text{sec.} \tag{4.88}$$

Other decay channels involving $\mathrm{U}(1)_F$ gauge boson exchange are also possible. The general point is that the heavy fermions have at least one chirality with color and electroweak quantum numbers that match those of a standard model fermion, which makes it possible to construct operators that lead to the rapid decays of these states. As a result we do not have to worry about direct search limits and cosmological consequences of heavy, long-lived

[2]Here, Q_L^3 is the third-generation standard model quark doublet.

charged particles. If dark matter consists, in part, of light, neutral fermions, in addition to the flaxion component, we expect that a similar decays of the heavy to light neutral states can also be arranged. We will not consider the issue of the stability of the heavy states further, since even in the case where they are exactly stable, it is possible that their abundance might be so low after re-heating [244] that there would be no negative consequences as far as direct searches or cosmology is concerned.

4.3.2 Extension with Leptons

The model presented in our previous work, Ref. [201], applied the flavor group discussed in Sec. 4.3.1 to both the quarks and leptons. A global fit to quark and lepton masses and CKM mixing angles demonstrated the viability of the model, with a flavor scale of $M_F = 4 \times 10^{16}$ GeV, and running between the flavor scale and the Z boson mass taken into account. Operator coefficients were found via this fit to be consistent with the expectations of naive dimensional analysis.

In this section, we present a model that is a closer match to the one of Ref. [201] in that both quarks and leptons are subject to the $T' \times Z_3 \times \mathrm{U}(1)_F$ flavor symmetry and M_F is again fixed to 4×10^{16} GeV, with $f_a = 10^{-2} M_F$ as suggested by the fit results. In this way, all the numerical results of Ref. [201] are unchanged. We will assume the most general set of M_F-suppressed higher-dimension operators, including those that could spoil the axion quality. Despite the fact that the ultraviolet (UV) cut off M_F is smaller than M_*, the flavor-scale assumed in our quark-sector model, we will find that axion quality is sufficiently preserved.

With f_a and M_F fixed, there are two remaining free parameters, f_b and N, which will be constrained by

(a) the axion quality bound that we have previously derived, which is now written as

$$f_b < \left[3.2387 \times 10^{-13}\ \mathrm{GeV}^4\right]^{1/N} (\sqrt{2})^{1-\frac{1}{N}} M_F^{1-\frac{4}{N}}, \tag{4.89}$$

(b) axion dark matter: If the PQ symmetry breaking happens before the inflationary phase, the axion can account for the DM relic density for decay constants on the order $f_A \sim 10^{11}$ to 10^{13} GeV [245–247] without fine tuning of the misalignment angle. However other production mechanisms can also be implemented that allow for a lower axion decay constant, see for example Ref. [248]. Thus we only impose the upper bound $f_A \leq 10^{13}$ GeV. It is also possible that dark matter has multiple components so that the relic density need not be saturated by the axion's contribution.

(c) the requirement that the Landau pole of the hypercharge gauge coupling remain above our UV cutoff, the flavor scale M_F. This constraint is relevant given the multiplicity of states with non-zero hypercharge in our extended heavy sector.

Besides the above constraints, there are also constraints from the flavor-changing couplings of the axion. It was shown in Ref. [201] that the most stringent limit comes from the meson decay $K^+ \to \pi^+ a$ (see Eq. (3.19) in that reference). Since the most relevant limit concern quarks lets focus on that sector for now. Derivatively coupled, flavor-changing axion couplings were obtained in Ref. [201] by applying the nonlinear field redefinition

$$d_R^3 \to e^{-ia/f_a} d_R^3 \ , \tag{4.90}$$

where a was the axion field in that model, and then rotating to the quark mass eigenstate basis. In the scenario we consider here, however, the analogous redefinition will involve the $\tilde{a}$ field instead, which is not the axion field. Re-expressing the derivative interaction in terms of the linear combination of the $\tilde{a}$ and $\tilde{b}$ fields identified with the axion (*c.f.*, Eqs. (4.65) and (4.66)), then the bound on f_a given in (3.19) of Ref. [201] is modified to:

$$f_A < \frac{f_a^2}{6.3 \times 10^{10} \text{GeV}}. \tag{4.91}$$

which is trivially satisfied for our choice $f_a = 4 \times 10^{14}$ GeV. Therefore we will not be concerned by the flavor-changing neutral current constraints henceforth. We will show

how other relevant constraints can be satisfied below.

4.3.3 The Model

The scalar fields and colored fermions charged under the gauged $U(1)_F$ of our quark-sector model remain unchanged while new color singlets are introduced to cancel gauge anomalies. The charge assignments of this model are presented in Table 4.7.

	s	s'	d_R^3	D_R^i	$\overline{D_L^i}$
$\mathrm{U}(1)_F$	1	$-\frac{1}{N}$	-1	$\frac{1}{N}+x$	$-x$
$\mathrm{SU}(3)_C\times\mathrm{SU}(2)_W\times\mathrm{U}(1)_Y$	$(\mathbf{1},\mathbf{1},0)$	$(\mathbf{1},\mathbf{1},0)$	$(\mathbf{3},\mathbf{1},-1/3)$	$(\mathbf{3},\mathbf{1},-1/3)$	$(\overline{\mathbf{3}},\mathbf{1},+1/3)$
$\mathrm{U}(1)\times\mathrm{U}(1)'$	$(1,0)$	$(0,1)$	$(-1,0)$	$(0,-1)$	$(0,0)$

	L^3	λ_L^i	λ_R^i
$\mathrm{U}(1)_F$	1	$-x-\frac{1}{N}$	$-x$
$\mathrm{SU}(3)_C\times\mathrm{SU}(2)_W\times\mathrm{U}(1)_Y$	$(\mathbf{1},\mathbf{2},-\frac{1}{2})$	$(\mathbf{1},\mathbf{2},-\frac{1}{2})$	$(\mathbf{1},\mathbf{2},-\frac{1}{2})$
$\mathrm{U}(1)\times\mathrm{U}(1)'$	$(1,0)$	$(0,1)$	(0,0)

	F_L^j	F_R^j	G_L^k	G_R^k
$\mathrm{U}(1)_F$	-1	0	$x+\frac{1}{N}$	x
$\mathrm{SU}(3)_C\times\mathrm{SU}(2)_W\times\mathrm{U}(1)_Y$	$(\mathbf{1},\mathbf{1},0)$	$(\mathbf{1},\mathbf{1},0)$	$(\mathbf{1},\mathbf{1},0)$	$(\mathbf{1},\mathbf{1},0)$
$\mathrm{U}(1)\times\mathrm{U}(1)'$	$(-1,0)$	$(0,0)$	$(0,-1)$	$(0,0)$

Table 4.7: Charge assignments under the gauged flavor symmetry, $\mathrm{U}(1)_F$, the standard model gauge group, $\mathrm{SU}(3)_C\times\mathrm{SU}(2)_W\times\mathrm{U}(1)_Y$, and the accidental global $\mathrm{U}(1)\times\mathrm{U}(1)'$ symmetries discussed in the text. Indices range from $i=1\ldots N$, $j=1\ldots 5$ and $k=1\ldots 5N$. Aside from d_R^3 and L^3, all other standard model fields are $\mathrm{U}(1)_F$ singlets. The parameters N and x are determined later by phenomenological constraints.

In this model the heavy λ_L and λ_R fields transform in the fundamental representation of

$SU(2)_W$. The extra fermion exotics, $F_{L/R}$ and $G_{L/R}$, cancel the $U(1)_F^3$ and $U(1)_F \times \text{Grav}^2$ gauge anomalies and are neutral under the SM gauge group.

Mass terms for the exotics are given by

$$\mathcal{L}_1 = s'(\kappa_1 \overline{D}_L D_R + \kappa_2 \overline{\lambda}_L \lambda_R + \kappa_3 \overline{G}_R G_L) + s\ \kappa_4 \overline{F}_R F_L + \text{h.c.}, \tag{4.92}$$

where the κ's are Yukawa couplings and the flavor indices on the heavy fields are omitted. From this expression, we see how the accidental U(1) and U(1)$'$ symmetries of the scalar potential may be extended to the Yukawa couplings, with the global charges identified in the third row of Table 4.7.

The induced axion coupling to the $G\widetilde{G}$ term is given by the same formulas presented in the last section since the charges of the colored fermions under the accidental $U(1) \times U(1)'$ group are the same. However the axion coupling to photon pairs will be modified by the differences in the heavy particle spectra, including the presence of the new heavy leptons that are doublets under $\text{SU}(2)_W$ in the present theory. For each of the U(1) global symmetries there is an $F\widetilde{F}$ interaction corresponding to the associated anomaly. These are given by [201]

$$\mathcal{L} \supseteq \frac{\alpha_{em}}{8\pi} \left[\frac{\tilde{a}}{f_a} (2N_B + N_W)_{U(1)} + \frac{\tilde{b}}{f_b} (2N_B + N_W)_{U(1)'} \right] F_{\mu\nu} \widetilde{F}^{\mu\nu} \ , \tag{4.93}$$

where N_B and N_W are the anomaly coefficients for hypercharge and isospin respectively. The value of these coefficients is completely determined once the charges of the scalar fields are fixed. Using the values presented in Table 4.7 one obtains

$$(2N_B + N_W)_{U(1)} = \frac{8}{3}, \tag{4.94}$$

$$(2N_B + N_W)_{U(1)'} = \frac{8}{3} N, \tag{4.95}$$

leading to the axion-photon coupling

$$\mathcal{L} \supseteq -\frac{\alpha_{em}}{8\pi}\frac{8}{3}\frac{a}{f_A}F_{\mu\nu}\widetilde{F}^{\mu\nu}. \tag{4.96}$$

Note that the numerical coefficient is the same as what one would find in the simplest DFSZ axion models [249].

4.3.4 Model Constraints

Since the exotic fermions with non-zero hypercharge, in this case D^i and λ^i, for $i = 1 \ldots N$, obtain their masses from the same scalar, the running of the hypercharge gauge coupling will be modified above the threshold given approximately by the scalar s' vev. This is different from the model introduced in the last section where the heavy particles with hypercharge appeared at two distinct energy thresholds. At 1-loop order, the location of the Landau pole is determined here by

$$\alpha_Y^{-1}(m_b) = \alpha_Y^{-1}(m_Z) + \frac{b_{SM}}{2\pi}\ln\left(\frac{m_b}{m_Z}\right), \tag{4.97}$$

$$\alpha_Y^{-1}(\Lambda_{LP}) = \alpha_Y^{-1}(m_b) + \frac{b_{SM}+\Delta b_b}{2\pi}\ln\left(\frac{\Lambda_{LP}}{m_b}\right), \tag{4.98}$$

where the contribution to the beta function is

$$\Delta b_b = -\frac{10}{9}N. \tag{4.99}$$

Analogous to Table 4.6, we present the location of the Landau pole for different heavy particle multiplicities N, assuming that the scale f_b saturates the axion quality condition, Eq. (4.89). We also show the predicted value of the axion decay constant f_A.

N	f_b	f_A	Λ_{LP}
6	3.7×10^3 GeV	630 GeV	4.5×10^{22} GeV
7	2.8×10^5 GeV	4.1×10^4 GeV	1.6×10^{22} GeV
8	7.4×10^6 GeV	9.3×10^5 GeV	6.6×10^{21} GeV
9	9.3×10^7 GeV	1×10^7 GeV	3.0×10^{21} GeV
10	7.0×10^8 GeV	7×10^7 GeV	1.6×10^{21} GeV
11	3.7×10^9 GeV	3.35×10^8	8.6×10^{20} GeV
12	1.5×10^{10} GeV	1.21×10^9	5.1×10^{20} GeV
13	4.7×10^{10} GeV	3.6×10^9	3.1×10^{20} GeV
14	1.3×10^{11} GeV	9.1×10^9	2.0×10^{20} GeV
15	3.0×10^{11} GeV	2.0×10^{10}	1.4×10^{20} GeV

Table 4.8: Values of f_b that saturate the bound on axion quality given in Eq. (4.89) as a function of N, with the associated value of the axion decay constant and the Landau pole scale for standard model hypercharge.

Table 4.8 shows that the Landau pole always remains above the UV cut off for the range in N shown; in fact it is farther above the cut off than our earlier quark-sector model. The bounds on the axion-photon coupling that were quoted in Eq. (4.86), apply here to the quantity $g_{a\gamma\gamma} \equiv \frac{\alpha_{em}}{2\pi} \frac{8}{3} \frac{1}{f_A}$. Again, using the estimate for the axion mass in Eq. (4.77), one finds that the rows of Table 4.8 with $N \leq 9$ are ruled out. We thus find that $N \geq 10$ is necessary, similar to our quark sector-model.

4.4 Conclusion

In this chapter, we have studied a nonsupersymmetric flavor model based on the double tetrahedral group, T'. Improving on earlier work by [215], we formulate a simpler model that dispenses with the triplet flavon S and eliminates some small numerical coefficients that were assumed in one version of the model to arise from unspecified physics at higher

energy scales. Moreover, by replacing one of the Abelian discrete group factors by a continuous U(1) flavor symmetry, we endow the theory with a flavorful axion that solves the strong CP problem. The flavorful axion decay constant f_a is related to the flavor scale M_F (the cut off of the effective theory) and falls roughly two orders of magnitude beneath it. We present constraints on f_a coming from FCNC processes and find that the strongest lower bound comes from the process $K^+ \to \pi^+ a$, yielding $f_a > 1.2 \times 10^{11}$ GeV. We show that the Yukawa matrices predicted by the model provide a good fit to the observed charged fermion masses and mixing angles, taking into account the running from the flavor scale down to the weak scale. We then successfully extend the model to the neutrino sector, by introducing three generations of right-handed neutrinos and employing a Type-I see-saw mechanism to explain the smallness of the light neutrino masses. By charging only the first generation right-handed neutrino non-trivially under T', we show how the mass matrix for the light neutrino mass eigenstates, which must account for two large mixing angles and requires only a modest hierarchy between the neutrino masses, can be predicted by the same theory that yields the strong hierarchies of the charged fermion Yukawa matrices. For the particular extension to the neutrino sector presented here, the flavor scale is roughly five orders of magnitude higher than what is required to satisfy the flavorful axion bounds. This suggests that flavor-changing signals from the flavorful axion will not be easily observable unless additional symmetries are introduced to lower the scale associated with the right-handed neutrinos.

Since long time ago it has been argued that the Peccei-Quinn solution to the strong CP problem of QCD could be spoiled by the presence of higher dimensional operators that violate the PQ symmetry explicitly unless their accompanying coefficients are unnaturally suppressed or if they arise at sufficiently high order [233].

In this chapter we have extended our previous work [201] on a flavorful axion model to address the quality of the axion solution by implementing the mechanism of Ref. [243]. The general proof of concept was delineated in section 4.3.1 by presenting a specific model with only quark fields. In that section we assumed the UV cutoff to be fixed at the Planck

scale.

A model that incorporates charged leptons has also been given with the flavor scale taken to be $M_F = 4 \times 10^{16}$ GeV, to remain consistent with the our findings in [201]. In this case some parametric differences in the flavor changing neutral couplings of the axion with respect to [201] arise but it was shown that the most relevant bound from heavy meson decay is trivially satisfied.

The axion couplings to gluons and photons were also presented and found to be identical to the flavorful axion model.

In general the addition of vector-like fermions charged under the $U(1)_Y$ group accelerates the running of its gauge coupling and we have taken the 1-loop beta function to show that for given values of scalar vevs and number of extra fermions, the predicted Landau pole lies above the cutoff of the theory thereby not violating its self-consistency.

For the model with leptons we found it compatible with all experiments for $N \geq 10$. That simpler models exist, that implement the mechanism of [243], is conceivable and we expect this approach to solving the axion quality problem to be applicable to a vast range of axion models.

Chapter 5

Conclusions

In this thesis we have presented several investigations on scalar extensions of the SM. Motivation for these extensions and relevant literature has been discussed. Here we summarize the main results.

In chapter 2 the imposition of discrete Z_2 symmetries on the 3HDM was employed for two different purposes: i) a three doublet lepton-specific model with FCNCs in the lepton sector, only, was devised. This was motivated by the experimental evidence on leptonic flavor violating decays of the Higgs boson and the primary interest was to study regions of parameter space that predict experimentally accessible signals for a charged Higgs boson while consistent with B physics constraints. A significant value for the charged Higgs branching fraction into the $\mu\nu_\tau$ final state can be obtained without fine tuning the mixing angles although detection by this channel seems challenging. ii) An exact Z_2 symmetry on the scalar potential can be used to prevent one Higgs doublet to couple to fermions, rendering inert and its neutral component can account for the relic density of DM. This is called the I(1+2)HDM and a full scan of its parameter space was performed. The model displays two regions of the DM mass that are consistent with the most current data. The experimental predictions of this model, in particular the missing energy signals called mono-object processes were evaluated using simulated events and were found to be allowed by collider searches. A more dedicated analysis using different kinematical variables and

techniques coupled with the future increased luminosity at the LHC could shed some new light on this model and has been left for future work.

The Randall-Sundrum model was introduced in chapter 3 where the main interest was on the scalar fluctuations of the metric, the radion field. The status of the Higgs-radion unification in the GBS model was reassessed and found to be inconsistent with the branching fractions of the Higgs as measured at the LHC. Two extensions of the GBS model were investigated: i) allowing all SM fermions to propagate in the bulk of the extra dimension and scanning over the bulk profiles was found that the model cannot be put in agreement with the measured properties of the Higgs. ii) Adding an extra Higgs doublet on the bulk and using the superpotential generating technique, it was found that a physical zero mode survives in the spectrum, ruling the model out. Although stabilization by bulk Higgs fields seems excluded other stabilizing solutions that do not rely on a superpotential are possible in principle but are significantly more challenging. Also in chapter 3 we considered a 2HDM living on the visible brane of the extra dimension. The coupling of gauge invariant Higgs bilinears with the Ricci scalar lead to 2HDM-radion mixing and the phenomenological implications were studied. Non-trivial bulk effects produce Higgs coupling deviations that are small but could be observable in future Higgs factories such as the ILC. Furthermore due to small allowed mixing the extra scalars in this model from those of other extended Higgs scenarios could be distinguished by their characteristic branching fractions into bb and ZZ final states. It was found that heavy Higgs searches can rule out a lot of the parameter space.

For the last part of this manuscript, chapter 4, we studied how the axion solution to the strong CP problem can be combined with a non-supersymmetric flavor model based on the non-Abelian double tetrahedral group. Numerical fits were presented that showed how the predicted Yukawa textures in this construction can explain the observed pattern of fermion mass hierarchies and the CKM matrix. As a consequence of the flavor symmetries, the axion mediates FCNCs in the quark and lepton sectors and the most stringent bounds on its decay constant were found from heavy meson decays. It was also shown how the

neutrino sector can easily be incorporated by use of the type-I seesaw mechanism which fixed the flavor scale to a high value such that FCNC constraints are trivially satisfied. We showed how the axion quality problem can be averted by gauging the $U(1)$ flavor group and extending the model by introducing one extra scalar and a suitable number of vector-like fermions. Cosmological constraints on the axion were considered and self-consistency evaluated. We found that $N \geq 10$ number of copies is a necessary condition to suppress the gravitational effects that otherwise shift the minimum of the axion potential.

Appendix

Appendix A

Bulk Gauge bosons

Since the fermions are living in the bulk, then the gauge bosons must also reside in the bulk. We will focus on an Abelian $5D$ gauge boson for simplicity. The $5D$ action is given by

$$S_{gauge} = \int d^5x\sqrt{g}\left\{\frac{1}{4}B_{MN}B_{RS}g^{MR}g^{NS}\right\}, \tag{A.1}$$

where $B_{MN} = \partial_M B_N - \partial_N B_M$ is the field strength. After electroweak symmetry is broken by the background VEV of a bulk Higgs mass terms for the gauge bosons are generated. Here we take a rotation to the mass basis for granted and simply focus on the Z boson

$$S = \int d^5x\sqrt{g}\left[-\frac{1}{4}Z_{MN}Z_{RS}g^{MR}g^{NS} + \frac{g_5^2\phi_0^2}{4\cos^2\theta_W}Z_M Z_N g^{MN}\right], \tag{A.2}$$

where the Weinberg angle is given by $\tan\theta_W = g_5'/g_5$ and the KK decomposition is

$$Z_\mu(x,y) = \sum_{n=0}^{\infty}\frac{1}{\sqrt{y_c}}Z_\mu^{(n)}(x)f_n(y). \tag{A.3}$$

Inserting this expansion in the equation of motion and choosing the graviton gauge in which $Z_5 = 0$ and $\partial_\mu Z^\mu = 0$, the gauge boson profiles satisfy the equation

$$\left[\partial_y(e^{-2A(y)}\partial_y) - \frac{g_5^2}{2c_{\theta_W}^2}\phi_0^2 e^{-2A(y)} + m_n^2\right]f_n(y) = 0 \tag{A.4}$$

To obtain the mass of the gauge boson notice that the second term in the above equation is proportional to the backreaction, viz.,

$$\phi_0 = \frac{l}{\sqrt{5}\kappa} e^{2ky}$$

and since the mass should also be proportional to the backreaction ($m_0^2 = l^2 \tilde{m}_0^2$)we can solve this differential equation perturbatively by expanding the zero mode profile in powers of the backreaction l as

$$f_0 = f_0^{(0)} + l^2 f_0^{(1)} + ...$$

The boundary conditions are that the derivative of the profile vanish at the brane locations. So the zeroth order profile gives just a constant $f^{(0)} = \text{constant} \equiv C$, while the second order equation is

$$f_0''^{(1)} - 2k f_0'^{(1)} = \frac{g_5^2}{10 c_{\theta_W}^2 \kappa^2} C e^{4ky} - C\tilde{m}_0^2 e^{2ky}, \tag{A.5}$$

the general solution to this equation is

$$f_0'^{(1)} = \frac{g_5^2}{10 c_{\theta_W}^2 \kappa^2} \frac{C}{2k} e^{4ky} - C\tilde{m}_0^2 y c e^{2ky} + C_2 e^{2ky}, \tag{A.6}$$

where C_2 is an integration constant. Solving the boundary condtions yield the gauge boson mass

$$m_Z^2 = l^2 \frac{g_5^2}{2y_c c_{\theta_W}^2} \frac{e^{2ky_c}}{10k\kappa^2} = (\frac{g_4 v_{eff}}{2c_{\theta_W}})^2 \tag{A.7}$$

where $g_4 = g_5/\sqrt{2y_c}$ is the $4D$ coupling. The mass of the $W^{\pm}$ bosons is found in a similar way to have the SM form

$$m_W = \frac{g_4 v_{eff}}{2}. \tag{A.8}$$

The constant C is determined by the normalization conditions of the profile functions, namely [128]

$$\int_0^{y_c} dy f_n^2 = 1, \tag{A.9}$$

which yields $C = 1/\sqrt{y_c}$.

Appendix B

Bulk Fermions

Fermions propagating in a slice of AdS_5 have been studied in [126, 127, 175, 254–256]. Here we make a brief review. The 5D action of a bulk Dirac fermion is given by [175]

$$S = \int d^5x\sqrt{g}\left(\frac{i}{2}(\bar{\Psi}\Gamma^M D_M\Psi - D_M\bar{\Psi}\Gamma^M\Psi) - m\mathrm{sgn}(y)\bar{\Psi}\Psi\right) \tag{B.1}$$

Capital letters are used to denote curved space and lower-case indices will be used for objects defined in the tangent frame. The matrices contracted with the covariant derivative are $\Gamma^M = E_a^M\gamma^a$ where $\gamma^a = (\gamma^\mu, i\gamma_5)$ give a 4D representation of the Dirac matrices in 5D flat space and E_a^M is the inverse verbein $E_a^A E_b^B\eta^{ab} = g^{AB}$.

The covariant derivative $D_M = \partial_M - \frac{i}{4}\omega_M^{ab}\sigma_{ab}$ and ω_M^{ab} is the spin connection. A straightforward evaluation of the spin connection yields [256]

$$D_\mu = \partial_\mu - \frac{ie^{-\sigma}\sigma'}{4r_c}[\gamma_\mu, \gamma_5], \qquad D_5 = \partial_5.$$

Since the metric is diagonal, the only nonvanishing entries of the spin connection have $b = M$ or $c = M$, giving no contribution to the action. Therefore we can write

$$S = \int d^5x\sqrt{g}\left\{E_a^M\frac{i}{2}\bar{\Psi}\gamma^a(\partial_M - \overleftarrow{\partial_M})\Psi - m\mathrm{sgn}(y)\bar{\Psi}\Psi\right\} \tag{B.2}$$

where the upper arrow in the differential operator indicates the direction of action and act only on the Dirac fermions and not on the metric factors.

Notice that the bulk mass term in the action is odd under Z_2 parity. This is a requirement bacause the fermion transforms under Z_2 as $\Psi(-y) = \pm\gamma_5\Psi(y)$.

Using integration by parts and expanding the spinor into its left- and right-handed components, the action can be written as [126]

$$S = \int d^4x \int d\phi r_c \Big\{ e^{-3A(y)} \left(\bar{\Psi}_L i\not{\partial}\Psi_L + \bar{\Psi}_R i\not{\partial}\Psi_R \right) - e^{-4A(y)} m \mathrm{sgn}(y) (\bar{\Psi}_L \Psi_R + \bar{\Psi}_R \Psi_L) \\ -\frac{1}{2}\left[\bar{\Psi}_L (e^{-4A(y)}\partial_y + \partial_y e^{-4A(y)})\Psi_R - \bar{\Psi}_R \left(e^{-4A(y)}\partial_y + \partial_y e^{-4A(y)} \right) \Psi_L \right] \Big\}, \qquad \text{(B.3)}$$

and periodic boundary condtitions that respect the orbifold symmetry are imposed on the fields. Notice that the action is invariant either if the left-handed component of the field is odd and the right-handed component is even or viceversa.

The action (B.2) is the most general expression for a bulk fermion and one can also show that it is equivalent to write it as

$$S = \int d^5x \sqrt{g} \left\{ i\bar{\Psi}\Gamma^M D_M \Psi - msgn(\phi)\bar{\Psi}\Psi \right\}. \qquad \text{(B.4)}$$

The Kaluza Klein expansion of the fermion, the orthogonality conditions and coupled differential equations for the profiles $\hat{f}_n^{L,R}(y)$ are given in reference [126]. Here we closely follow their notation.

In the fermion sector of the SM, fermions of different quiralities transform under different representations of the gauge group $SU(2)$. For each generation, the left-handed up (neutrino) and down quarks (charged lepton) form a $SU(2)$ doublet while their right-handed counterparts are $SU(2)$ singlet fields each. Therefore in the SM only one Dirac fermion is needed for each particle.

In our case notice from (B.3) that having different quiralities of a particle belonging to

different representations would imediately forbid having the last two terms in the action. Thus for each particle we need to introduce two $5D$ Dirac fields, e.g., for the quarks case we need, for each generation, an $SU(2)$-doublet $Q = (q_u, q_d)^T$ and two $SU(2)$-singlets u and d.

The $5D$ action for quarks should read

$$S_{fermions} = \int d^5x\sqrt{g}\left[i\bar{Q}\Gamma^M D_M Q + i\bar{u}\Gamma^M D_M u + i\bar{d}\Gamma^M D_M d \right. \\ \left. -\text{sgn}(y)(m_Q\bar{Q}Q + m_u\bar{u}u + m_d\bar{d}d)\right] \tag{B.5}$$

with generation indices omitted and a similar expression for leptons should be included.

For fermions in the bulk we have two different options of boundary conditions. In "option-L" the left handed-field is odd and the right-handed one is even and viceversa for "option-R". The key point is that odd fields do not have a zero mode profile. Since SM fields should correspond to the KK zero modes then we choose "option-R" for the $SU(2)$-doublets and "option-L" for $SU(2)$- singlets. So we expand these fields as [257]

$$Q(x,\phi) = Q_L + Q_R = \sum_n e^{2\sigma}\left\{Q_L^{(n)}(x)\chi_Q^{(n)}(y) + Q_R^{(n)}(x)\tau_Q^{(n)}(y)\right\}, \tag{B.6}$$

$$u(x,\phi) = u_L + u_R = \sum_n e^{2\sigma}\left\{u_L^{(n)}(x)\tau_u^{(n)}(y) + u_R^{(n)}(x)\chi_u^{(n)}(y)\right\} \tag{B.7}$$

where $\chi^{(n)}(y)$ ($\tau^{(n)}(y)$) are even (odd) functions of y and a the singlet d has a similar expansion as u above. In particular the zero mode profiles satisfy the differential equations (see equation (2.5) of [126])

$$(\partial_y - m_Q)\chi_Q^{(0)}(y) = 0, \tag{B.8}$$

$$(\partial_y + m_u)\chi_u^{(0)}(y) = 0, \tag{B.9}$$

with normalization conditions

$$\int_0^{y_c} dy e^{A(y)}\chi_\psi^{(m)}(y)\chi_\psi^{(n)}(y) = \delta_{mn}. \tag{B.10}$$

The solution for the zero mode profiles are

$$\chi_Q^{(0)}(y) = \chi_Q^{(0)}(0)e^{m_Q y}, \quad \chi_u^{(0)}(y) = \chi_u^{(0)}(0)e^{-m_u y} \tag{B.11}$$

with normalization constants given by

$$|\chi_Q^{(0)}(0)|^2 = \frac{ky_c(1+2\frac{m_Q}{k})}{e^{ky_c(1+2\frac{m_Q}{k})}-1}, \quad |\chi_u^{(0)}(0)|^2 = \frac{kr_c(1-2\frac{m_u}{k})}{e^{ky_c(1-2\frac{m_u}{k})}-1}, \tag{B.12}$$

the solutions for $\chi_d^{(0)}(y)$ look exactly the same as those for the u profile given above but with the respective mass replaced.

Appendix C

Background Solution

In this section we justify our choice of brane potentials (3.74), (3.75) and give the formulas for the coefficients of the bulk potential in terms of the superpotential parameters. A derivation of the VEV profiles, equations (C.15) and (C.16), of the system (3.77) is also given.

For notational convenience we define the values of the VEV profiles in the branes by

$$\phi_i(0) \equiv \bar{\phi}_i, \quad \phi_i(y_c) \equiv v_i. \tag{C.1}$$

Notice that given the physical input into the model, namely the bulk and brane potentials V and λ_{UV} and λ_{IR}, equation (3.70) is a non-linear partial differential equation for W that has two integration constants. Equations (3.71) are first order and provide three integration constants giving a total of five integration constant as before. The superpotential method provides the solution to the boundary value problem provided we have

$$\lambda_{UV}(\bar{\phi}_1, \bar{\phi}_2) = +W(\bar{\phi}_1, \bar{\phi}_2), \quad \lambda_{IR}(v_1, v_2) = -W(v_1, v_2), \tag{C.2}$$

and

$$\left.\frac{\lambda_{UV}(\phi_1, \phi_2)}{\partial \phi_i}\right|_0 = \left.\frac{\partial W(\phi_1, \phi_2)}{\partial \phi_i}\right|_0, \quad \left.\frac{\lambda_{IR}(\phi_1, \phi_2)}{\partial \phi_i}\right|_{y_c} = -\left.\frac{\partial W(\phi_1, \phi_2)}{\partial \phi_i}\right|_{y_c}, \tag{C.3}$$

this fact justifies our choice of brane potentials in (3.74) and (3.75). It should be empha-

sized that brane potentials have to be evaluated at the background first, $\Phi_i = \phi_i$ and then at the orbifold fixed points.

The parameters of the 2HDM bulk potential (3.73) are given in terms of the superpotential parameters by

$$\frac{\bar{m}_{11}^2}{k^2} = \frac{u_{11}^2 + u_{12}^2}{8} - 2u_{11}, \quad \frac{\bar{m}_{22}^2}{k^2} = \frac{u_{22}^2 + u_{12}^2}{8} - 2u_{22}, \quad \frac{m_{12}^2}{k^2} = u_{12}\left(\frac{u_{11} + u_{22}}{8} - 2\right), \tag{C.4}$$

$$\lambda_1 = -\frac{k^2\kappa^2}{6}u_{11}^2, \quad \lambda_2 = -\frac{k^2\kappa^2}{6}u_{22}^2, \quad \lambda_3 = \frac{-k^2\kappa^2}{3}u_{11}u_{22}, \quad \lambda_4 = -\frac{k^2\kappa^2}{6}u_{12}^2, \tag{C.5}$$

$$\lambda_6 = -\frac{k^2\kappa^2}{3}u_{12}u_{11}, \quad \lambda_7 = -\frac{k^2\kappa^2}{3}u_{12}u_{22} \tag{C.6}$$

therefore this choice of superpotential generates a bulk 2HDM potential with quartic interactions. Notice that quartic terms in the bulk are higher dimensional operators that one would expect to be suppressed.

To find the solutions for the VEV profiles we notice that the system of equations can be written in matrix form as $\mathbf{M}\vec{\phi} = 0$, where $\mathbf{M}$ is the matrix of coefficients. Equilibrium solutions are found by solving $\mathbf{M}\vec{\phi} = 0$. We assume that $det\mathbf{M} \neq \mathbf{0}$, so $\phi = 0$ is the only equilibrium solution. This assumption puts a contraint on the parameters of the bulk potential, namely

$$\det \mathbf{M} \equiv d \equiv u_{11}u_{22} - u_{12}^2 \neq 0. \tag{C.7}$$

The system (3.77) can be solved easily by the inserting the ansatz

$$\vec{\phi}(y) = \vec{\xi}e^{rky}, \tag{C.8}$$

with ξ a constant vector. We get

$$(\mathbf{M} - rk\mathbf{I})\vec{\xi} = 0, \tag{C.9}$$

which is a simple eigenvalue problem. The eigenvalues are given by

$$r_\pm = u(2 \pm \nu), \tag{C.10}$$

where we defined

$$u \equiv \frac{u_{11} + u_{22}}{4}, \quad \nu \equiv \sqrt{4 - \frac{d}{u^2}}, \tag{C.11}$$

and from now on we trade the parameters $\{u_{11}, u_{22}, u_{12}\}$ for $\{u, \nu, u_{12}\}$. The most general solution can be written as

$$\vec{\phi}(y) = e^{2ku y} \left(c_+ \vec{\xi}_+ e^{ku\nu y} + c_- \vec{\xi}_- e^{-ku\nu y} \right), \tag{C.12}$$

where

$$\vec{\xi}_\pm = \frac{1}{\sqrt{2u\nu \left[u\nu \mp \sqrt{u^2\nu^2 - u_{12}^2} \right]}} \begin{pmatrix} -u_{12} \\ \sqrt{u^2\nu^2 - u_{12}^2} \mp u\nu \end{pmatrix}. \tag{C.13}$$

are the orthonormal set of eigenvectors and the $c_\pm$'s are integration constants of mass dimension 3/2. From the discussion above, these integration constants are fixed by requiring $\phi_1(y_c) = v_1$ and $\phi_2(y_c) = v_2$ to be simultaneously satisfied. It is straightforward to find that

$$c_\pm = -e^{-(2\pm\nu)uky_c} \frac{u_{12}v_1 \pm v_2(u\nu \mp \sqrt{u^2\nu^2 - u_{12}^2})}{\sqrt{2u\nu \left[u\nu + \sqrt{u^2\nu^2 - u_{12}^2} \right]}} \tag{C.14}$$

and the background vev profiles are found to be

$$\phi_1(y) = \frac{e^{2ku(y-yc)} \left[\left(v_1 \sqrt{\nu^2u^2 - u_{12}^2} + u_{12}v_2 \right) \sinh(k\nu u(y - y_c)) + \nu u v_1 \cosh(k\nu u(y - y_c)) \right]}{\nu u}, \tag{C.15}$$

$$\phi_2(y) = \frac{e^{2ku(y-y_c)} \left[\left(u_{12}v_1 - v_2 \sqrt{\nu^2u^2 - u_{12}^2} \right) \sinh(k\nu u(y - y_c)) + \nu u v_2 \cosh(k\nu u(y - y_c)) \right]}{\nu u}. \tag{C.16}$$

Appendix D

LHC Data

Decay	Production	Measured Signal Strength R_m
$\gamma\gamma$	ggF+tth	$1.19^{+0.20}_{-0.18}$ [CMS] [258]
	VBF +Vh	$1.01^{+0.57}_{-0.51}$ [CMS] [258]
	ggF	$0.8^{+0.19}_{-0.18}$ [ATLAS] [259]
	VBF	$2.1^{+0.6}_{-0.6}$ [ATLAS] [259]
	Vh	$0.7^{+0.9}_{-0.8}$ [ATLAS] [259]
WW*	ggF	$1.02^{+0.29}_{-0.26}$ [ATLAS] [260]
	VBF	$1.27^{+0.53}_{-0.45}$ [ATLAS] [260]
	ggF	0.76 ± 0.21 [CMS] [261]
	VBF	$1.7^{+1.1}_{-0.9}$ [ATLAS] [262]
	Wh	$3.2^{+4.4}_{-4.2}$ [ATLAS] [262]
ZZ*	ggF	$1.7^{+0.5}_{-0.4}$ [ATLAS] [263]
	VBF + Vh	$0.3^{+1.6}_{-0.9}$ [ATLAS] [263]
	ggF	$1.20^{+0.35}_{-0.31}$ [CMS] [264]
	VBF	$0.00^{+1.37}_{-0.00}$ [CMS] [264]
bb	VBF	$-3.7^{+2.4}_{-2.5}$ [CMS] [265]
	Vh	$1.20^{+0.42}_{-0.36}$ [ATLAS] [266]
	Vh	1.2 ± 0.4 [CMS] [267]
$\tau\tau$	VBF	1.2 ± 0.4 [ATLAS] [268]
	ggF	$2.0^{+1.5}_{-1.2}$ [ATLAS] [269]
	VBF + Vh	$1.24^{+0.59}_{-0.54}$ [ATLAS] [269]
	WH	2.3 ± 1.6 [ATLAS] [270]
	tth	$1.5^{+1.2}_{-1.0}$ [ATLAS] [271]

Table D.0.1: Measured Higgs Signal Strengths

Bibliography

[1] G. Aad *et al.* [ATLAS Collaboration], Phys. Lett. B **716**, 1 (2012) doi:10.1016/j.physletb.2012.08.020 [arXiv:1207.7214 [hep-ex]].

[2] S. Chatrchyan *et al.* [CMS Collaboration], Phys. Lett. B **716**, 30 (2012) doi:10.1016/j.physletb.2012.08.021 [arXiv:1207.7235 [hep-ex]].

[3] P. A. M. Dirac, Proc. Roy. Soc. Lond. A **165**, 199 (1938). doi:10.1098/rspa.1938.0053

[4] M. Gell-Mann, Nuovo Cim. **4**, no. S2, 848 (1956). doi:10.1007/BF02748000

[5] G. 't Hooft, NATO Sci. Ser. B **59**, 135 (1980). doi:10.1007/978 − 1 − 4684 − 7571 − 5_9

[6] S. P. Martin, Adv. Ser. Direct. High Energy Phys. **21**, 1 (2010) [Adv. Ser. Direct. High Energy Phys. **18**, 1 (1998)] *doi* : 10.1142/9789812839657$_0$001, 10.1142/9789814307505_0001 [hep-ph/9709356].

[7] T. Kaluza, Sitzungsber. Preuss. Akad. Wiss. Berlin (Math. Phys.) **1921**, 966 (1921) [Int. J. Mod. Phys. D **27**, no. 14, 1870001 (2018)] doi:10.1142/S0218271818700017 [arXiv:1803.08616 [physics.hist-ph]].

[8] O. Klein, Z. Phys. **37**, 895 (1926) [Surveys High Energ. Phys. **5**, 241 (1986)]. doi:10.1007/BF01397481

[9] P. W. Graham, D. E. Kaplan and S. Rajendran, Phys. Rev. Lett. **115**, no. 22, 221801 (2015) doi:10.1103/PhysRevLett.115.221801 [arXiv:1504.07551 [hep-ph]].

[10] N. Arkani-Hamed, T. Cohen, R. T. D'Agnolo, A. Hook, H. D. Kim and D. Pinner, Phys. Rev. Lett. **117**, no. 25, 251801 (2016) doi:10.1103/PhysRevLett.117.251801 [arXiv:1607.06821 [hep-ph]].

[11] K. Agashe, R. Contino and A. Pomarol, Nucl. Phys. B **719**, 165 (2005) doi:10.1016/j.nuclphysb.2005.04.035 [hep-ph/0412089].

[12] R. N. Mohapatra and J. C. Pati, Phys. Rev. D **11**, 566 (1975). doi:10.1103/PhysRevD.11.566

[13] Z. Chacko, H. S. Goh and R. Harnik, Phys. Rev. Lett. **96**, 231802 (2006) doi:10.1103/PhysRevLett.96.231802 [hep-ph/0506256].

[14] V. Khachatryan *et al.* [CMS], Eur. Phys. J. C **75**, no.5, 212 (2015) doi:10.1140/epjc/s10052-015-3351-7 [arXiv:1412.8662 [hep-ex]].

[15] [ATLAS], ATLAS-CONF-2015-007.

[16] H. E. Haber and G. L. Kane, Phys. Rept. **117**, 75 (1985). doi:10.1016/0370-1573(85)90051-1

[17] R. D. Peccei and H. R. Quinn, Phys. Rev. Lett. **38**, 1440 (1977). doi:10.1103/PhysRevLett.38.1440

[18] J. E. Kim, Phys. Rept. **150**, 1 (1987). doi:10.1016/0370-1573(87)90017-2

[19] J. M. Cline and P. A. Lemieux, Phys. Rev. D **55**, 3873 (1997) doi:10.1103/PhysRevD.55.3873 [hep-ph/9609240].

[20] M. Joyce, T. Prokopec and N. Turok, Phys. Rev. D **53**, 2958 (1996) doi:10.1103/PhysRevD.53.2958 [hep-ph/9410282].

[21] K. Funakubo, A. Kakuto and K. Takenaga, Prog. Theor. Phys. **91**, 341 (1994) doi:10.1143/PTP.91.341, 10.1143/ptp/91.2.341 [hep-ph/9310267].

[22] A. T. Davies, C. D. froggatt, G. Jenkins and R. G. Moorhouse, Phys. Lett. B **336**, 464 (1994). doi:10.1016/0370-2693(94)90559-2

[23] J. M. Cline, K. Kainulainen and A. P. Vischer, Phys. Rev. D **54**, 2451 (1996) doi:10.1103/PhysRevD.54.2451 [hep-ph/9506284].

[24] M. Laine and K. Rummukainen, Nucl. Phys. B **597**, 23 (2001) doi:10.1016/S0550-3213(00)00736-7 [hep-lat/0009025].

[25] L. Fromme, S. J. Huber and M. Seniuch, JHEP **0611**, 038 (2006) doi:10.1088/1126-6708/2006/11/038 [hep-ph/0605242].

[26] N. G. Deshpande and E. Ma, Phys. Rev. D **18**, 2574 (1978). doi:10.1103/PhysRevD.18.2574

[27] E. Ma, Phys. Rev. D **73**, 077301 (2006) doi:10.1103/PhysRevD.73.077301 [hep-ph/0601225].

[28] R. Barbieri, L. J. Hall and V. S. Rychkov, Phys. Rev. D **74**, 015007 (2006) doi:10.1103/PhysRevD.74.015007 [hep-ph/0603188].

[29] L. Lopez Honorez, E. Nezri, J. F. Oliver and M. H. G. Tytgat, JCAP **0702**, 028 (2007) doi:10.1088/1475-7516/2007/02/028 [hep-ph/0612275].

[30] C. Arina, F. S. Ling and M. H. G. Tytgat, JCAP **0910**, 018 (2009) doi:10.1088/1475-7516/2009/10/018 [arXiv:0907.0430 [hep-ph]].

[31] E. Nezri, M. H. G. Tytgat and G. Vertongen, JCAP **0904**, 014 (2009) doi:10.1088/1475-7516/2009/04/014 [arXiv:0901.2556 [hep-ph]].

[32] X. Miao, S. Su and B. Thomas, Phys. Rev. D **82**, 035009 (2010) doi:10.1103/PhysRevD.82.035009 [arXiv:1005.0090 [hep-ph]].

[33] M. Gustafsson, S. Rydbeck, L. Lopez-Honorez and E. Lundstrom, Phys. Rev. D **86**, 075019 (2012) doi:10.1103/PhysRevD.86.075019 [arXiv:1206.6316 [hep-ph]].

[34] A. Arhrib, R. Benbrik and N. Gaur, Phys. Rev. D **85**, 095021 (2012) doi:10.1103/PhysRevD.85.095021 [arXiv:1201.2644 [hep-ph]].

[35] B. Swiezewska and M. Krawczyk, Phys. Rev. D **88**, no. 3, 035019 (2013) doi:10.1103/PhysRevD.88.035019 [arXiv:1212.4100 [hep-ph]].

[36] A. Goudelis, B. Herrmann and O. Stål, JHEP **1309**, 106 (2013) doi:10.1007/JHEP09(2013)106 [arXiv:1303.3010 [hep-ph]].

[37] A. Arhrib, Y. L. S. Tsai, Q. Yuan and T. C. Yuan, JCAP **1406**, 030 (2014) doi:10.1088/1475-7516/2014/06/030 [arXiv:1310.0358 [hep-ph]].

[38] M. Krawczyk, D. Sokolowska, P. Swaczyna and B. Swiezewska, JHEP **1309**, 055 (2013) doi:10.1007/JHEP09(2013)055 [arXiv:1305.6266 [hep-ph]].

[39] M. Krawczyk, D. Soko?owska, P. Swaczyna and B. ?wie?ewska, Acta Phys. Polon. B **44**, no. 11, 2163 (2013) doi:10.5506/APhysPolB.44.2163 [arXiv:1309.7880 [hep-ph]].

[40] A. Ilnicka, M. Krawczyk and T. Robens, Phys. Rev. D **93**, no. 5, 055026 (2016) doi:10.1103/PhysRevD.93.055026 [arXiv:1508.01671 [hep-ph]].

[41] M. A. Díaz, B. Koch and S. Urrutia-Quiroga, Adv. High Energy Phys. **2016**, 8278375 (2016) doi:10.1155/2016/8278375 [arXiv:1511.04429 [hep-ph]].

[42] K. P. Modak and D. Majumdar, Astrophys. J. Suppl. **219**, no. 2, 37 (2015) doi:10.1088/0067-0049/219/2/37 [arXiv:1502.05682 [hep-ph]].

[43] F. S. Queiroz and C. E. Yaguna, JCAP **1602**, 038 (2016) doi:10.1088/1475-7516/2016/02/038 [arXiv:1511.05967 [hep-ph]].

[44] C. Garcia-Cely, M. Gustafsson and A. Ibarra, JCAP **1602**, 043 (2016) doi:10.1088/1475-7516/2016/02/043 [arXiv:1512.02801 [hep-ph]].

[45] M. Hashemi and S. Najjari, Eur. Phys. J. C **77**, no. 9, 592 (2017) doi:10.1140/epjc/s10052-017-5159-0 [arXiv:1611.07827 [hep-ph]].

[46] P. Poulose, S. Sahoo and K. Sridhar, Phys. Lett. B **765**, 300 (2017) doi:10.1016/j.physletb.2016.12.022 [arXiv:1604.03045 [hep-ph]].

[47] A. Alves, D. A. Camargo, A. G. Dias, R. Longas, C. C. Nishi and F. S. Queiroz, JHEP **1610**, 015 (2016) doi:10.1007/JHEP10(2016)015 [arXiv:1606.07086 [hep-ph]].

[48] A. Datta, N. Ganguly, N. Khan and S. Rakshit, Phys. Rev. D **95**, no. 1, 015017 (2017) doi:10.1103/PhysRevD.95.015017 [arXiv:1610.00648 [hep-ph]].

[49] A. Belyaev, G. Cacciapaglia, I. P. Ivanov, F. Rojas-Abatte and M. Thomas, Phys. Rev. D **97**, no. 3, 035011 (2018) doi:10.1103/PhysRevD.97.035011 [arXiv:1612.00511 [hep-ph]].

[50] G. C. Branco, P. M. Ferreira, L. Lavoura, M. N. Rebelo, M. Sher and J. P. Silva, Phys. Rept. **516**, 1 (2012) doi:10.1016/j.physrep.2012.02.002 [arXiv:1106.0034 [hep-ph]].

[51] G. Bhattacharyya and D. Das, Pramana **87**, no. 3, 40 (2016) doi:10.1007/s12043-016-1252-4 [arXiv:1507.06424 [hep-ph]].

[52] G. D'Ambrosio, G. F. Giudice, G. Isidori and A. Strumia, Nucl. Phys. B **645**, 155 (2002) doi:10.1016/S0550-3213(02)00836-2 [hep-ph/0207036].

[53] S. L. Glashow and S. Weinberg, Phys. Rev. D **15**, 1958 (1977). doi:10.1103/PhysRevD.15.1958

[54] E. A. Paschos, Phys. Rev. D **15**, 1966 (1977). doi:10.1103/PhysRevD.15.1966

[55] A. Pich and P. Tuzon, Phys. Rev. D **80**, 091702 (2009) doi:10.1103/PhysRevD.80.091702 [arXiv:0908.1554 [hep-ph]].

[56] P. Tuzon and A. Pich, Acta Phys. Polon. Supp. **3**, 215 (2010) [arXiv:1001.0293 [hep-ph]].

[57] I. P. Ivanov and E. Vdovin, Phys. Rev. D **86**, 095030 (2012) doi:10.1103/PhysRevD.86.095030 [arXiv:1206.7108 [hep-ph]].

[58] I. P. Ivanov and C. C. Nishi, JHEP **1501**, 021 (2015) doi:10.1007/JHEP01(2015)021 [arXiv:1410.6139 [hep-ph]].

[59] I. P. Ivanov, V. Keus and E. Vdovin, J. Phys. A **45**, 215201 (2012) doi:10.1088/1751-8113/45/21/215201 [arXiv:1112.1660 [math-ph]].

[60] V. Keus, S. F. King and S. Moretti, JHEP **1401**, 052 (2014) doi:10.1007/JHEP01(2014)052 [arXiv:1310.8253 [hep-ph]].

[61] D. Das and U. K. Dey, Phys. Rev. D **89**, no. 9, 095025 (2014) Erratum: [Phys. Rev. D **91**, no. 3, 039905 (2015)] doi:10.1103/PhysRevD.91.039905, 10.1103/PhysRevD.89.095025 [arXiv:1404.2491 [hep-ph]].

[62] D. Das, U. K. Dey and P. B. Pal, Phys. Lett. B **753**, 315 (2016) doi:10.1016/j.physletb.2015.12.038 [arXiv:1507.06509 [hep-ph]].

[63] J. Heeck, M. Holthausen, W. Rodejohann and Y. Shimizu, Nucl. Phys. B **896**, 281 (2015) doi:10.1016/j.nuclphysb.2015.04.025 [arXiv:1412.3671 [hep-ph]].

[64] S. Moretti and K. Yagyu, Phys. Rev. D **91**, 055022 (2015) doi:10.1103/PhysRevD.91.055022 [arXiv:1501.06544 [hep-ph]].

[65] A. Aranda, C. Bonilla, F. de Anda, A. Delgado and J. Hernandez-Sanchez, Phys. Lett. B **725**, 97 (2013) doi:10.1016/j.physletb.2013.06.047 [arXiv:1302.1060 [hep-ph]].

[66] A. Aranda, J. E. Barradas-Guevara, A. Cordero-Cid, F. de Anda, A. Delgado, O. Felix-Beltran and J. Hernandez-Sanchez, arXiv:1404.7829 [hep-ph].

[67] A. Crivellin, G. D'Ambrosio and J. Heeck, Phys. Rev. D **91**, no. 7, 075006 (2015) doi:10.1103/PhysRevD.91.075006 [arXiv:1503.03477 [hep-ph]].

[68] A. G. Akeroyd, S. Moretti, K. Yagyu and E. Yildirim, Int. J. Mod. Phys. A **32**, no. 23n24, 1750145 (2017) doi:10.1142/S0217751X17501457 [arXiv:1605.05881 [hep-ph]].

[69] K. Yagyu, Phys. Lett. B **763**, 102 (2016) doi:10.1016/j.physletb.2016.10.028 [arXiv:1609.04590 [hep-ph]].

[70] A. G. Akeroyd, S. Moretti, K. Yagyu and E. Yildirim, PoS CHARGED **2016**, 024 (2016) doi:10.22323/1.286.0024 [arXiv:1612.05194 [hep-ph]].

[71] M. Merchand and M. Sher, Phys. Rev. D **95**, no. 5, 055004 (2017) doi:10.1103/PhysRevD.95.055004 [arXiv:1611.06887 [hep-ph]].

[72] M. Merchand and M. Sher, arXiv:1911.06477 [hep-ph].

[73] V. Khachatryan *et al.* [CMS Collaboration], Phys. Lett. B **749**, 337 (2015) doi:10.1016/j.physletb.2015.07.053 [arXiv:1502.07400 [hep-ex]].

[74] A. M. Sirunyan *et al.* [CMS Collaboration], JHEP **1806**, 001 (2018) doi:10.1007/JHEP06(2018)001 [arXiv:1712.07173 [hep-ex]].

[75] G. Aad *et al.* [ATLAS Collaboration], Eur. Phys. J. C **77**, no. 2, 70 (2017) doi:10.1140/epjc/s10052-017-4624-0 [arXiv:1604.07730 [hep-ex]].

[76] T. P. Cheng and M. Sher, Phys. Rev. D **35**, 3484 (1987). doi:10.1103/PhysRevD.35.3484

[77] H. E. Logan and D. MacLennan, Phys. Rev. D **79**, 115022 (2009) doi:10.1103/PhysRevD.79.115022 [arXiv:0903.2246 [hep-ph]].

[78] P. A. R. Ade *et al.* [Planck Collaboration], Astron. Astrophys. **594**, A13 (2016) doi:10.1051/0004-6361/201525830 [arXiv:1502.01589 [astro-ph.CO]].

[79] A. Belyaev *et al.*, Phys. Rev. D **99**, no. 1, 015011 (2019) doi:10.1103/PhysRevD.99.015011 [arXiv:1809.00933 [hep-ph]].

[80] J. Kalinowski, W. Kotlarski, T. Robens, D. Sokolowska and A. F. Zarnecki, JHEP **1812**, 081 (2018) doi:10.1007/JHEP12(2018)081 [arXiv:1809.07712 [hep-ph]].

[81] D. Dercks and T. Robens, Eur. Phys. J. C **79**, no. 11, 924 (2019) doi:10.1140/epjc/s10052-019-7436-6 [arXiv:1812.07913 [hep-ph]].

[82] B. Grzadkowski, O. M. Ogreid and P. Osland, Phys. Rev. D **80**, 055013 (2009) doi:10.1103/PhysRevD.80.055013 [arXiv:0904.2173 [hep-ph]].

[83] B. Grzadkowski, O. M. Ogreid, P. Osland, A. Pukhov and M. Purmohammadi, JHEP **1106**, 003 (2011) doi:10.1007/JHEP06(2011)003 [arXiv:1012.4680 [hep-ph]].

[84] P. Osland, A. Pukhov, G. M. Pruna and M. Purmohammadi, JHEP **1304**, 040 (2013) doi:10.1007/JHEP04(2013)040 [arXiv:1302.3713 [hep-ph]].

[85] S. Moretti, D. Rojas and K. Yagyu, JHEP **1508**, 116 (2015) doi:10.1007/JHEP08(2015)116 [arXiv:1504.06432 [hep-ph]].

[86] V. Keus, S. F. King, S. Moretti and D. Sokolowska, JHEP **1411**, 016 (2014) doi:10.1007/JHEP11(2014)016 [arXiv:1407.7859 [hep-ph]].

[87] V. Keus, S. F. King, S. Moretti and D. Sokolowska, JHEP **1511**, 003 (2015) doi:10.1007/JHEP11(2015)003 [arXiv:1507.08433 [hep-ph]].

[88] A. Cordero, J. Hernandez-Sanchez, V. Keus, S. F. King, S. Moretti, D. Rojas and D. Sokolowska, JHEP **1805**, 030 (2018) doi:10.1007/JHEP05(2018)030 [arXiv:1712.09598 [hep-ph]].

[89] V. Keus, S. F. King and S. Moretti, Phys. Rev. D **90**, no. 7, 075015 (2014) doi:10.1103/PhysRevD.90.075015 [arXiv:1408.0796 [hep-ph]].

[90] A. Ahriche, G. Faisel, S. Y. Ho, S. Nasri and J. Tandean, Phys. Rev. D **92**, no. 3, 035020 (2015) doi:10.1103/PhysRevD.92.035020 [arXiv:1501.06605 [hep-ph]].

[91] A. Cordero-Cid, J. Hernández-Sánchez, V. Keus, S. F. King, S. Moretti, D. Rojas and D. Soko?owska, JHEP **1612**, 014 (2016) doi:10.1007/JHEP12(2016)014 [arXiv:1608.01673 [hep-ph]].

[92] A. Aranda, D. Hernández-Otero, J. Hernández-Sanchez, S. Moretti, D. Rojas-Ciofalo and T. Shindou, arXiv:1907.12470 [hep-ph].

[93] A. Arbey, F. Mahmoudi, O. Stal and T. Stefaniak, Eur. Phys. J. C **78**, no. 3, 182 (2018) doi:10.1140/epjc/s10052-018-5651-1 [arXiv:1706.07414 [hep-ph]].

[94] M. Baak *et al.* [Gfitter Group], Eur. Phys. J. C **74**, 3046 (2014) doi:10.1140/epjc/s10052-014-3046-5 [arXiv:1407.3792 [hep-ph]].

[95] S. Schael *et al.* [ALEPH and DELPHI and L3 and OPAL and LEP Electroweak Collaborations], Phys. Rept. **532**, 119 (2013) doi:10.1016/j.physrep.2013.07.004 [arXiv:1302.3415 [hep-ex]].

[96] [Tevatron Electroweak Working Group], arXiv:1003.2826 [hep-ex].

[97] G. Altarelli, R. Kleiss and C. Verzegnassi, CERN-89-08, CERN-89-08-V-1, CERN-YELLOW-89-08-V-1.

[98] E. Lundstrom, M. Gustafsson and J. Edsjo, Phys. Rev. D **79**, 035013 (2009) doi:10.1103/PhysRevD.79.035013 [arXiv:0810.3924 [hep-ph]].

[99] G. Abbiendi *et al.* [ALEPH and DELPHI and L3 and OPAL and LEP Collaborations], Eur. Phys. J. C **73**, 2463 (2013) doi:10.1140/epjc/s10052-013-2463-1 [arXiv:1301.6065 [hep-ex]].

[100] A. Pierce and J. Thaler, JHEP **0708**, 026 (2007) doi:10.1088/1126-6708/2007/08/026 [hep-ph/0703056 [HEP-PH]].

[101] A. M. Sirunyan *et al.* [CMS Collaboration], Phys. Lett. B **793**, 520 (2019) doi:10.1016/j.physletb.2019.04.025 [arXiv:1809.05937 [hep-ex]].

[102] J. Bernon and B. Dumont, Eur. Phys. J. C **75**, no. 9, 440 (2015) doi:10.1140/epjc/s10052-015-3645-9 [arXiv:1502.04138 [hep-ph]].

[103] P. Bechtle, O. Brein, S. Heinemeyer, G. Weiglein and K. E. Williams, Comput. Phys. Commun. **182**, 2605 (2011) doi:10.1016/j.cpc.2011.07.015 [arXiv:1102.1898 [hep-ph]].

[104] N. Aghanim *et al.* [Planck Collaboration], arXiv:1807.06209 [astro-ph.CO].

[105] E. Aprile *et al.* [XENON Collaboration], Phys. Rev. Lett. **121**, no. 11, 111302 (2018) doi:10.1103/PhysRevLett.121.111302 [arXiv:1805.12562 [astro-ph.CO]].

[106] Digitized XENON1T results at PhenoData project,. https://hepmdb.soton.ac.uk/phenodata/view.php?id=595e239abb817586383e929d

[107] A. Alloul, N. D. Christensen, C. Degrande, C. Duhr and B. Fuks, Comput. Phys. Commun. **185**, 2250 (2014) doi:10.1016/j.cpc.2014.04.012 [arXiv:1310.1921 [hep-ph]].

[108] G. Belanger, F. Boudjema, A. Pukhov and A. Semenov, arXiv:1305.0237 [hep-ph].

[109] G. Belanger, F. Boudjema, A. Pukhov and A. Semenov, arXiv:1005.4133 [hep-ph].

[110] G. Belanger, F. Boudjema, A. Pukhov and A. Semenov, arXiv:0803.2360 [hep-ph].

[111] G. Belanger, F. Boudjema, A. Pukhov and A. Semenov, Comput. Phys. Commun. **176** (2007) 367 [arXiv:hep-ph/0607059].

[112] J. Haller, A. Hoecker, R. Kogler, K. Mönig, T. Peiffer and J. Stelzer, Eur. Phys. J. C **78**, no. 8, 675 (2018) doi:10.1140/epjc/s10052-018-6131-3 [arXiv:1803.01853 [hep-ph]].

[113] D. S. Akerib *et al.* [LZ Collaboration], arXiv:1509.02910 [physics.ins-det].

[114] B. Eiteneuer, A. Goudelis and J. Heisig, Eur. Phys. J. C **77**, no. 9, 624 (2017) doi:10.1140/epjc/s10052-017-5166-1 [arXiv:1705.01458 [hep-ph]].

[115] D. Dercks, N. Desai, J. S. Kim, K. Rolbiecki, J. Tattersall and T. Weber, Comput. Phys. Commun. **221**, 383 (2017) doi:10.1016/j.cpc.2017.08.021 [arXiv:1611.09856 [hep-ph]].

[116] J. de Favereau *et al.* [DELPHES 3 Collaboration], JHEP **1402**, 057 (2014) doi:10.1007/JHEP02(2014)057 [arXiv:1307.6346 [hep-ex]].

[117] M. Cacciari, G. P. Salam and G. Soyez, Eur. Phys. J. C **72**, 1896 (2012) doi:10.1140/epjc/s10052-012-1896-2 [arXiv:1111.6097 [hep-ph]].

[118] M. Cacciari and G. P. Salam, Phys. Lett. B **641**, 57 (2006) doi:10.1016/j.physletb.2006.08.037 [hep-ph/0512210].

[119] M. Cacciari, G. P. Salam and G. Soyez, JHEP **0804**, 063 (2008) doi:10.1088/1126-6708/2008/04/063 [arXiv:0802.1189 [hep-ph]].

[120] A. L. Read, J. Phys. G **28**, 2693 (2002). doi:10.1088/0954-3899/28/10/313

[121] T. Sjöstrand *et al.*, Comput. Phys. Commun. **191**, 159 (2015) doi:10.1016/j.cpc.2015.01.024 [arXiv:1410.3012 [hep-ph]].

[122] A. Belyaev, N. D. Christensen and A. Pukhov, Comput. Phys. Commun. **184**, 1729 (2013) doi:10.1016/j.cpc.2013.01.014 [arXiv:1207.6082 [hep-ph]].

[123] M. Aaboud *et al.* [ATLAS Collaboration], JHEP **1801**, 126 (2018) doi:10.1007/JHEP01(2018)126 [arXiv:1711.03301 [hep-ex]].

[124] L. Randall and R. Sundrum, Phys. Rev. Lett. **83**, 3370 (1999) doi:10.1103/PhysRevLett.83.3370 [hep-ph/9905221].

[125] H. Davoudiasl, J. L. Hewett and T. G. Rizzo, Phys. Rev. Lett. **84**, 2080 (2000) doi:10.1103/PhysRevLett.84.2080 [hep-ph/9909255].

[126] Y. Grossman and M. Neubert, Phys. Lett. B **474**, 361 (2000) doi:10.1016/S0370-2693(00)00054-X [hep-ph/9912408].

[127] T. Gherghetta and A. Pomarol, Nucl. Phys. B **586**, 141 (2000) doi:10.1016/S0550-3213(00)00392-8 [hep-ph/0003129].

[128] A. Pomarol, Phys. Lett. B **486**, 153 (2000) doi:10.1016/S0370-2693(00)00737-1 [hep-ph/9911294].

[129] W. D. Goldberger and M. B. Wise, Phys. Lett. B **475**, 275 (2000) doi:10.1016/S0370-2693(00)00099-X [hep-ph/9911457].

[130] R. Rattazzi and A. Zaffaroni, JHEP **0104**, 021 (2001) doi:10.1088/1126-6708/2001/04/021 [hep-th/0012248].

[131] W. D. Goldberger and M. B. Wise, Phys. Rev. Lett. **83**, 4922 (1999) doi:10.1103/PhysRevLett.83.4922 [hep-ph/9907447].

[132] O. DeWolfe, D. Z. Freedman, S. S. Gubser and A. Karch, Phys. Rev. D **62**, 046008 (2000) doi:10.1103/PhysRevD.62.046008 [hep-th/9909134].

[133] C. Csaki, M. L. Graesser and G. D. Kribs, Phys. Rev. D **63**, 065002 (2001) doi:10.1103/PhysRevD.63.065002 [hep-th/0008151].

[134] C. Charmousis, R. Gregory and V. A. Rubakov, Phys. Rev. D **62**, 067505 (2000) doi:10.1103/PhysRevD.62.067505 [hep-th/9912160].

[135] S. J. Huber and Q. Shafi, Phys. Rev. D **63**, 045010 (2001) doi:10.1103/PhysRevD.63.045010 [hep-ph/0005286].

[136] H. Davoudiasl, J. L. Hewett and T. G. Rizzo, Phys. Rev. D **63**, 075004 (2001) doi:10.1103/PhysRevD.63.075004 [hep-ph/0006041].

[137] S. Chang, J. Hisano, H. Nakano, N. Okada and M. Yamaguchi, Phys. Rev. D **62**, 084025 (2000) doi:10.1103/PhysRevD.62.084025 [hep-ph/9912498].

[138] H. Davoudiasl, B. Lillie and T. G. Rizzo, JHEP **0608**, 042 (2006) doi:10.1088/1126-6708/2006/08/042 [hep-ph/0508279].

[139] P. R. Archer, JHEP **1209**, 095 (2012) doi:10.1007/JHEP09(2012)095 [arXiv:1204.4730 [hep-ph]].

[140] P. R. Archer, M. Carena, A. Carmona and M. Neubert, JHEP **1501**, 060 (2015) doi:10.1007/JHEP01(2015)060 [arXiv:1408.5406 [hep-ph]].

[141] G. Cacciapaglia, C. Csaki, G. Marandella and J. Terning, JHEP **0702**, 036 (2007) doi:10.1088/1126-6708/2007/02/036 [hep-ph/0611358].

[142] N. Haba, K. y. Oda and R. Takahashi, Acta Phys. Polon. B **41**, 1291 (2010) [arXiv:0910.4528 [hep-ph]].

[143] M. Quiros, Mod. Phys. Lett. A **30**, no. 15, 1540012 (2015) doi:10.1142/S021773231540012X [arXiv:1311.2824 [hep-ph]].

[144] F. Mahmoudi, U. Maitra, N. Manglani and K. Sridhar, JHEP **1611**, 075 (2016) doi:10.1007/JHEP11(2016)075 [arXiv:1608.07407 [hep-ph]].

[145] N. Haba, K. y. Oda and R. Takahashi, JHEP **1105**, 125 (2011) doi:10.1007/JHEP05(2011)125 [arXiv:1102.1970 [hep-ph]].

[146] K. Agashe, A. Delgado, M. J. May and R. Sundrum, JHEP **0308**, 050 (2003) doi:10.1088/1126-6708/2003/08/050 [hep-ph/0308036].

[147] M. Geller, S. Bar-Shalom and A. Soni, Phys. Rev. D **89**, no. 9, 095015 (2014) doi:10.1103/PhysRevD.89.095015 [arXiv:1312.3331 [hep-ph]].

[148] A. Ahmed, B. Grzadkowski, J. F. Gunion and Y. Jiang, Acta Phys. Polon. B **46**, no. 11, 2205 (2015) doi:10.5506/APhysPolB.46.2205 [arXiv:1510.04116 [hep-ph]].

[149] V. O. Egorov and I. P. Volobuev, J. Phys. Conf. Ser. **798**, no. 1, 012085 (2017). doi:10.1088/1742-6596/798/1/012085

[150] L. Vecchi, JHEP **1111**, 102 (2011) doi:10.1007/JHEP11(2011)102 [arXiv:1012.3742 [hep-ph]].

[151] M. Merchand, M. Sher and K. Thrasher, J. Phys. G **46**, no. 7, 075004 (2019) doi:10.1088/1361-6471/ab0ecc [arXiv:1809.10277 [hep-ph]].

[152] D. P. George, Phys. Rev. D **83**, 104025 (2011) doi:10.1103/PhysRevD.83.104025 [arXiv:1102.0564 [hep-th]].

[153] G. Aad *et al.* [ATLAS and CMS Collaborations], JHEP **1608**, 045 (2016) doi:10.1007/JHEP08(2016)045 [arXiv:1606.02266 [hep-ex]].

[154] The ATLAS collaboration [ATLAS Collaboration], ATLAS-CONF-2018-031.

[155] D. Dominici, B. Grzadkowski, J. F. Gunion and M. Toharia, Nucl. Phys. B **671**, 243 (2003) doi:10.1016/j.nuclphysb.2003.08.020 [hep-ph/0206192].

[156] A. Chakraborty, U. Maitra, S. Raychaudhuri and T. Samui, Nucl. Phys. B **922**, 41 (2017) doi:10.1016/j.nuclphysb.2017.06.006 [arXiv:1701.07471 [hep-ph]].

[157] K. Agashe, G. Perez and A. Soni, Phys. Rev. D **71**, 016002 (2005) doi:10.1103/PhysRevD.71.016002 [hep-ph/0408134].

[158] G. F. Giudice, R. Rattazzi and J. D. Wells, Nucl. Phys. B **595**, 250 (2001) doi:10.1016/S0550-3213(00)00686-6 [hep-ph/0002178].

[159] S. M. Aybat and D. P. George, JHEP **1009**, 010 (2010) doi:10.1007/JHEP09(2010)010 [arXiv:1006.2827 [hep-th]].

[160] J. L. Hewett and T. G. Rizzo, JHEP **0308**, 028 (2003) doi:10.1088/1126-6708/2003/08/028 [hep-ph/0202155].

[161] M. Chaichian, A. Datta, K. Huitu and Z. h. Yu, Phys. Lett. B **524**, 161 (2002) doi:10.1016/S0370-2693(01)01378-8 [hep-ph/0110035].

[162] A. Datta and K. Huitu, Phys. Lett. B **578**, 376 (2004) doi:10.1016/j.physletb.2003.10.055 [hep-ph/0306241].

[163] H. de Sandes and R. Rosenfeld, Phys. Rev. D **85**, 053003 (2012) doi:10.1103/PhysRevD.85.053003 [arXiv:1111.2006 [hep-ph]].

[164] H. Kubota and M. Nojiri, Phys. Rev. D **87**, 076011 (2013) doi:10.1103/PhysRevD.87.076011 [arXiv:1207.0621 [hep-ph]].

[165] N. Desai, U. Maitra and B. Mukhopadhyaya, JHEP **1310**, 093 (2013) doi:10.1007/JHEP10(2013)093 [arXiv:1307.3765 [hep-ph]].

[166] E. Boos, S. Keizerov, E. Rahmetov and K. Svirina, Phys. Rev. D **90**, no. 9, 095026 (2014) doi:10.1103/PhysRevD.90.095026 [arXiv:1409.2796 [hep-ph]].

[167] E. E. Boos, V. E. Bunichev, M. A. Perfilov, M. N. Smolyakov and I. P. Volobuev, Phys. Rev. D **92**, no. 9, 095010 (2015) doi:10.1103/PhysRevD.92.095010 [arXiv:1505.05892 [hep-ph]].

[168] M. Frank, K. Huitu, U. Maitra and M. Patra, Phys. Rev. D **94**, no. 5, 055016 (2016) doi:10.1103/PhysRevD.94.055016 [arXiv:1606.07689 [hep-ph]].

[169] A. Ahmed, B. M. Dillon, B. Grzadkowski, J. F. Gunion and Y. Jiang, Phys. Rev. D **95**, no. 9, 095019 (2017) doi:10.1103/PhysRevD.95.095019 [arXiv:1512.05771 [hep-ph]].

[170] M. Merchand, M. Sher and K. Thrasher, JHEP **1809**, 029 (2018) doi:10.1007/JHEP09(2018)029 [arXiv:1805.07282 [hep-ph]].

[171] C. Csaki, J. Erlich and J. Terning, Phys. Rev. D **66**, 064021 (2002) doi:10.1103/PhysRevD.66.064021 [hep-ph/0203034].

[172] K. Agashe, R. Contino, L. Da Rold and A. Pomarol, Phys. Lett. B **641**, 62 (2006) doi:10.1016/j.physletb.2006.08.005 [hep-ph/0605341].

[173] H. E. Haber and D. O'Neil, Phys. Rev. D **83**, 055017 (2011) doi:10.1103/PhysRevD.83.055017 [arXiv:1011.6188 [hep-ph]].

[174] A. Pomarol and R. Vega, Nucl. Phys. B **413**, 3 (1994) doi:10.1016/0550-3213(94)90611-4 [hep-ph/9305272].

[175] C. Csaki, J. Hubisz and S. J. Lee, Phys. Rev. D **76**, 125015 (2007) doi:10.1103/PhysRevD.76.125015 [arXiv:0705.3844 [hep-ph]].

[176] M. Aaboud *et al.* [ATLAS Collaboration], arXiv:1804.06174 [hep-ex].

[177] A. M. Sirunyan *et al.* [CMS Collaboration], JHEP **1801**, 054 (2018) doi:10.1007/JHEP01(2018)054 [arXiv:1708.04188 [hep-ex]].

[178] M. Aaboud *et al.* [ATLAS Collaboration], Eur. Phys. J. C **78**, no. 1, 24 (2018) doi:10.1140/epjc/s10052-017-5491-4 [arXiv:1710.01123 [hep-ex]].

[179] A. M. Sirunyan *et al.* [CMS Collaboration], arXiv:1804.01939 [hep-ex].

[180] V. Khachatryan *et al.* [CMS Collaboration], Phys. Lett. B **759**, 369 (2016) doi:10.1016/j.physletb.2016.05.087 [arXiv:1603.02991 [hep-ex]].

[181] CMS Collaboration [CMS Collaboration], CMS-PAS-HIG-16-010.

[182] M. Aaboud *et al.* [ATLAS Collaboration], arXiv:1804.01126 [hep-ex].

[183] C. Patrignani *et al.* [Particle Data Group], Chin. Phys. C **40**, no. 10, 100001 (2016). doi:10.1088/1674-1137/40/10/100001

[184] M. Misiak and M. Steinhauser, Eur. Phys. J. C **77**, no. 3, 201 (2017) doi:10.1140/epjc/s10052-017-4776-y [arXiv:1702.04571 [hep-ph]].

[185] R. J. Crewther, P. Di Vecchia, G. Veneziano and E. Witten, Phys. Lett. **88B**, 123 (1979) Erratum: [Phys. Lett. **91B**, 487 (1980)]. doi:10.1016/0370-2693(80)91025-4, 10.1016/0370-2693(79)90128-X

[186] C. A. Baker *et al.*, Phys. Rev. Lett. **97**, 131801 (2006) doi:10.1103/PhysRevLett.97.131801 [hep-ex/0602020].

[187] A. E. Nelson, Phys. Lett. **136B**, 387 (1984). doi:10.1016/0370-2693(84)92025-2

[188] S. M. Barr, Phys. Rev. Lett. **53**, 329 (1984). doi:10.1103/PhysRevLett.53.329

[189] R. D. Peccei and H. R. Quinn, Phys. Rev. D **16**, 1791 (1977). doi:10.1103/PhysRevD.16.1791

[190] R. D. Peccei, J. Korean Phys. Soc. **29**, S199 (1996) [hep-ph/9606475].

[191] J. E. Kim and G. Carosi, Rev. Mod. Phys. **82**, 557 (2010) Erratum: [Rev. Mod. Phys. **91**, no. 4, 049902 (2019)] doi:10.1103/RevModPhys.91.049902, 10.1103/RevModPhys.82.557 [arXiv:0807.3125 [hep-ph]].

[192] S. L. Adler, Phys. Rev. **177**, 2426 (1969). doi:10.1103/PhysRev.177.2426

[193] J. S. Bell and R. Jackiw, Nuovo Cim. A **60**, 47 (1969). doi:10.1007/BF02823296

[194] P. Di Vecchia and G. Veneziano, Nucl. Phys. B **171**, 253 (1980). doi:10.1016/0550-3213(80)90370-3

[195] C. D. Froggatt and H. B. Nielsen, Nucl. Phys. B **147**, 277 (1979). doi:10.1016/0550-3213(79)90316-X

[196] F. Wilczek, Phys. Rev. Lett. **49**, 1549 (1982). doi:10.1103/PhysRevLett.49.1549

[197] F. Björkeroth, E. J. Chun and S. F. King, JHEP **1808**, 117 (2018) doi:10.1007/JHEP08(2018)117 [arXiv:1806.00660 [hep-ph]].

[198] Y. Ema, K. Hamaguchi, T. Moroi and K. Nakayama, JHEP **1701**, 096 (2017) doi:10.1007/JHEP01(2017)096 [arXiv:1612.05492 [hep-ph]].

[199] L. Calibbi, F. Goertz, D. Redigolo, R. Ziegler and J. Zupan, Phys. Rev. D **95**, no. 9, 095009 (2017) doi:10.1103/PhysRevD.95.095009 [arXiv:1612.08040 [hep-ph]].

[200] M. Linster and R. Ziegler, JHEP **1808**, 058 (2018) doi:10.1007/JHEP08(2018)058 [arXiv:1805.07341 [hep-ph]].

[201] C. D. Carone and M. Merchand, Phys. Rev. D **100**, no. 3, 035006 (2019) doi:10.1103/PhysRevD.100.035006 [arXiv:1904.11059 [hep-ph]].

[202] Y. Nir and N. Seiberg, Phys. Lett. B **309**, 337 (1993) doi:10.1016/0370-2693(93)90942-B [hep-ph/9304307].

[203] M. Leurer, Y. Nir and N. Seiberg, Nucl. Phys. B **420**, 468 (1994) doi:10.1016/0550-3213(94)90074-4 [hep-ph/9310320].

[204] D. B. Kaplan and M. Schmaltz, Phys. Rev. D **49**, 3741 (1994) doi:10.1103/PhysRevD.49.3741 [hep-ph/9311281].

[205] M. Dine, R. G. Leigh and A. Kagan, Phys. Rev. D **48**, 4269 (1993) doi:10.1103/PhysRevD.48.4269 [hep-ph/9304299].

[206] L. J. Hall and H. Murayama, Phys. Rev. Lett. **75**, 3985 (1995) doi:10.1103/PhysRevLett.75.3985 [hep-ph/9508296].

[207] C. D. Carone, L. J. Hall and H. Murayama, Phys. Rev. D **53**, 6282 (1996) doi:10.1103/PhysRevD.53.6282 [hep-ph/9512399].

[208] P. H. Frampton and O. C. W. Kong, Phys. Rev. Lett. **77**, 1699 (1996) doi:10.1103/PhysRevLett.77.1699 [hep-ph/9603372].

[209] F. Gabbiani, E. Gabrielli, A. Masiero and L. Silvestrini, Nucl. Phys. B **477**, 321 (1996) doi:10.1016/0550-3213(96)00390-2 [hep-ph/9604387].

[210] R. Barbieri, G. R. Dvali and L. J. Hall, Phys. Lett. B **377**, 76 (1996) doi:10.1016/0370-2693(96)00318-8 [hep-ph/9512388].

[211] R. Barbieri, L. J. Hall and A. Romanino, Phys. Lett. B **401**, 47 (1997) doi:10.1016/S0370-2693(97)00372-9 [hep-ph/9702315].

[212] R. Barbieri, L. J. Hall, S. Raby and A. Romanino, Nucl. Phys. B **493**, 3 (1997) doi:10.1016/S0550-3213(97)00134-X [hep-ph/9610449].

[213] A. Aranda, C. D. Carone and R. F. Lebed, Phys. Lett. B **474**, 170 (2000) doi:10.1016/S0370-2693(99)01497-5 [hep-ph/9910392].

[214] A. Aranda, C. D. Carone and R. F. Lebed, Phys. Rev. D **62**, 016009 (2000) doi:10.1103/PhysRevD.62.016009 [hep-ph/0002044].

[215] C. D. Carone, S. Chaurasia and S. Vasquez, Phys. Rev. D **95**, no. 1, 015025 (2017) doi:10.1103/PhysRevD.95.015025 [arXiv:1611.00784 [hep-ph]].

[216] Y. H. Ahn, Phys. Rev. D **98**, no. 3, 035047 (2018) doi:10.1103/PhysRevD.98.035047 [arXiv:1804.06988 [hep-ph]].

[217] A. Falkowski, M. Nardecchia and R. Ziegler, "Lepton Flavor Non-Universality in B-meson Decays from a U(2) Flavor Model," JHEP **1511**, 173 (2015) [arXiv:1509.01249 [hep-ph]].

[218] L. M. Krauss and F. Wilczek, "Discrete Gauge Symmetry in Continuum Theories," Phys. Rev. Lett. **62**, 1221 (1989).

[219] D. J. E. Marsh, "Axion Cosmology," Phys. Rept. **643**, 1 (2016) [arXiv:1510.07633 [astro-ph.CO]].

[220] J. L. Feng, T. Moroi, H. Murayama and E. Schnapka, "Third generation familons, b factories, and neutrino cosmology," Phys. Rev. D **57**, 5875 (1998) [hep-ph/9709411].

[221] M. Bauer, T. Schell and T. Plehn, "Hunting the Flavon," Phys. Rev. D **94**, no. 5, 056003 (2016) [arXiv:1603.06950 [hep-ph]].

[222] A. Celis, J. Fuentes-Martin and H. Serodio, "An invisible axion model with controlled FCNCs at tree level," Phys. Lett. B **741**, 117 (2015) [arXiv:1410.6217 [hep-ph]].

[223] M. E. Albrecht, T. Feldmann and T. Mannel, "Goldstone Bosons in Effective Theories with Spontaneously Broken Flavour Symmetry," JHEP **1010**, 089 (2010) [arXiv:1002.4798 [hep-ph]].

[224] A. Davidson and M. A. H. Vozmediano, "The Horizontal Axion Alternative: The Interplay of Vacuum Structure and Flavor Interactions," Nucl. Phys. B **248**, 647 (1984).

[225] S. Adler *et al.* [E949 and E787 Collaborations], "Measurement of the $K^+ \to \pi^+ \nu\nu$ branching ratio," Phys. Rev. D **77**, 052003 (2008) [arXiv:0709.1000 [hep-ex]].

[226] J. K. Ahn *et al.* [KOTO Collaboration], "A new search for the $K_L \to \pi^0 \nu\overline{\nu}$ and $K_L \to \pi^0 X^0$ decays," PTEP **2017**, no. 2, 021C01 (2017) [arXiv:1609.03637 [hep-ex]].

[227] R. Ammar *et al.* [CLEO Collaboration], "Search for the familon via $B^{+-} \to \pi^{\pm} X^0$, $B^{\pm} \to K^{\pm} X^0$, and $B^0 \to K^0_S X^0$ decays," Phys. Rev. Lett. **87**, 271801 (2001) [hep-ex/0106038].

[228] M. Tanabashi *et al.* [Particle Data Group], "Review of Particle Physics," Phys. Rev. D **98**, no. 3, 030001 (2018).

[229] T. Banks, Physicalia Mag. **12**, 19 (1990).

[230] S. B. Giddings and A. Strominger, Nucl. Phys. B **307**, 854 (1988). doi:10.1016/0550-3213(88)90109-5

[231] S. R. Coleman, Nucl. Phys. B **310**, 643 (1988). doi:10.1016/0550-3213(88)90097-1

[232] G. Gilbert, Nucl. Phys. B **328**, 159 (1989). doi:10.1016/0550-3213(89)90097-7

[233] S. M. Barr and D. Seckel, Phys. Rev. D **46**, 539 (1992). doi:10.1103/PhysRevD.46.539

[234] M. Kamionkowski and J. March-Russell, Phys. Lett. B **282**, 137 (1992) doi:10.1016/0370-2693(92)90492-M [hep-th/9202003].

[235] L. Randall, Phys. Lett. B **284**, 77 (1992). doi:10.1016/0370-2693(92)91928-3

[236] B. Lillard and T. M. P. Tait, JHEP **1711**, 005 (2017) doi:10.1007/JHEP11(2017)005 [arXiv:1707.04261 [hep-ph]].

[237] L. Di Luzio, E. Nardi and L. Ubaldi, Phys. Rev. Lett. **119**, no. 1, 011801 (2017) doi:10.1103/PhysRevLett.119.011801 [arXiv:1704.01122 [hep-ph]].

[238] B. Lillard and T. M. P. Tait, JHEP **1811**, 199 (2018) doi:10.1007/JHEP11(2018)199 [arXiv:1811.03089 [hep-ph]].

[239] E. J. Chun and A. Lukas, Phys. Lett. B **297**, 298 (1992) doi:10.1016/0370-2693(92)91266-C [hep-ph/9209208].

[240] K. Harigaya, M. Ibe, K. Schmitz and T. T. Yanagida, Phys. Rev. D **88**, no. 7, 075022 (2013) doi:10.1103/PhysRevD.88.075022 [arXiv:1308.1227 [hep-ph]].

[241] K. Harigaya, M. Ibe, K. Schmitz and T. T. Yanagida, Phys. Rev. D **92**, no. 7, 075003 (2015) doi:10.1103/PhysRevD.92.075003 [arXiv:1505.07388 [hep-ph]].

[242] H. C. Cheng and D. E. Kaplan, hep-ph/0103346.

[243] H. Fukuda, M. Ibe, M. Suzuki and T. T. Yanagida, Phys. Lett. B **771**, 327 (2017) doi:10.1016/j.physletb.2017.05.071 [arXiv:1703.01112 [hep-ph]].

[244] M. Duerr, K. Schmidt-Hoberg and J. Unwin, Phys. Lett. B **780**, 553 (2018) doi:10.1016/j.physletb.2018.03.054 [arXiv:1712.01841 [hep-ph]].

[245] J. Preskill, M. B. Wise and F. Wilczek, "Cosmology of the Invisible Axion," Phys. Lett. **120B**, 127 (1983).

[246] L. F. Abbott and P. Sikivie, "A Cosmological Bound on the Invisible Axion," Phys. Lett. **120B**, 133 (1983).

[247] M. Dine and W. Fischler, "The Not So Harmless Axion," Phys. Lett. **120B**, 137 (1983).

[248] R. T. Co, L. J. Hall and K. Harigaya, "QCD Axion Dark Matter with a Small Decay Constant," Phys. Rev. Lett. **120**, no. 21, 211602 (2018) [arXiv:1711.10486 [hep-ph]].

[249] M. Dine, W. Fischler and M. Srednicki, "A Simple Solution to the Strong CP Problem with a Harmless Axion," Phys. Lett. B **104**, 199-202 (1981); A. Zhitnitsky, "On Possible Suppression of the Axion Hadron Interactions. (In Russian)," Sov. J. Nucl. Phys. **31**, 260 (1980).

[250] J. E. Kim, Phys. Rev. D **58**, 055006 (1998) doi:10.1103/PhysRevD.58.055006 [hep-ph/9802220].

[251] F. Arias-Aragon and L. Merlo, "The Minimal Flavour Violating Axion," JHEP **1710**, 168 (2017) Erratum: [JHEP **1911**, 152 (2019)] [arXiv:1709.07039 [hep-ph]].

[252] J. Jaeckel and M. Spannowsky, "Probing MeV to 90 GeV axion-like particles with LEP and LHC," Phys. Lett. B **753**, 482 (2016) [arXiv:1509.00476 [hep-ph]].

[253] M. Bauer, M. Neubert and A. Thamm, "Collider Probes of Axion-Like Particles," JHEP **1712**, 044 (2017) [arXiv:1708.00443 [hep-ph]].

[254] C. Csaki, C. Grojean, J. Hubisz, Y. Shirman and J. Terning, Phys. Rev. D **70**, 015012 (2004) doi:10.1103/PhysRevD.70.015012 [hep-ph/0310355].

[255] T. Gherghetta, Phys. Rev. Lett. **92**, 161601 (2004) doi:10.1103/PhysRevLett.92.161601 [hep-ph/0312392].

[256] A. M. Iyer and S. K. Vempati, Phys. Rev. D **88**, no. 7, 073005 (2013) doi:10.1103/PhysRevD.88.073005 [arXiv:1307.5773 [hep-ph]].

[257] C. S. Kim, J. D. Kim and J. h. Song, Phys. Rev. D **67**, 015001 (2003) doi:10.1103/PhysRevD.67.015001 [hep-ph/0204002].

[258] CMS Collaboration [CMS Collaboration], CMS-PAS-HIG-16-040.

[259] The ATLAS collaboration [ATLAS Collaboration], ATLAS-CONF-2017-045.

[260] G. Aad *et al.* [ATLAS Collaboration], Phys. Rev. D **92**, no. 1, 012006 (2015) doi:10.1103/PhysRevD.92.012006 [arXiv:1412.2641 [hep-ex]].

[261] S. Chatrchyan *et al.* [CMS Collaboration], JHEP **1401**, 096 (2014) doi:10.1007/JHEP01(2014)096 [arXiv:1312.1129 [hep-ex]].

[262] The ATLAS collaboration [ATLAS Collaboration], ATLAS-CONF-2016-112.

[263] G. Aad *et al.* [ATLAS Collaboration], Phys. Rev. D **91**, no. 1, 012006 (2015) doi:10.1103/PhysRevD.91.012006 [arXiv:1408.5191 [hep-ex]].

[264] CMS Collaboration [CMS Collaboration], CMS-PAS-HIG-16-041.

[265] CMS Collaboration [CMS Collaboration], CMS-PAS-HIG-16-003.

[266] M. Aaboud *et al.* [ATLAS Collaboration], JHEP **1712**, 024 (2017) doi:10.1007/JHEP12(2017)024 [arXiv:1708.03299 [hep-ex]].

[267] A. M. Sirunyan *et al.* [CMS Collaboration], Phys. Lett. B **780**, 501 (2018) doi:10.1016/j.physletb.2018.02.050 [arXiv:1709.07497 [hep-ex]].

[268] G. Aad *et al.* [ATLAS Collaboration], JHEP **1504**, 117 (2015) doi:10.1007/JHEP04(2015)117 [arXiv:1501.04943 [hep-ex]].

[269] G. Aad *et al.* [ATLAS Collaboration], Eur. Phys. J. C **76**, no. 1, 6 (2016) doi:10.1140/epjc/s10052-015-3769-y [arXiv:1507.04548 [hep-ex]].

[270] G. Aad *et al.* [ATLAS Collaboration], Phys. Rev. D **93**, no. 9, 092005 (2016) doi:10.1103/PhysRevD.93.092005 [arXiv:1511.08352 [hep-ex]].

[271] M. Aaboud *et al.* [ATLAS Collaboration], Phys. Rev. D **97**, no. 7, 072003 (2018) doi:10.1103/PhysRevD.97.072003 [arXiv:1712.08891 [hep-ex]].